A CHEMICAL AND KINETIC EVALUATION OF SPIN TRAPPING BY 5,5-DIMETHYL-1-PYRROLINE-N-OXIDE IN THE REACTION OF $[Fe^{III}EDTA]^{-1}$ WITH PEROXIDE

BY

FRANCES Y. SAUNDERS

A DISSERTATION PRESENTED TO THE GRADUATE SCHOOL
OF THE UNIVERSITY OF FLORIDA IN PARTIAL FULFILLMENT
OF THE REQUIREMENTS FOR THE DEGREE OF
DOCTOR OF PHILOSOPHY

UNIVERSITY OF FLORIDA

1990

ACKNOWLEDGMENTS

This work was completed by the grace of God and the prayers of many. I would like to give credit and thanks to all those who gave of themselves to assist me in this endeavor. I would first like to thank Dr. David Richardson for his patience, ideas and instruction and the Richardson research group for their support and friendship. I would also like to thank Dr. Robert Hanrahan for his assistance with kinetic simulations and the gamma radiolysis experiments. Special thanks go to the NCASI staff for their patient, wholehearted support. I am indebted to my parents and family for their support and encouragement throughout my many years in school, and I am also grateful to Dr. and Mrs. Ted Goodman for their continued concern and encouragement. I wish to give special thanks to Dr. Shannon Davis for her constant friendship through the good and the bad. Finally, I have been enabled to complete this work by the love, counsel, friendship and prayers of Mike, Maribel, Christopher and Michelle Lisk, Mike and Theresa Williams, Arty and Jackie Hart, Al and Cindy Dompe, Margaret Brouwer and many other members of the Vineyard Christian Fellowship. I would like to thank all of them for their help in completing this work.

TABLE OF CONTENTS

	Page
ACKNOWLEDGMENTS	ii
LIST OF TABLES	vi
LIST OF FIGURES	vii
LIST OF ABBREVIATIONS	x
ABSTRACT	xi
CHAPTERS	
1 INTRODUCTION	1
Free Radicals: an Historical Overview	1
Biological Free Radicals	4
History	4
Effects of Biological Radicals	4
In Vivo Radical Production	5
Beneficial Biological Radicals	7
Summary	8
Free Radical Detection	9
General Methods	9
Spin Trapping	10
Free Radical Generation	17
2 EXPERIMENTAL	20
Instrumentation and Special Appararatus	20
Instrumentation	20
Thermostatted pH Stat System	20
EPR Recirculation System	22
UV Photolysis	23
Gamma Irradiation Apparatus	23
Removal of Adventitious Metal Ions	27
Stock Solution Preparation	28
General Methods	28
DMPO and Other Spin Trap Solutions	28
TEMPO Solutions	29
Analytical Methods	29
Peroxide Titration	29

Quantification of EPR Spectra..... 31
Iron(II)/Cysteine Reaction..... 31
Stock Solutions..... 31
Procedure..... 32
Iron-imidazole/Peroxide Reaction..... 32
Stock Solutions..... 32
$[Fe(CN)_5IM]^{-2}$ (Iron-imidazole) Preparation.. 33
Procedure..... 34
$[Fe^{III}DCYTA]^{-1}$/Peroxide Reaction..... 34
Stock Solutions..... 34
Procedure..... 35
$[[Fe^{III}EDTA]^{-1}$/Peroxide Reaction..... 35
Stock Solutions..... 35
Procedure..... 36
DMPO-OH Decay Experiments..... 38
Spin Trap Competition Experiments..... 39
Gamma Radiolysis..... 39
$[[Fe^{II}EDTA]^{-2}/H_2O_2$ Reaction..... 40
Protein Experiments..... 41
Bovine Serum Albumin..... 41
Metallothionein..... 41
Kinetic Simulations..... 42

3 RESULTS..... 44

Introduction..... 44
Radical Generating Reactions..... 45
Iron/Cysteine..... 45
Pentacyano(Imidazole) Iron(III)/Peroxide.... 45
$[Fe^{III}DCYTA]^{-1}/H_2O_2$..... 48
$[Fe^{III}EDTA]^{-1}/H_2O_2$..... 48
Replication Experiments..... 49
Organic Substrate Effects..... 49
pH Effects..... 53
Precision Measurements..... 53
Substrate and Buffer Effects
on the $[Fe^{III}EDTA]^{-1}/H_2O_2$ Reaction..... 58
DMPO Effect..... 58
Phosphate Buffer Effect..... 58
Protein Effect..... 62
Spin-Trapping Experiments..... 63
DMPO in the $[Fe^{III}EDTA]^{-1}/H_2O_2$ Reaction..... 64
Protein Effect on the $[Fe^{III}EDTA]^{-1}/H_2O_2$
Reaction..... 69
DMPO-OH Decay Experiments..... 69
TEMPO Decay..... 75
Spin Trap Competition Experiments..... 76

4 DISCUSSION..... 83

Introduction..... 83

Spin-Trapping and the $[Fe^{III}EDTA]^{-1}/H_2O_2$ Reaction..... 84
Choice of Radical Generating System..... 84
$[Fe^{III}EDTA]^{-1}$ and $[Fe^{III}EDTA]^{-2}$ Chemistry.... 85
Critical Observations..... 86
Formation of DMPO-OH..... 87
Proposed Reactive Intermediates for Iron/Peroxide Reactions..... 91
Hydroxyl Radical..... 92
Iron(V) Ferryl..... 98
Iron(IV) Ferryl..... 100
Summary..... 104
Spin Trap Competition Experiments..... 105
DMPO-OH Production in the $[Fe^{III}EDTA]^{-1}/H_2O_2$ Reaction..... 113
DMPO-OH Decay in the $[Fe^{III}EDTA]^{-1}/H_2O_2$ Reaction..... 119
$[Fe^{III}EDTA]^{-1}/H_2O_2$ Spin-Trapping Reaction Mechanism..... 121
Proteins in the $[Fe^{III}EDTA]^{-1}/H_2O_2$ Reaction.... 146
Peroxide Decomposition..... 146
DMPO-OH Production..... 146

5 CONCLUSIONS..... 149

APPENDICES

A KINETIC SIMULATIONS..... 157

B RATE CONSTANTS FOR ELEMENTARY REACTION STEPS... 161

REFERENCES..... 163

BIOGRAPHICAL SKETCH..... 169

LIST OF TABLES

Table Number	Title	Page
3-1	Peroxide decomposition as a function of acetone concentration.....	51
3-2	First and second order peroxide decomposition rate constants as a function of acetone concentration.....	54
3-3	Replication data for peroxide decomposition as a function of pH.....	55
3-4	First and second order peroxide decomposition rate constants as a function of pH.....	57
3-5	Peroxide decomposition data for the $[Fe^{III}EDTA]^{-1}/H_2O_2$ reaction in the presence of DMPO.....	59
3-6	Experimental k_{1st} and k_{2nd} values from peroxide decomposition experiments in the presence of DMPO.....	61
3-7	Data from [DMPO-OH] versus time curves in the $[Fe^{III}EDTA]^{-1}/H_2O_2$ reaction.....	67
3-8	First order rate constant for DMPO-OH decay under different conditions.....	74

LIST OF FIGURES

Figure Number	Title	Page
2-1	Thermostatted pH-stat apparatus.....	21
2-2	^{60}Co gamma ray source.....	25
2-3	Circular cell holder for ^{60}Co experiments..	26
3-1	EPR spectra from different radical generating reactions using the spin trap DMPO.....	47
3-2	Representative plots of peroxide decomposition in the presence of various acetone concentrations.....	50
3-3	Dependence of k_{2nd} on organic substrate concentration in the $[Fe^{III}EDTA]^{-1}/H_2O_2$ reaction.....	52
3-4	Peroxide decompostion as pH was varied in replication experiments.....	56
3-5	Plots of peroxide decomposition in the $[Fe^{III}EDTA]^{-1}/H_2O_2$ reaction in the presence of DMPO or acetone.....	60
3-6	[DMPO-OH] versus time curves for the $[Fe^{III}EDTA]^{-1}/H_2O_2$ reaction.....	64
3-7	EPR spectrum of hydroxyl radical and ethanol radical adducts of DMPO generated during the $[Fe^{III}EDTA]^{-1}/H_2O_2$ reaction...	68
3-8	The effect of metallothionein on DMPO-OH production in the $[Fe^{III}EDTA]^{-1}/H_2O_2$ reaction.....	70
3-9	DMPO-OH decay plots.....	73

Figure Number	Title	Page
3-10	TEMPO decay in the $[Fe^{III}EDTA]^{-1}/H_2O_2$ reaction	77
3-11	Spin adduct formation from radiolysis experiments	78
3-12	Spin adduct formation from radiolysis experiments	79
3-13	Spin adduct formation from the $[Fe^{II}EDTA]^{-2}/H_2O_2$ reaction	81
4-1	Mechanism proposed by Walling for the $[Fe^{III}EDTA]^{-1}/H_2O_2$ reaction	93
4-2	Mechanism proposed by Kremer for the Fe^{III}/H_2O_2 reaction	99
4-3	Two equivalent ways of expressing the oxidizing intermediate steps using O_x as an unidentified oxidizing intermediate	114
4-4	Proposed mechanism for the $[Fe^{III}EDTA]^{-1}/H_2O_2$ reaction in the presence of DMPO	115
4-5	Simulated DMPO-OH production using the proposed spin trap mechanism in Figure 4-4	117
4-6	Mechanism attempting to model DMPO-OH and H_2O_2 behavior in the $[Fe^{III}EDTA]^{-1}/H_2O_2$ reaction	123
4-7	Simulations of the Figure 4-6 mechanism	125
4-8	Alteration of Figure 4-6 mechanism	127
4-9	Simulations of the Figure 4-8 mechanism	128
4-10	An accurate mechanism for H_2O_2 decomposition	132
4-11	Figure 4-10 mechanism fit of simulated peroxide decomposition data to experimental data	136

Figure Number	Title	Page
4-12	Invariance of peroxide decomposition to trap concentration using the Figure 4-10 mechanism.....	137
4-13	DMPO-OH production curve form the Figure 4-10 mechanism.....	138
4-14	DMPO-OH production curve using the Figure 4-10 mechanism without the DMPO-OH decay step (p).....	140
4-15	Inclusion of a catalytic DMPO-OH decay cycle in the Figure 4-10 mechanism.....	141
4-16	Simulation of the Figure 4-15 mechanism....	143

LIST OF ABBREVIATIONS

BSA	bovine serum albumin
DCYTA	trans,1,2-diaminocyclohexane-N,N,N',N'-tetraacetic acid
DMPO	5,5-dimethyl-1-pyrroline-N-oxide
EDTA	ethylenediaminetetraacetic acid
EPR	electron paramagnetic resonance
ICP	inductively coupled argon plasma spectrometer
4-MePyBN	4-(N-methyl pyridinium) tertbutylnitrone
NHE	normal hydrogen electrode
PBN	N-tert-butyl-α-phenylnitrone
4-POBN	α-(4-pyridyl 1-oxide)-N-tert-butylnitrone
SOD	superoxide dismutase
TEMPO	tetramethyl-1-piperidinyloxy, free radical
TMPO	3,3,5,5-tetramethyl-1-pyrroline-N-oxide

Abstract of Dissertation Presented to the Graduate School of the University of Florida in Partial Fulfillment of the Requirements for the Degree of Doctor of Philosophy

A CHEMICAL AND KINETIC EVALUATION OF SPIN TRAPPING BY 5,5-DIMETHYL-1-PYRROLINE-N-OXIDE IN THE REACTION OF $[Fe^{III}EDTA]^{-1}$ WITH PEROXIDE

By

Frances Y. Saunders

December 1990

Chairman: David E. Richardson
Major Department: Chemistry

Free radicals are implicated in many biological processes and in the etiology of certain pathological conditions. The spin-trapping technique has emerged as a major tool in free radical research, both in vivo and in vitro. However, the technique is not without problems, and indiscriminate use may lead to erroneous results and conclusions.

The current study undertakes the chemical and kinetic evaluation of spin trapping by 5,5-dimethyl-1-pyrroline-N-oxide (DMPO) in the $[Fe^{III}EDTA]^{-1}/H_2O_2$ reaction under conditions appropriate for biological free radical studies. The formation and decay of the DMPO-OH spin adduct and the decomposition of peroxide were examined quantitatively in these experiments. Computer simulations of reaction kinetics were used to model the experimental observations in

an attempt to describe the mechanism of the $[Fe^{III}EDTA]^{-1}/H_2O_2$ reaction in the presence of DMPO. Unexpected DMPO-OH behavior was observed and the validity of conclusions drawn from spin-trapping investigations is discussed in light of these results. The $[Fe^{III}EDTA]^{-1}/H_2O_2$ reaction was chosen as a hydroxyl radical generating system, but the identity of the chain-carrying intermediate in this reaction is controversial. In addition to the hydroxyl radical, the iron(IV) or iron(V) ferryl ions have been proposed as intermediates. This controversy has not been resolved, but is addressed in the current study.

CHAPTER 1
INTRODUCTION

Free Radicals: an Historical Overview

The term "radical" was first used in 1789 by Lavoisier in his definition of acids.[1] Lavoisier described acids as oxygenated substances and called the element or combination of elements to which oxygen was bound a "radical." As more accurate descriptions of acids evolved, this definition of a radical was discarded. The term "radical" persisted, however, and was often used to refer to commonly observed combinations of elements in a series of related compounds.[1]

In 1828, a new definition of "radical" was proposed by Dumas and Boullay.[2] A radical was described as a basic organic unit that could be combined with water, HCl, acetic acid and other substances to form a class of compounds. The first such unit proposed by Dumas and Boullay was called etherin (C_4H_4) and compounds containing etherin were called ethers. The radical unit was hoped to provide systematic organization to organic chemistry and other radical units such as benzoyl ($C_{14}H_{10}O_2$), methyl (C_2H_3), cetyl ($C_{32}H_{32}$) etc. were proposed.[1]

The concept of radical units rather than organizing organic chemistry generated confusion as many observations could not be explained in terms of radical units. The radical designation was eventually abandoned as the valency concept and new theories on the combination of carbon atoms were developed. Again, the term "radical" persisted in the background referring to a group of atoms which remained joined together through a series of reactions.[1]

The term "radical" was reintroduced in 1900 by Moses Gomberg who reported the isolation of a solid free radical compound.[3] He identified the highly reactive white solid as the triphenylmethyl ($(C_6H_5)_3C$) radical. Though his findings were greeted with skepticism, Gomberg devoted much of his 36 year career to the study of free radicals. The white solid was later determined by molecular weight measurements to be hexaphenylethane, the dimer of triphenylmethyl, but strong evidence based on solution color properties was gathered to support a dimer/free radical equilibrium in solutions of the compound. The solution was yellow, which was unexpected for hexaphenylethane. When oxygen was added the color disappeared but returned with time. This effect could be demonstrated repeatedly until all the hydrocarbon was removed. These results suggested an equilibrium in which the colored species was reactive with oxygen. It was further observed that the color intensity of the solution increased as the solution was diluted showing a deviation

from Beer's law. Color intensity was also observed to increased as the solution was heated. Both of these observations were used to support the dimer/radical theory.[3]

Gomberg's free radical designation gained acceptance as other organic compounds with similar properties were discovered. There was uncertainty regarding the distribution of electrons as the dimer separated, but color and resonance stability arguments ultimately led to the conclusion that the dimer split homolytically to form two identical radicals each containing an unpaired electron. This conclusion led to a definition of the term "free radical" in the thirties that has persisted and is still generally accepted today.[1]

Free radicals are currently defined as atoms or molecules with one or more unpaired electrons. By this definition free radicals can be any species with an unpaired electron including paramagnetic transition metals and may be charged or neutral species. The most commonly considered free radicals are organic radicals and radical species derived from oxygen. Radicals are generally highly reactive, but some organic radicals are stable enough to be isolated as solids and to persist in solution for days or weeks. Radicals are often involved in catalytic chain reactions and are known to take part in combustion, polymerization, photolysis and radiolysis reactions.[1]

Biological Free Radicals

History

Though free radicals were defined and accepted in the mid-thirties, no serious consideration was given to their participation in biological systems until 1968. Enzymatic reactions were suggested early on to result in the formation of free radicals but this idea was refuted and formation from non-enzymatic sources was not considered. It was proposed in 1954 that most of the damaging effects of elevated oxygen concentration could be attributed to the formation of free radicals.[4] This idea generated little interest until 1968 when the enzyme superoxide dismutase (SOD) was discovered by McCord and Fridovich.[5]

SOD is an enzyme that is specific for the catalytic removal of superoxide. SOD is found in aerobic bacteria and many mammalian tissues. The discovery of an enzyme specific for the removal of superoxide was thought to confirm the importance of radical reactions in biological systems, and these reactions rapidly became a major research concern.

Effects of Biological Radicals

Since the discovery of free radicals in biological systems, their reactions both *in vivo* and *in vitro* have been studied extensively. These studies have led to the implication of radical processes in the etiology of many diseases. Evidence exists for free radical tissue damage

resulting in rheumatoid arthritis, immune injury to lungs and kidneys and cerebral trauma.[6] Tissue damage in heart attack and stroke victims is thought to be partially accounted for by free radical formation upon blood reperfusion to the temporarily blocked areas.[6,7] Radicals have been implicated in the degenerative effects of ageing,[8] in the cancer causing effects of radiation and in the mutagenic and carcinogenic properties of many substances.[8,9] A review of radical related diseases by Halliwell lists over sixty clinical conditions in which their involvement has been suggested.[6]

In Vivo Radical Production

Biochemical free radical production is linked usually to the presence of transition metals, typically iron or copper. Trace amounts of these metals can catalyze the formation of radicals from hydrogen peroxide, lipid peroxides, thiols and other oxidizable molecules.[6] The most common production pathway is thought by many to involve, the reaction of superoxide, peroxide and a metal catalyst to form the hydroxyl radical (equation 1-1).[10]

$$O_2 + e^- \longrightarrow O_2^-$$

$$2O_2 + 2H^+ \longrightarrow H_2O_2 + O_2$$

$$H_2O_2 + Fe(II) \longrightarrow OH\cdot + OH^- + Fe(III)$$

$$O_2^- + OH\cdot \longrightarrow O_2 + OH^-$$

$$OH\cdot + H_2O_2 \longrightarrow OH^- + HO_2\cdot$$

$$OH\cdot + \text{biological target} \longrightarrow \text{prods.} \qquad (1\text{-}1)$$

The superoxide radical forms due to various stresses, excess O_2 concentrations, toxins, radiation, etc. Superoxide is also generated by phagocytes to aid in killing bacteria. When a large number of phagocytes are activated, excess superoxide and peroxide may be generated and result in tissue damage.[6] Superoxide is a relatively unreactive radical and cannot alone account for the cellular damage that is often observed. In contrast $OH\cdot$ is a highly reactive species ($E°(NHE) = 1.77$ V; $OH\cdot + e^- = OH^-$)[11] and will react with most biological molecules at nearly diffusion controlled rates. The formation of $OH\cdot$, as shown in equation 1-1, thus explains the cellular damage observed in the presence of peroxide and superoxide. The hydroxyl radical, because of its high reactivity, will react near the site of its formation. The nature of radical damage in an organism is thus dependent on the area in which the coincidence of radical-generating reactants occurs.

In general, free radical production in vivo is not expected unless there is a loss of control in or damage to the cell. Organisms are thought to control and limit

radical production by the use of catalase and peroxidase enzymes to remove peroxide and possibly by the use of SOD to remove superoxide. Radical production may also be controlled by keeping metal ions compartmentalized or sequestered in unreactive forms.[10]

Iron, which is one of the most prevalent biological metals, is usually sequestered in storage or transport proteins. The small pool of low molecular weight iron used for biosynthesis is thought to be compartmentalized within the cell. Stresses may cause the release of iron from the compartments or sequestering proteins. In some cases superoxide or peroxide may cause iron to be released from proteins, and cellular damage can release iron by disrupting storage compartments.[6,12]

Once metal ions have been released and hydroxyl radicals generated, a large number of damaging reactions may occur. DNA appears to be a primary target for radical damage, but proteins, enzymes, tissues and membranes are also targets. Lipid peroxidation is a major reaction pathway for *in vivo* free radicals and is believed to be one mechanism by which radical-induced cellular damage occurs.[6]

Beneficial Biological Radicals

Though most research has focused on the damaging effects of uncontrolled radicals *in vivo*, there are some biochemical processes that require the production of free radicals. A review by Williams[13] describes the desirable

biochemical production of radicals and discusses several of these processes. Radical production is required mechanistically in some enzyme reactions, for polymerization reactions to form exoskeletons, shells (as in the crab) or waxy coatings on plants, for energy capture and transduction in photosynthesis, for the destruction of invading organisms and for removing more dangerous radicals.[13] Compartmentalization prevents radical damage in these processes by confining radicals to their area of usefulness and maintaining reaction component separation until radicals are required.[13]

Summary

A large amount of research has been devoted to characterizing the production and reactions of biological radicals. Radical formation has been linked to stresses or toxins which promote the simultaneous occurrence of peroxide, superoxide and metal ions. The damaging effects of radical production have been implicated in many biological disorders,[6-8] and desirable biochemical radical reactions have been identified.[13] Finally, some biochemical protection mechanisms against undesirable free radical reactions have been identified.[10]

Research continues in this area to further characterize radical reactions in vivo, to confirm the link between radicals and biological disorders, to identify other radical promoting agents or stresses and to develop methods of

protection against radical damage. Most damage is thought to be caused by the highly reactive hydroxyl radical, which is therefore of considerable interest to researchers.

Free Radical Detection

General Methods

Free radical research is complicated by the high reactivity and consequent short life times of these reactive species. Special techniques are thus required to detect and monitor radical reactions, production and decay. Since the $OH\cdot$ is thought to be responsible for the most radical damage and $OH\cdot$ formation is linked to the presence of superoxide, techniques that are applicable to superoxide and/or hydroxyl radical detection are desirable.

Chemical and optical methods have found some use as radical detection methods but are limited in their usefulness.[14] Electron paramagnetic resonance spectroscopy (EPR) is a direct method of detection and radicals species, which are long-lived, are easily and conveniently observed in the EPR. Short-lived radicals such as $OH\cdot$ must be frozen or generated continuously using special flow through techniques in order to be detected in the EPR.[15] These techniques have only limited use in biochemical studies; freezing is usually not practical, and the large quantities of reactants required for flow through techniques are often not available or are prohibitively expensive.[15]

Spin Trapping

In 1968 a special technique called spin-trapping was developed by several independent groups for the detection and identification of short-lived radicals.[12,16] Spin trapping involves the capture of short-lived radicals by a diamagnetic molecule to form a long-lived radical species, which is referred to as a spin adduct and can be easily observed by EPR. Spin trapping is a convenient, readily applicable technique which is used extensively in the study of biochemical radical processes.

Spin traps

Nitrone and nitroso (equation 1-2) compounds are the

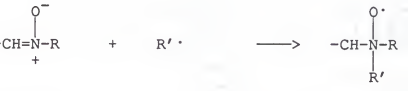

Nitrone Nitroxide

(1-2)

Nitroso Nitroxide

most commonly used spin traps. The nitroxide spin adducts which form from these traps are resonance stabilized by delocalization of the unpaired electron between oxygen and nitrogen (1-3).[17] This stabilization allows spin

(1-3)

adducts to persist in solution for several minutes or even several hours.

Carbon-, oxygen-, nitrogen- and phosphorous-centered radicals can be trapped, but nitroso traps do not form stable adducts with oxygen centered radicals.[12] Therefore, superoxide and hydroxyl radical studies normally employ nitrone traps. Though a variety of different radicals occur in biochemical systems, the precursors to these radicals are often superoxide and hydroxyl radicals. Nitrones are thus the traps of choice in biological radical studies.

There are a variety of nitrone traps commercially available, but the most commonly used are PBN (phenyl-t-butylnitrone) and DMPO (5,5-dimethyl-1-pyrroline-N-oxide) (equation 1-4). Both traps form relatively long-lived,

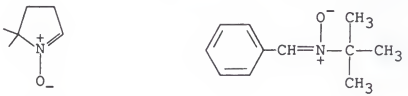

DMPO PBN (1-4)

readily identifiable adducts with superoxide and hydroxyl radicals. DMPO is superior to PBN for identifying radicals and for studies of the hydroxyl radical. The β-H hyperfine

splitting for DMPO spin adducts is more sensitive to the nature of the trapped radical than that of PBN. Thus, with DMPO the identity of unknown radical species can be more easily determined by analysis of the EPR spectrum.[18] The hydroxyl radical adduct of DMPO (DMPO-OH) yields a unique 1:2:2:1 quartet spectrum due to an accidental equality of the nitrogen and hydrogen hyperfine coupling constants ($A_N = A_H$ = 14.77 - 15.3 G).[12] The DMPO-OH EPR spectrum can thus be quickly distinguished from the six line spectra of other DMPO radical adducts.

The hydroxyl radical reacts rapidly with DMPO ($k_{OH\cdot}$ = 3.4 X 10^9 M^{-1} s^{-1}; pH 7.4, 25° C).[19] The resulting spin adduct is believed to decay slowly via disproportionation (equation 1-5)[20]. A first order $t_{½}$ of 2.6 h (pH 7.4 and 25° C)[19] has been reported and is generally accepted for aqueous solutions, but spin adduct decay processes and rates have not been examined extensively

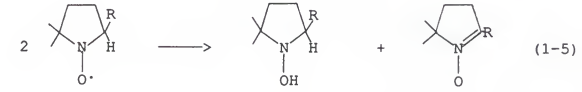

(1-5)

under varying conditions. Decay could conceivably occur by other pathways with varying rates. Dimerization was proposed as a potential decay pathway but was ruled out by Castelhano and coworkers.[20]

Superoxide reacts much more slowly with DMPO than the hydroxyl radical ($k = 10\ M^{-1}s^{-1}$ pH 7.8, 25° C)[19] forming a six line EPR spectrum with $A_N = 14.3$ G and $A_H = 11.7$ G.[21] The superoxide adduct of DMPO is relatively unstable, decaying with a $t_{½}$ of 27 sec at pH 9.0 into DMPO-OH and a non-radical product.[22,23]

Precautions for spin trapping studies

Spin trapping is a powerful research technique for biological radical studies both in vitro and in vivo. Though a large amount of information has been derived from these studies, one must critically evaluate this information to rule out experimental oversights that may lead to inaccurate conclusions. Spin adducts may be observed in the absence of radicals if traps are involved in side reactions. If a short-lived spin adduct is formed, spin adduct production may not be observed even in the presence of radicals.

Several criteria must be met for successful spin-trapping experiments: (1) The spin trap must be inert to all non-radical reagents (or reaction intermediates) in the system. (2) The radical/spin trap reaction should be more rapid than competing reactions. (3) Spin adducts must be long-lived species in order to allow detection. (4) The EPR parameters of spin adducts must be sensitive to the nature of the trapped radical so that radicals can be identified.[24] Reviews by Finkelstein et al.,[25] Buettner,[26] and Janzen[12]

detail experimental precautions and spin-trapping verification techniques as well as helpful information on the application of spin-trapping.

Spin trapping applications

In vivo applications. The spin-trapping technique has been applied in a variety of different biological studies, both in vivo and in vitro. In vivo experiments often involve the injection of a spin trap into the test animal. The animal is then exposed to a potential radical generating stress after which the spin adduct is extracted from the blood, tissues, or organs of interest and analyzed via EPR spectroscopy. This procedure has been used for the determination of free radical formation during carbon tetrachloride metabolism using rats as test animals.[27,28] The in vivo generation of radicals in the brain, spleen and liver of mice during gamma irradiation has been studied.[29] Kubow et al.[30] have studied the in vivo metabolism and resultant free radical formation that occurs upon administration of 3-methylindole. Radical generation following blood reperfusion in dogs has been demonstrated by Bolli et al.[7] Other in vivo experiments may be conducted by including the spin trap in living cell cultures. In vivo radical formation promoted by the anti-cancer drug, adriamycin, was studied in this manner.[31]

Because of the complexity of in vivo systems, critical analysis of experimental techniques and observations is

necessary to determine if biochemical conclusions are valid. It is important that all radical forming reactions other than the one of interest be ruled out. Also, reactions that may result in spin adduct formation in the absence of radicals must be ruled out. A determination of the stability of the radical spin adduct and the trapping rate of the spin trap is also necessary. For in vivo tissue or organ studies and cell culture studies, a determination of the diffusion of spin trap into the tissues, organs or cells must be made. Qualitative in vivo studies demonstrating radical formation are most likely reliable, provided adequate blank samples have been analyzed. However, if no spin adduct is observed, the conclusion that no radicals were formed cannot be assumed without consideration of the above factors.

Quantitative studies of radical formation require very rigorous characterization of the spin adduct production, decay and side reactions to assure that the spin adduct concentration is representative of the radical formation. Conclusions based on the absence of observable spin adduct formation or that depend on quantitative spin adduct measurements should be accepted cautiously.

In vitro applications

In vitro experiments require the same experimental precautions as in vivo experiments. Additionally, in the case of quantitative studies involving radical generation

systems, it is essential to have correct mechanisms and rate constants for both the radical generating reactions and the spin adduct formation reactions. In vitro studies allow careful control of the reaction matrix and can be used to study the effects of in vivo components individually.

In vitro studies usually include the spin trap in a biochemical reaction mixture in order to detect radical formation. Such studies may explore radical production by proteins, enzymes, amino acids, DNA, etc. Radical production of iron-binding proteins have been studied by Sibelle et al.[32] using this approach. Radical formation from DNA- bound iron(II) in the presence of peroxide has also been examined in this manner.[8,33] In many in vitro studies, species of biochemical interest are included in radical generating systems in order to study their reactions with radicals. The lipid peroxidation studies of Lai and Piette[31] and Davies[15] fall into this category. Another example is the study of protein response to radicals generated during photolysis or radiolysis.[34] Often, radical generating systems are used to evaluate potential radical scavengers. Kinetic competition measurements of spin adduct production in the presence and absence of a radical scavenger are used to determine the substrate's scavenging rate and efficiency. Thornallay and Vasak[35] have used this approach to study the radical scavenging ability of the protein metallothionein.

The above examples of *in vitro* and *in vivo* spin-trapping applications illustrate the wide-spread use of the spin-trapping technique in biochemical radical research. Although *in vivo* studies are common, careful *in vitro* work is necessary to validate the observations and conclusions from these studies. *In vitro* characterization of spin trap behavior in the presence of radical generating systems is a valuable approach to understanding *in vivo* spin-trapping results.

Free Radical Generation

Sonolysis, radiolysis, photolysis and chemical or biochemical reactions have been used as free radical sources for *in vitro* experiments. Some common hydroxyl radical generating methods are UV photolysis of H_2O_2,[18,36] sonolysis of aqueous solutions (which generates radicals via cavitation),[37,38] gamma irradiation of N_2O saturated aqueous solutions[39,40] and the reaction of chelated iron complexes with peroxide.[41] The xanthine-xanthine oxidase reaction is also frequently used to generate superoxide radicals.[19,35] Each method has advantages and disadvantages. Photolysis, sonolysis and gamma irradiation are well characterized hydroxyl radical generating systems, are easy to use, and contain no potential substrates for competing reactions. A disadvantage of photolysis is the potential for the biochemical substrate to absorb light at the wavelengths

used, possibly causing unexpected side reactions and decreasing the radical production capacity of the system. In competition experiments, lower radical production could be mistaken for a scavenging effect of a biochemical substrate. Irradiation and sonolysis have the disadvantage of potentially disrupting a biochemical substrate directly so that the true radical reactions cannot be observed.

Certain disadvantages of photolysis, radiolysis and sonolysis may be avoided by using the chelated iron/peroxide reaction to generate hydroxyl radicals. This reaction has the disadvantage of being chemically complex and must be used with great care. However, iron chelate/peroxide reactions are used quite frequently in a variety of spin-trapping and biochemical studies. Though complex, the in vitro reaction of iron and peroxide is a much simpler system and is easier to study than the in vivo reaction.

Since iron and peroxide are believed to be major contributors to in vivo free radical production, an understanding of iron/peroxide reaction in vitro is essential. Spin trapping is an ideal method for probing these reactions, but for quantitative and kinetic competition studies, the manner in which the spin trap enters the reaction mechanism must be determined. The common assumption that radical generating reactions proceed by their accepted mechanisms unaltered by the presence of a

spin trap should be tested. In addition, all the spin-trapping precautions mentioned earlier must be observed.

Although spin traps are frequently used in systems that may contain both iron and peroxide, there is often little characterization of the interaction of the trap and the iron/peroxide reactions.[8,32,42-44] General experimental precautions are usually taken, but these often leave many ambiguities and potential sources of error. The current study addresses this deficiency by a detailed examination of an iron/peroxide reaction in the presence of a spin trap. The $[Fe^{III}EDTA]^{-1}/H_2O_2$ reaction was chosen as a relatively simple reaction for which the kinetics have been previously studied. The findings of the current study show the difficulties encountered with the $[Fe^{III}EDTA]^{-1}/H_2O_2$ reaction mechanism in the presence of the spin trap DMPO. Unexpected spin-trapping problems that could be easily overlooked following the established literature procedures have been identified.

CHAPTER 2
EXPERIMENTAL

Instrumentation and Special Apparatus

Instrumentation

UV analyses were performed on an IBM model 9420 UV-VIS spectrophotometer. EPR spectra were obtained by using a Bruker ER200D-SRC spectrometer equipped with a variable temperature unit, ER 022 signal channel controller, ER 001 time base controller, ER 031M field controller, ER 082 power supply and ER 040XR microwave bridge. Quartz flat cells (Wilmad) were used for all EPR analyses. Quantitative elemental analyses were performed by using a Perkin Elmer PlasmaII inductively coupled plasma spectrometer (ICP) with vacuum UV detection capability.

Thermostatted pH Stat System

All $[Fe^{III}EDTA]^{-1}/H_2O_2$ reactions were performed using a thermostatted pH stat system (Figure 2-1) unless otherwise noted. Temperature control was achieved by using a Haake-F3 thermostatted circulator bath to recirculate water at the desired temperature through a double walled glass reaction vessel. The pH control unit was comprised of a Model 8103

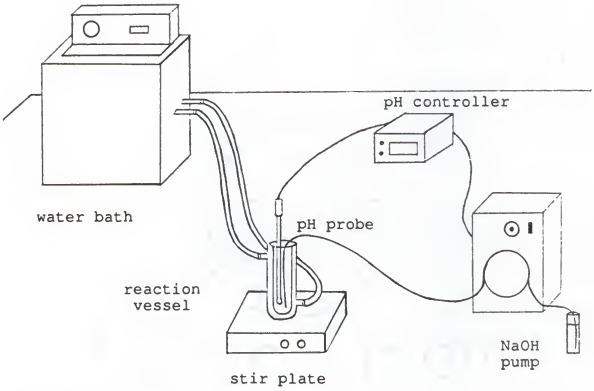

Figure 2-1. Thermostatted pH-stat apparatus.

Ross combination pH electrode coupled to an Omega PHCN-36 pH/ORP controller. The controller functioned to switch on a Buchler multistatic pump which delivered NaOH solution to the reaction mixture as pH dropped below the set point. The use of 0.01" ID Tygon microbore tubing for the base solution allowed precise pH control within 0.10 pH units throughout the reaction. Reactions were stirred continuously by using teflon coated magnetic stir bars and a Sybron-NuovaII stirring plate.

EPR Recirculation System

For EPR experiments, reactions were carried out in the thermostatted pH stat apparatus. Continuous monitoring of these reactions was achieved by recirculating the reaction mixture through a quartz EPR flat cell that remained in the EPR cavity throughout the experiment. The recirculation system consisted of and ISCO, Tris multichannel pump and 0.05" ID Tygon microbore tubing. The reacting solution was thermostatted during recirculation by encasing the recirculation tubing in 0.5" ID Tygon tubing through which circulator bath water was flowed. Further insulation was provided by a foam rubber covering over the entire recirculation system.

The recirculation system presented one drawback when TEMPO (2,2,6,6-tetramethyl-1-piperidinyloxy, free radical) solutions were used. TEMPO concentrations slowly but steadily decreased as they were recirculated. This decrease

did not occur if TEMPO was allowed to remain stationary in the cell after being recirculated. The addition of ethanol to aqueous TEMPO solutions prevented the concentration decrease during recirculation. This effect was attributed to adsorption of TEMPO by the tubing. To avoid this problem TEMPO standards were pumped into the cell, but not recirculated. The short amount of tubing exposure while TEMPO was pumped into the cell did not detectably decrease the TEMPO signal intensity. DMPO-OH did not show accelerated decay during recirculation, so no special measures were necessary for DMPO-OH analyses.

UV Photolysis

A Hanovia low pressure UV lamp was the source for UV photolysis experiments. Solutions were photolyzed in a 1 cm quartz UV cell which was placed about 2 cm from the source.

Gamma Irradiation Apparatus

Gamma irradiation experiments were performed with the assistance of Dr. R. J. Hanrahan using the ^{60}Co source shown in Figure 2-2. The source had a nominal intensity of 600 curies as of May 1988. At a fall off rate of 1% per month the intensity at the time of the experiments was 88% of the original. Samples were held in place 1" from the cobalt source in a specially made circular holder (Figure 2-3) with a depression in the middle for the cobalt rod.

Figure 2-2. ^{60}Co gamma ray source. (A) counterweight; (B) upper support; (C) control rod handle; (D) extra top shielding; (E) storage turret; (F) ^{60}Co rod; (G) shutter, shown open; (H) rear wall; (I) door; (J) downward shielding; (K) door carriage; (L) door crank; (M) door frame.

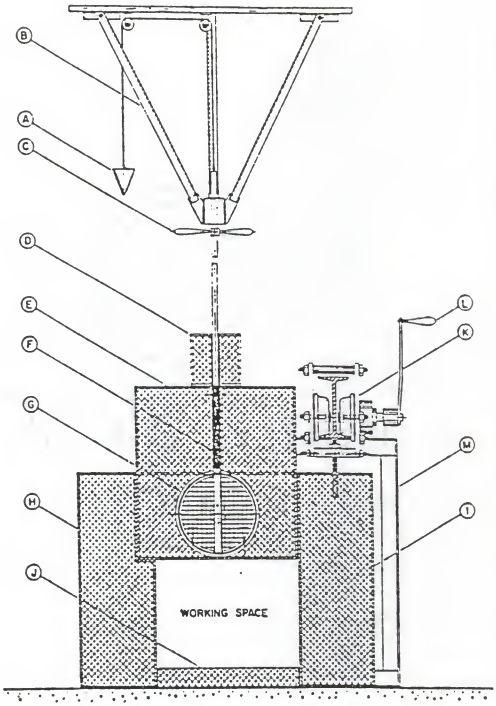
B
A
C
D
E
F
G
H
J
L
K
M
I
WORKING SPACE

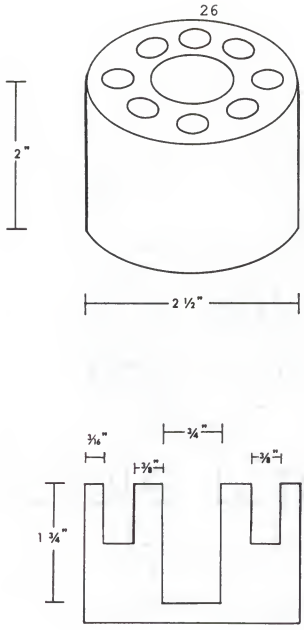

Figure 2-3. Circular cell holder for ^{60}Co experiments.

Removal of Adventitious Metal Ions

Water used for stock solutions, dilutions and cleaning was specially purified by the Barnstead, Nanopure system and then passed through a column of chelating resin (sodium form, dry mesh 50-100, Sigma Chemical Company) to remove all adventitious metal ions. Stock solutions (except for iron, peroxide and EDTA), after preparation using purified water, were treated with small quantities of chelating resin to remove any metal impurities from the reagent solutions.

Glassware was cleaned by rinsing with concentrated nitric acid, followed by purified water. The glassware was then soaked in basic EDTA solution. Prior to use the glassware was rinsed thoroughly with purified water. The EPR recirculating system was cleaned by rinsing with purified water and then recirculating basic EDTA solution. Prior to use the recirculating system was rinsed thoroughly with purified water.

Gilson micropipettors with disposable tips were used to make up reaction mixtures from stock solutions. Sample aliquots were micropipetted from reaction mixtures using a fresh tip for each sample. Samples were collected in disposable centrifuge tubes and covered with parafilm until analysis.

Stock Solution Preparation

General Methods

All stock solutions were prepared with purified water using reagent grade chemicals. The reagents used and stock solution concentrations are all listed in the relevant sections. Spin trap and spin label solutions requiring special storage or purification are described below.

DMPO and Other Spin Trap Solutions

DMPO was purchased from Aldrich or Sigma Chemical Companies. DMPO, a liquid at room temperature, was shipped frozen in sealed vials and was kept frozen prior to use to prevent degradation. Stock solutions of DMPO (FW = 113.16 g) were prepared by dissolving the entire contents of a 1 g vial in about 16 mL of purified water to form a solution of about 0.6 M DMPO. The solution was then purified by filtering through activated charcoal followed by treatment with chelating resin.

The concentration of DMPO solutions was determined by UV spectroscopy. A 1:1000 dilution of a DMPO solution was made in 95% ethanol and the concentration was calculated from the absorbance at 234 nm (ε_{234} = 7700 l/cm mole in 95% ethanol).[45] DMPO stock solutions were stored frozen and were tested periodically for changes in concentration and spurious EPR signals.

Other spin traps used were solids at room temperature. Solutions of these traps were prepared by dissolving known weights of solid in purified water. These solutions were not further purified and were stored frozen.

TEMPO Solutions

TEMPO solutions were used as standards for the EPR determination of DMPO-OH concentration. TEMPO, an orange solid at room temperature, was stored in the freezer to prevent degradation. TEMPO solutions were made by dissolving the solid in purified water and ranged in concentration from 10^{-7} to 10^{-3} M. TEMPO standards were stored in the refrigerator. Fresh solutions were made every two or three days even though EPR signal intensity remained constant for standards stored for 2 weeks or longer.

Analytical Methods

Peroxide Titration[46]

Stock solutions. Stock solutions for peroxide titrations were 3% ammonium molybdate solution, concentrated sulfuric acid diluted 1:5, 0.002 to 0.10 M (depending on peroxide concentration range) sodium thiosulfate solution. Starch solution was made by gently heating 2 or 3 g of starch in 100 mL of water until the solution was clear. Solid potassium iodide was used as purchased.

Procedure. One mL of the peroxide containing sample was delivered into 10 mL of the sulfuric acid solution in a 15 mL disposable centrifuge tube. In a 100 mL Erlenmeyer flask 3 g of potassium iodide were dissolved in 10 mL of water and several drops of ammonium molybdate solution were added. The peroxide solution was then added to the flask contents producing an instantaneous deep orange/red color. The centrifuge tube was rinsed into the flask with about 15 mL of water. With continuous magnetic stirring the flask contents were titrated with sodium thiosulfate solution until the solution color was pale yellow. Then 1 mL of starch solution was added turning the solution deep purple, and the titration was continued until the solution was colorless. Two moles of thiosulfate are required to titrate 1 mole of peroxide as shown in equation 2-1.

$$H_2O_2 + 2H^+ + 2I^- \longrightarrow I_2 + 2H_2O$$
$$I_2 + 2S_2O_3^{-2} \longrightarrow 2I^- + S_4O_6^{-2} \qquad (2\text{-}1)$$

Thiosulfate standardization.[46] A 9.29 X 10^{-3} M solution of potassium iodate was prepared as a primary standard solution. One mL of this solution was added to a flask containing 2 g of potassium iodide dissolved in 10 mL of 0.5 M sulfuric acid. The contents of the flask were titrated with thiosulfate solution until no orange/yellow color remained. Thiosulfate concentration was calculated based on reaction 2-2.

$$IO_3^- + 5I^- + 6H^+ \longrightarrow 3I_2 + 3\ H_2O$$
$$I_2 + 2S_2O_3^{-2} \longrightarrow 2I^- + S_4O_6^{-2} \qquad (2\text{-}2)$$

Quantification of EPR Spectra

EPR spectral peak areas were used to determine spin adduct concentration. Peak areas were calculated using the double integration formula 2-3 where P is the peak to peak separation and H is the peak height.[47] TEMPO solutions of

$$\text{Peak Area} = (2\pi)^{\frac{1}{2}}\ (e^{\frac{1}{2}})\ (\tfrac{1}{2}P)^2\ H \qquad (2\text{-}3)$$

known concentration were used as standards to generate calibration curves.

The EPR was set up to record only the second peak of the DMPO-OH spectrum. The spectrum was expanded to allow more accurate area determinations. Likewise a single peak of the three peak TEMPO standard spectrum was measured. The second DMPO-OH peak has a 1:1 spin correspondence to any one of the TEMPO peaks allowing direct area/concentration comparisons.

Iron(II)/Cysteine Reaction[48]

Stock Solutions

Solid cysteine (Sigma Chemical Company) was dissolved in water to make a 2.05 X 10^{-3} M cysteine solution. Cysteine solution concentration was confirmed by ICP analysis for sulfur concentration. A 3.8 X 10^{-3} M iron(II)

solution was prepared by dissolving ferrous ammonium sulfate in nitrogen purged water immediately prior to use. A 0.18 M DMPO stock solution was prepared as previously described. Phosphate buffer solution (pH 7.8, μ 0.2) was used to maintain pH at 7.8.

Procedure

The reaction mixture was made up of phosphate buffer solution and appropriate volumes of stock solutions to yield a 2 mL reaction volume with 0.054 M DMPO, 125 µl cysteine and 12.5 µl iron(II). Components were added in the order listed with reaction initiation occurring upon addition of the iron(II). The reaction was carried out at ambient temperature. An aliquot of the reacting solution was immediately transferred to an EPR flat cell for analysis.

Iron-imidazole/Peroxide Reaction

Stock Solutions

A 0.13 M DMPO solution was prepared in pH 7.8, μ 0.2 phosphate buffer. Peroxide was used undiluted as purchased (30%). Peroxide concentration was determined by titration to be 9.84 M. A 2.90 M solution of pentacyanoiron(III)-imidazole ($[Fe(CN)_5IM]^{-2}$) was prepared as described below.[49] The $[Fe(CN)_5IM]^{-2}$ concentration was determined by UV absorbance at 402 nm ($\varepsilon_{402} = 1.163 \times 10^3$ l/mole cm).[49]

$[Fe(CN)_5IM]^{-2}$ (iron-imidazole) Preparation

Solid imidzole (0.60421 g, 8.9 X 10^{-3} moles) (Sigma Chemical Company) was dissolved in 15 mL of purified water. Pentacyanoamine-ferroateammonium disodium salt penta hydrate ($Na_2NH_4[Fe(CN)_5NH_3]\cdot 5H_2O$) (0.30144 g, 8.4 X 10^{-4} moles) was added slowly with stirring to the imidazole solution and allowed to react for 15 minutes. Concentrated hydrochloric acid was then added slowly to adjust the pH to 8 or 9. In a dark area and using foil to prevent light exposure 10 mL of 1 M hydrogen peroxide were added slowly with stirring while the pH was maintained at 8 or 9. The solution was allowed to stir for 1 hour with no light exposure. Still excluding light, a small amount of dry AG 3-X4A anion exchange resin (Biorad) was added and stirring was maintained until the dark red color of the solution had greatly diminished. More resin was added as necessary to reduce solution color. At this point working under normal light, the resin was filtered out and rinsed with purified water. The product was eluted from the resin by rinsing with 100 mL of 4 M potassium chloride solution. Imidazole (0.61757 g, 9.1 X 10^{-3} moles) was added immediately to the eluted product solution. The $[Fe(CN)_5IM]^{-2}$ solution was stored at 4° C in a foil covered flask and was used within a day or two of preparation.

Procedure

Using the stock solutions $[Fe(CN)_5IM]^{-2}$, DMPO and peroxide solutions were mixed in order to form a 2 mL reaction solution. Component concentrations were 7.13×10^{-4} M $[Fe(CN)_5IM]^{-2}$, 0.099 M DMPO and 0.160 M peroxide. The solution pH was maintained at 7.8 by the phosphate buffer in which DMPO was prepared. Reaction initiation occurred upon the addition of peroxide. A sample was transferred to an EPR flat cell for analysis immediately following initiation. The reaction was performed at ambient temperature.

$[Fe^{III}DCYTA]^{-1}$/Peroxide Reaction

Stock Solutions

Fifty mL of the iron(III)-DCYTA (trans,1,2-diaminocyclohexane-N,N,N',N'-tetraacetic acid hydrate) chelate complex was prepared as follows. DCYTA (0.06936 g, 2.0×10^{-4} moles) was dissolved in 50 mL of pH 7.8, μ 0.2 phosphate buffer. Ferric ammonium sulfate ($Fe(III)NH_4(SO_4)_2 \ 12H_2O$) (0.09829 g, 2.0×10^{-4} moles) was added to the DCYTA solution with stirring. The solution clouded upon iron addition and was heated gently with stirring for about 2 hours after which any remaining solid was filtered out. Concentration of the iron(III)-DCYTA solution was determined by ICP elemental iron analysis to be

2.13×10^{-3} M. The same DMPO and peroxide stock solutions that were used for the $[Fe(CN)_5IM]^{-2}$ reaction were used for the iron(III)-DCYTA/peroxide reaction.

Procedure

Phosphate buffer, 0.054 M DMPO, 2.0×10^{-4} M iron(III)-DCYTA and 1.35 M peroxide were combined in order for a total reaction volume of 1.8 mL. The solution was buffered at pH 7.8, μ 0.2. The reaction was initiated upon addition of peroxide. A sample was transferred to the EPR flat cell for EPR analysis immediately following initiation. The reaction was carried out at ambient temperature.

$[Fe^{III}EDTA]^{-1}$/Peroxide Reaction

Stock Solutions

Stock solutions for the $[Fe^{III}EDTA]^{-1}/H_2O_2$ reaction were 0.997 M sodium perchlorate, 7.45×10^{-2} M iron(III) perchlorate (concentration determined by ICP iron analysis) and 0.100 M EDTA (from the disodium salt of EDTA). Peroxide was used as purchased (30%). Peroxide concentration was determined by titration prior to use. DMPO solutions were prepared, purified and stored as described previously. The concentration of DMPO stock solutions was typically around 0.65 M. Organic substrates were used as purchased without further purification. Protein solutions were prepared when

necessary by dissolving freeze dried protein (Sigma Chemical Company) in phosphate buffer solutions of the desired pH.

Procedure

The standard reaction mixture was composed of 1.55×10^{-3} EDTA, 1.20×10^{-3} iron(III) perchlorate, 0.42 M sodium perchlorate (to adjust ionic strength to 0.43) and 1.52×10^{-2} M peroxide. DMPO or acetone were included in the reaction mixture as necessary. Concentrations of these substrates varied according to the experiment but were typically in the range of 0.01 to 0.10 M.

These reactions were carried out in the thermostatted pH-stat system. The pH was adjusted and maintained by using 1 M sodium hydroxide solution. The pH values used for these experiments ranged from 7 to 9. The order of components and sodium hydroxide addition was crucial to prevent iron precipitation. Purified water (to provide desired reaction mixture volume of 5 to 8 mL), sodium perchlorate and EDTA solutions were added first directly into the thermostatted reaction vessel. The pH stat was then turned on, and pH was adjusted slowly with continuous stirring. The pH stat system was left on as iron solution was added to the reaction vessel. Iron was added slowly and the pH adjusted continuously so that the pH did not fall below 6 or 7. The solution was allowed to stir for a few minutes following iron addition to equilibrate. The DMPO or the organic substrate was then added and after complete mixing, the

reaction was initiated by the addition of peroxide. A 0.2 to 0.3 pH drop occurred upon peroxide addition. The reaction time was started when the desired pH was reestablished (usually less than 30 s after adding the peroxide). The first analysis was taken immediately after the timer was started. Reactions were monitored by following either the change in peroxide concentration or the formation of DMPO-OH spin adduct as described below.

Peroxide decomposition. To follow peroxide decomposition 1 mL aliquots were taken from the reaction mixture at regular time intervals as the reaction progressed. The aliquots were immediately added to 10 mL of 1:5 diluted sulfuric acid solution in order to quench the reaction. The solution was then titrated iodometrically to determine the peroxide concentration. Titrations were usually performed within 30 minutes after taking the sample, but samples that were stored overnight at 4° C before analysis provided acceptable results.

EPR detection of DMPO-OH. Recirculation of the reacting mixture through the EPR flat cell allowed the spin adduct signal to be monitored as the reaction progressed. Recirculation was started after the reaction was initiated and had reached the proper pH. The first sample spectrum was usually taken about 1 minute after the reaction was initiated and spectra were taken at regular time intervals. To reduce instrumental error the flat cell was placed in the

EPR cavity and attached to the recirculation system prior to a reaction. The instrument was tuned using TEMPO standard solutions. The instrumental setting were left unchanged and the cell was not moved during the course of the experiment.

DMPO-OH Decay Experiments

Decay rates for DMPO-OH were determined under various conditions. DMPO-OH for decay rate experiments was generated by UV photolysis of DMPO or DMPO/peroxide solutions. For DMPO photolysis, 1 mL of approximately 0.4 M DMPO solution was placed in a 1 cm quartz cuvette and exposed to the UV light for about 1 hour. After irradiation the contents of the cuvette were added to the desired reaction component mixture in the thermostatted, pH stat reaction vessel and circulated through the EPR cell. The total volume (including the DMPO solution) in the reaction vessel was usually 8 mL. EPR spectra were taken at regular time intervals and quantified as described previously. No difference was noted in decay rates of solutions that were continuously recirculated and those that were not recirculated. The typical initial DMPO-OH concentration in the recirculating mixture was on the order of 3×10^{-6} M. For DMPO/peroxide photolysis, the procedure was the same. The photolysis solution contained 0.08 M DMPO and 0.03 M

peroxide (1 mL total volume) and only 10 to 15 minutes exposure time was required to generate a 1 X 10^{-5} M DMPO-OH solution.

Spin Trap Competition Experiments

Gamma Radiolysis

Stock solutions. Four different spin trap solutions were prepared in purified water and stored frozen until use. The solutions were 0.490 M DMPO, 0.153 M PBN, 0.420 M TMPO (3,3,5,5-tetramethylpyrroline-N-oxide) and 0.510 M 4-POBN (α-(4-pyridyl-1-oxide)-N-tert-butylnitrone).

Procedure. Solutions (0.5 mL total volume) containing 10 mM each of two different spin traps or 10 mM of a single spin trap buffered at pH 7.0 with 80 mM phosphate buffer were prepared in 7 X 75 mm glass test tubes. The test tubes were capped with rubber septa and purged with N_2O for 20 minutes prior to gamma irradiation. The holder containing the test tubes was then placed in the irradiation chamber and the ^{60}Co rod was lowered into the center of the holder. Solutions were exposed to the ^{60}Co source for 20 minutes. The solutions were frozen in liquid nitrogen immediately upon removal from the irradiation chamber. Samples remained frozen until just before EPR analysis. They were then thawed rapidly and immediately placed in the EPR for analysis.

$[Fe^{II}EDTA]^{-2}/H_2O_2$ Reaction

Stock solutions. POBN and DMPO spin trap solutions used in this experiment were the same as those used in the gamma radiolysis experiments. EDTA solution (1×10^{-2} M) was prepared in 30 mM, pH 8.0 phosphate buffer. Twenty mL of this solution was purged with nitrogen. Ferrous ammonium sulfate (1.03×10^{-4} moles) was placed into a nitrogen purged 10 mL volumetric flask. Phosphate buffer/EDTA solution was transferred via syringe into the volumetric flask. Continuous nitrogen purge was maintained and the flask contents were heated gently and stirred until all solid was dissolved. The solution was kept under a nitrogen atmosphere until use, and no oxidized iron was observed. The $[Fe^{II}EDTA]^{-2}$ stock solution concentration was 1×10^{-2} M.

Procedure. The reaction mixtures had a total volume of 0.5 mL and contained 10 mM of either 4-POBN or DMPO or 10 mM of each. The $[Fe^{II}EDTA]^{-2}$ and H_2O_2 concentrations were both 1 mM. Twenty-six mM phosphate buffer was used to control pH to 8.0. The reactions were carried out at room temperature. The spin trap solutions and the peroxide were mixed and purged with nitrogen. The reaction was then initiated by the addition of $[Fe^{II}EDTA]^{-2}$ and the nitrogen purge was continued for about 20 seconds to allow complete mixing and reaction to occur. The reaction solution was then frozen in

liquid nitrogen and later analyzed by EPR as described for the gamma radiolysis experiments.

Protein Experiments

Bovine Serum Albumin

Freeze dried bovine serum albumin (BSA) was purchased from Sigma Chemical Company. Stock solutions of BSA were prepared by dissolving a known weight of solid protein in pH 7.8, μ 0.2 phosphate buffer. BSA solutions were used without further purification and were stored at 4° C. Peroxide decomposition was studied in the $[Fe^{III}EDTA]^{-1}/H_2O_2$ reaction at pH 9.0 and 30° C using BSA as an organic substrate following the procedure as previously described.

Metallothionein

Rat liver metallothionein was purchased from Sigma Chemical Company or donated by Dr. John Bell or Dr. Robert Cousins. The protein was purified, when necessary, by ion exchange chromatography using DEAE Sephacel ion exchange resin (Sigma). The protein sample was loaded onto the column and rinsed with 50 mL of 0.01 M Tris-HCl (Sigma) pH 7.8 buffer solution, followed by a 400 mL gradient of 0 to 0.15 M KCl in 0.01 M Tris-HCl (pH 7.8) buffer solution. The protein fractions (identified by UV absorption at 209 nm) were pooled and concentrated. The monomeric protein was then collected by passing the protein solution through a

Sephadex G-75 (Sigma) gel permeation column using pH 7.8, μ 0.2 phosphate buffer as the mobile phase. Metallothionein eluted at an apparent molecular weight of 10,000 g. Metallothionein concentration was determined by ICP analysis for sulfur (21 S atoms per mole of metallothionein). Metallothionein solutions were stored at 4° C.

In preliminary $[Fe^{III}EDTA]^{-1}/H_2O_2$ spin-trapping studies, the protein metallothionein was included in the reaction mixture. The reaction mixture used for these studies contained 1.6 X 10^{-4} M $[Fe^{III}EDTA]^{-1}$, 1.3 M H_2O_2, 0.06 M DMPO and either 12 μM metallothionein or 12 μM ethanol in pH 7.8, μ 0.2 phosphate buffered solution. These reactions were performed at room temperature. The reaction was initiated by the addition of H_2O_2 and DMPO-OH production was monitored by EPR (the first DMPO spectrum was obtained within 30 s of the initiation). The DMPO-OH formation was followed for the first five minutes of the reaction.

Kinetic Simulations

Computer simulations of kinetic mechanisms were performed by using a program provided by Dr. R. J. Hanrahan. This program analyzes the kinetics of a reaction mechanism by numerical integration of simultaneous differential equations. The program is capable of handling mechanisms of up to 16 first or second order elementary reaction steps and can be run on any PC with a math coprocessor. A description

of the program input, output and parameters for use are included in Appendix A.

CHAPTER 3
RESULTS

Introduction

Unless otherwise noted the peroxide decomposition and EPR spin-trapping experiments involving the reaction of $[Fe^{III}EDTA]^{-1}$ with H_2O_2 included in this section use reactant concentrations taken from the work of Walling et al.[41] These concentrations are 1.2 X 10^{-3} M $Fe(ClO_4)_3$, 1.5 X 10^{-3} M Na_2EDTA, 1.5 X 10^{-2} M H_2O_2 and $NaClO_4$ solution to adjust the ionic strength to 0.43. The reactions were carried out as described in the experimental section.

Errors are expressed where appropriate as ± one standard deviation and are relative, not absolute, errors. Data from precision experiments are also presented in this section. The errors generated from these measurements represent the overall instrumental and technique errors. This precision error is not factored into the relative error values that are presented but should be kept in mind when using the experimental numbers.

Radical Generating Reactions

Several reactions were explored for their potential as radical generating systems. These reactions, with the exception of the $[Fe^{III}EDTA]^{-1}/H_2O_2$ reaction, were carried out in test tubes at ambient temperature using phosphate buffer for pH control. EPR spectra of each reaction mixture were recorded as soon as possible after initiation (< 5 minutes).

Iron/Cysteine

Hydroxyl radical generation was attempted using the reaction of cysteine with iron(II).[48] Cysteine solution (1.25×10^{-4} M) was mixed with 1.25×10^{-5} M ferrous ammonium sulfate in the presence of 0.054 M DMPO. The solution was buffered at pH 7.8 with phosphate buffer (μ 0.2). The resulting EPR spectrum is shown in Figure 3-1 (B). The spectral lines of the hydroxyl radical ($A_N = A_H = 15$ G),[12] adduct were not observed, and the radical species responsible for the EPR signal was not identified.

Pentacyano(Imidazole) Iron(III)/Peroxide

Pentacyano(imidazole) Iron(III) was allowed to react with peroxide in an attempt to generate hydroxyl radicals.[43] $[Fe(CN)_5(imidazole)]^{-2}$ solution (7.1×10^{-4} M) was mixed with 0.16 M H_2O_2 in the presence of 0.0994 M DMPO. The

Figure 3-1. EPR spectra from different radical generating reactions using the spin trap DMPO.
A. Pentacyano(imidazole) iron(III)/H_2O_2
B. Iron(II)/Cysteine
C. $[Fe^{III}_{DCYTA}]^{-1}/H_2O_2$
D. $[Fe^{III}_{EDTA}]^{-1}/H_2O_2$.

EPR Parameters:
Sweep Width = 200 G_{pp}; Sweep Time = 200 s; Mid Range = 3450 G; Power = 10 dB
Frequency = 9.73 GHz

Gain: A,B = 4.0×10^5
C = 8.0×10^4
D = 1.6×10^5.

Modulation: A,C = 2.5×10^{-1} G_{pp}
B,D = 1.6×10^{-1} G_{pp}.

Time Constant: A = 500 ms
B = 1000 ms
C = 50 ms
D = 100 ms

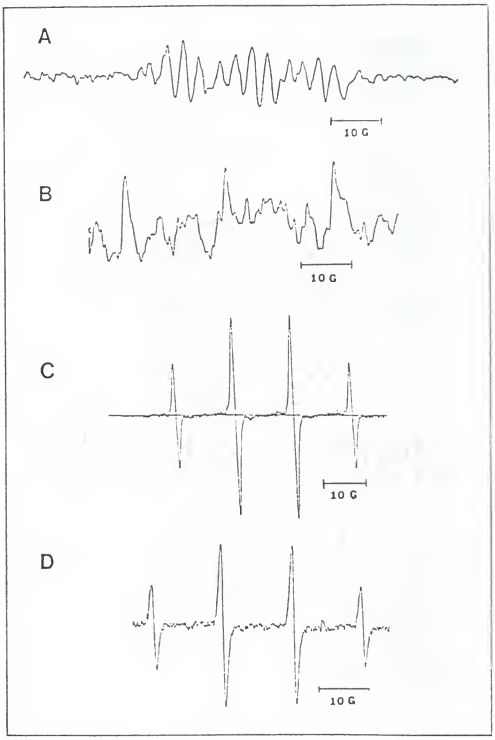
A
10 G
B
10 G
C
10 G
D
10 G

solution was buffered at pH 7.8 with phosphate buffer (μ 0.2). The resulting EPR spectrum is shown in Figure 3-1 (A). The DMPO-OH signal was not observed in this spectrum, and the radical adducts responsible for this spectrum were not identified.

$[Fe^{III}DCYTA]^{-1}/H_2O_2$

The DMPO-OH adduct was successfully generated by the reaction of the iron chelate of trans,1,2-Diamino-cyclohexane-N,N,N',N'-tetraacetic acid hydrate (DCYTA) with peroxide. The DMPO-OH spectrum ($A_N = A_H = 15$ G)[12] resulting from this reaction is shown in Figure 3-1 (C). The reaction was carried out in phosphate buffered solution at pH 7.8, μ 0.2 and 0.054 M DMPO was included in the reaction mixture of 2.0×10^{-4} M $[Fe^{III}DCYTA]^{-1}$ and 1.35 M H_2O_2.

$[Fe^{III}EDTA]^{-1}/H_2O_2$

The DMPO-OH adduct was also successfully generated by the $[Fe^{III}EDTA]^{-1}/H_2O_2$ reaction. The reaction mixture contained 1.2×10^{-3} M $[Fe^{III}EDTA]^{-1}$, 1.5×10^{-2} M H_2O_2 and 0.05 to 0.10 M DMPO. The reaction pH was maintained at either 7.8 or 9.0 by the pH stat system that was previously described. The resulting DMPO-OH spectral parameters were the same at both pH values, and the pH 9.0 spectrum is shown in Figure 3-1 (D).

Replication Experiments

Organic Substrate Effects

Standard experimental procedures were established and validated by replication of the Walling et al.[41] experiment using the thermostatted pH stat apparatus. Replication experiments were done under the experimental conditions of Walling et al.[41] in the high pH $[Fe^{III}EDTA]^{-1}/H_2O_2$ studies where acetone was used as the organic substrate. In reproducing the published experiments, peroxide decomposition was monitored in the presence of various concentrations of acetone at pH 9.0 and 30° C. Peroxide decomposition was found to be first order in peroxide, and first order rate constants (k_{1st}) were obtained from log plots of the data. Figure 3-2 shows representative replication plots of peroxide decomposition in the presence of different acetone concentrations. The data for all replication trials are shown in Table 3-1. Based on the simplified rate law presented by Walling et al.[41] (equation D-20) pseudo second order (k_{2nd}) rate constants were obtained by dividing k_{1st} by the $[Fe^{III}EDTA]^{-1}$ concentration. Walling et al.[41] presented the results for various organic substrate concentrations in a plot of k_{2nd} versus 1/RH with a y intercept of 0.294 and a slope of 0.0180. Replication experiments (Figure 3-3) showed reasonable agreement with the work of Walling et al.[41] Peroxide decomposition rate constant values decreased as

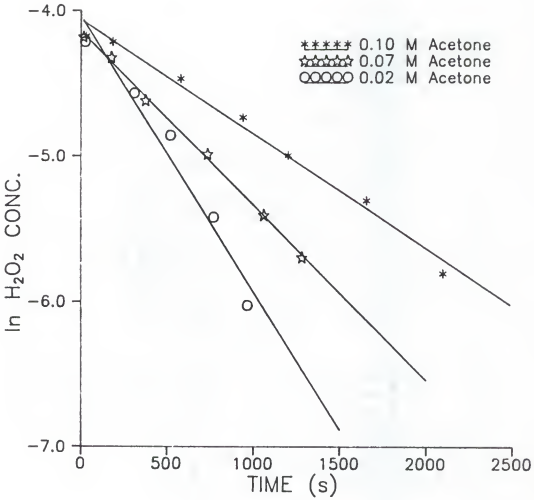

Figure 3-2. Representative plots of peroxide decomposition in the presence of various acetone concentrations.

Table 3-1. Peroxide decomposition as a function of acetone concentration. Data from replication experiments. T = 30° C.

Acetone (M)	Time (s)	$[H_2O_2]$ X 10^2
0.10	32	1.54
	187	1.48
	581	1.15
	941	0.88
	1203	0.67
	1656	0.49
	2098	0.30
0.07	15	1.53
	177	1.33
	375	0.99
	735	0.68
	1061	0.45
	1282	0.34
0.05	19	1.59
	207	1.28
	462	0.90
	633	0.69
	883	0.46
	1093	0.31
	1323	0.26
0.04	15	1.27
	300	0.95
	417	0.80
	552	0.66
	710	0.51
	946	0.37
0.02	25	1.48
	310	1.04
	519	0.77
	770	0.44
	966	0.24

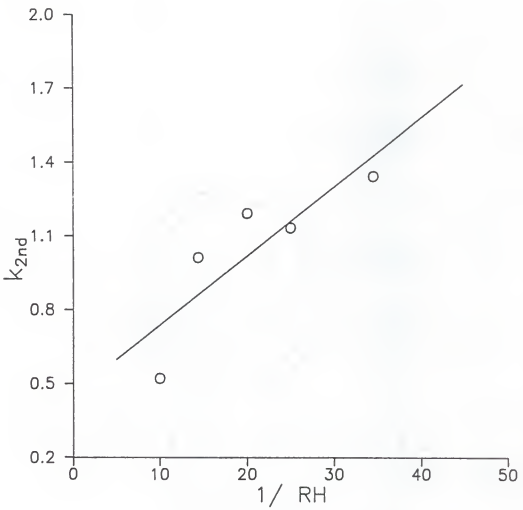

Figure 3-3. Dependence of k_{2nd} on organic substrate concentration in the $[Fe^{III}EDTA]^{-1}/H_2O_2$ reaction. Replication experiments. pH 9.0, 30° C.

acetone concentration was increased (Table 3-2), and a plot of k_{2nd} vs 1/RH yielded a y intercept of 0.450 ± 0.194 with a slope of 0.0281 ± 0.0099.

pH Effects

Walling et al.[41] observed that the rate of peroxide decomposition was inversely dependent on $[H^+]$. A factor of 10 decrease in the rate was reported when pH was lowered from 9.0 to 7.7. Peroxide decomposition data from replication of the 30° C, 0.10 M acetone experiment at different pH values again show reasonable agreement with the Walling et al.[41] results. A decrease in k_{obs} from 0.50 to 0.075 $M^{-1}s^{-1}$ resulted as pH was lowered from 9.0 to 7.6. Replication data for peroxide decomposition at different pH values are included in Table 3-3 and plotted in Figure 3-4. The values of k_{1st} and k_{2nd} for each pH are shown in Table 3-4.

Precision Measurements

The precision of peroxide decomposition rate constant measurements was determined by replication of the pH 9.0 $[Fe^{III}EDTA]^{-1}/H_2O_2$ reaction in the presence of 0.10 M acetone at 30° C. The data from three consecutive identical trials yieled k_{2nd} values of 0.49, 0.46 and 0.54 $M^{-1}s^{-1}$. The mean k_{2nd} = 0.50 ± 0.04 $M^{-1}s^{-1}$, and the measurement error was ±24% at the 95% confidence level.

Table 3-2. First and second order peroxide decomposition rate constants as a function of acetone concentration. Derived from replication experimental data. T = 30° C.

Acetone (M)	k_{1st} (s^{-1})	k_{2nd} ($M^{-1}s^{-1}$)
0.10	7.64×10^{-4}	0.64
0.07	1.21×10^{-3}	1.01
0.05	1.43×10^{-3}	1.19
0.04	1.35×10^{-3}	1.13
0.02	1.61×10^{-3}	1.34

Table 3-3. Replication data for peroxide decomposition as a function of pH. T = 30° C.

pH	Time (s)	$[H_2O_2] \times 10^2$
9.0	17	1.6
	192	1.48
	343	1.35
	605	1.15
	951	0.88
8.7	25	1.57
	292	1.49
	613	1.43
	907	1.36
	1238	1.22
	1544	1.10
	1812	1.08
7.6	20	1.55
	312	1.52
	653	1.47
	955	1.44
	1314	1.38
	2009	1.29
	2728	1.22

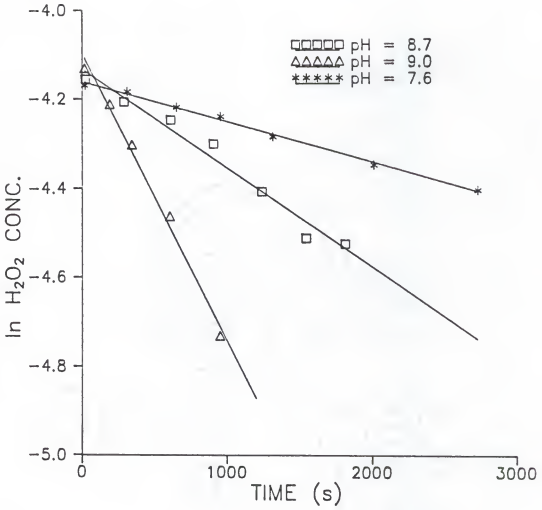

Figure 3-4. Peroxide decomposition as pH was varied in replication experiments.

Table 3-4. First and second order peroxide decomposition rate constants as a function of pH (from replication experiment data). T = 30° C.

pH	k_{1st} (s^{-1})	k_{2nd} ($M^{-1}s^{-1}$)
9.0	6.5×10^{-4}	0.54
8.7	2.2×10^{-4}	0.19
7.6	9.0×10^{-5}	0.075

Substrate and Buffer Effects on the $[Fe^{III}EDTA]^{-1}/H_2O_2$ Reaction

DMPO Effect

The rate of peroxide decomposition is significantly decreased by the inclusion of DMPO in the $[Fe^{III}EDTA]^{-1}/H_2O_2$ reaction mixture. Further, the rate is almost independent of the DMPO concentration used over a range of 0.001 M to 0.10 M. The peroxide decomposition data are presented in Table 3-5. Figure 3-5 shows representative plots of this data compared to the 0.10 M acetone $[Fe^{III}EDTA]^{-1}/H_2O_2$ reaction. k_{1st} and k_{2nd} values for peroxide decomposition in the presence of DMPO are shown in Table 3-6.

Phosphate Buffer Effect

The Walling et al.[41] experiments were done in the absence of buffering agents; however, phosphate buffered solutions are commonly used in studies involving iron chelates. Therefore, peroxide decomposition was studied using solutions containing phosphate buffer. Peroxide decomposition was followed in the $[Fe^{III}EDTA]^{-1}/H_2O_2$ reaction with pH 9.0, 0.10 M acetone, 30° C, in the presence of 33 mM phosphate buffer. The average k_{2nd} over five trials was $0.40 \pm 0.04\ M^{-1}s^{-1}$ which is 20% lower than the corresponding rate in the absence of phosphate buffer. This decrease however, is within the 95% confidence level measurement error.

Table 3-5. Peroxide decomposition data for the $[Fe^{III}EDTA]^{-1}/H_2O_2$ reaction in the presence of DMPO.

[DMPO]	Time (s)	$[H_2O_2]$ X 10^2
0.10	23	1.62
	286	1.57
	889	1.43
	1464	1.41
	2062	1.26
	2684	1.19
	3381	1.12
0.05	17	1.69
	341	1.60
	711	1.54
	1662	1.35
	2166	1.20
	2709	1.12
	3277	1.00
0.025	21	1.99
	379	1.88
	724	1.82
	1209	1.73
	1622	1.66
	2222	1.41
	3006	1.32
0.01	22	1.96
	287	1.91
	827	1.77
	1450	1.71
	2047	1.54
	2648	1.49
	3245	1.39
0.001	17	1.70
	204	1.64
	831	1.48
	1476	1.39
	1995	1.29
	2587	1.20
	3201	1.07

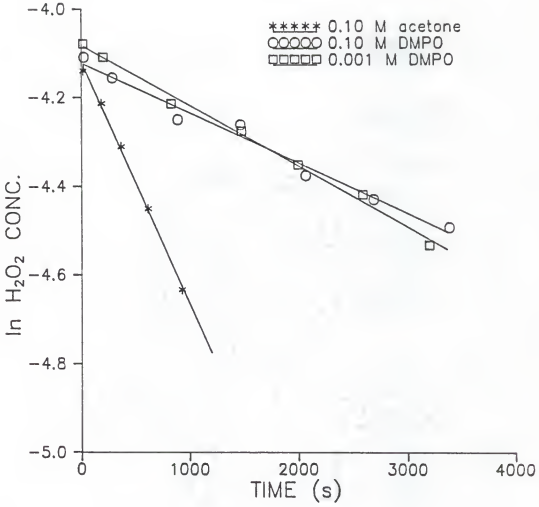

Figure 3-5. Plots of peroxide decomposition data in the $[Fe^{III}EDTA]^{-1}/H_2O_2$ reaction in the presence of DMPO or acetone.

Table 3-6. Experimental k_{1st} and k_{2nd} values from peroxide decomposition experiments in the presence of DMPO.

[DMPO]	k_{1st} (s^{-1})	k_{2nd} ($M^{-1}s^{-1}$)	calc. k_{2nd}* ($M^{-1}s^{-1}$)
0.10	1.13×10^{-4}	0.0945	0.360
0.10	0.79×10^{-4}	0.065	0.360
0.05	1.59×10^{-4}	0.132	0.360
0.05	1.16×10^{-4}	0.097	0.360
0.025	1.42×10^{-4}	0.118	0.361
0.01	1.07×10^{-4}	0.0892	0.362
0.001	1.37×10^{-4}	0.114	0.375

Average $k_{1st} = 1.2 \times 10^{-4}\ s^{-1}$
Average $k_{2nd} = 0.101\ M^{-1}s^{-1}$

* Calculated using the Walling et al.[41] rate law (equation D-19).

Although the reduction in k_{2nd} is statistically insignificant, some effect might be expected as a result of phosphate binding to the iron couple. Constant pH UV titrations of $[Fe^{III}EDTA]^{-1}$ with KH_2PO_4 solution produced small shifts in the λ_{max} of $[Fe^{III}EDTA]^{-1}$ (246.0 nm to 250.8 nm). Some complex formation between phosphate ion and $[Fe^{III}EDTA]^{-1}$ is thus indicated and may account for the consistent rate decrease in the presence of phosphate buffer.

Protein Effect

The effect of a protein as an organic substrate was examined by including the protein bovine serum albumin (BSA) in the $[Fe^{III}EDTA]^{-1}/H_2O_2$. The $[Fe^{III}EDTA]^{-1}/H_2O_2$ reaction was again carried out at pH 9.0 and 30° C with varying concentrations of BSA. All reaction mixtures also included 17 mM phosphate buffer. A blank reaction was run under the same conditions substituting 0.10 M acetone for the BSA. No protein effect was observed in these experiments. The k_{2nd} for the blank reaction was 0.38 $M^{-1}s^{-1}$. With 2.25 mg and 4.45 mg of BSA the k_{2nd} values were 0.38 and 0.32 $M^{-1}s^{-1}$ respectively.

Spin-Trapping Experiments

DMPO in the $[Fe^{III}EDTA]^{-1}/H_2O_2$ Reaction

General observations. The $[Fe^{III}EDTA]^{-1}/H_2O_2$ reaction was studied as described in the peroxide decomposition experiments using the spin trap DMPO instead of an organic substrate. DMPO spin adduct formation was monitored by recirculating the reacting mixture through the EPR cell and taking spectra periodically. DMPO-OH concentrations for these studies were estimated from peak intensity relative to TEMPO standards. The DMPO-OH adduct was cleanly formed in the reaction, and no other adduct signals were noted for the duration of the reaction.

In the $[Fe^{III}EDTA]^{-1}/H_2O_2$ reaction at pH 9.0 and 30° C the DMPO-OH adduct signal was formed, but disappeared completely in about 6 min. The reaction at 30° C was too rapid to be studied effectively with the EPR method used here. All further reactions studied were slowed by reducing the temperature to 20° C.

Figure 3-6 shows DMPO-OH concentration versus time curves in the $[Fe^{III}EDTA]^{-1}/H_2O_2$ reaction at different pH values and DMPO concentrations. In all cases the same behavior was observed: DMPO was formed, reached a maximum, and decayed until no signal could be detected. The time to reach maximum DMPO-OH concentration (t_{max}), the maximum DMPO-OH concentration (C_{max}) and the total decay time (t_{dk})

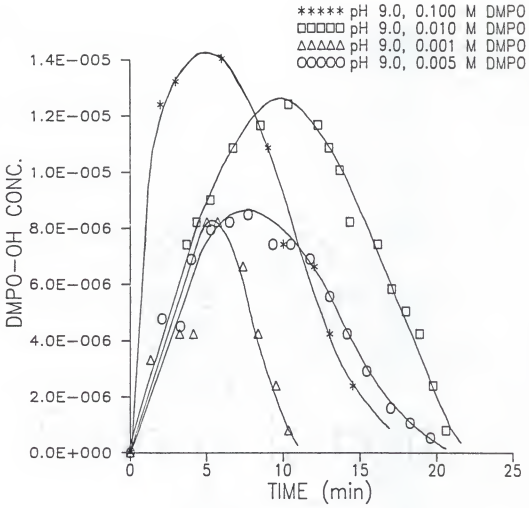

Figure 3-6. [DMPO-OH] versus time curves for the $[Fe^{III}EDTA]^{-1}/H_2O_2$ reaction. 20° C.

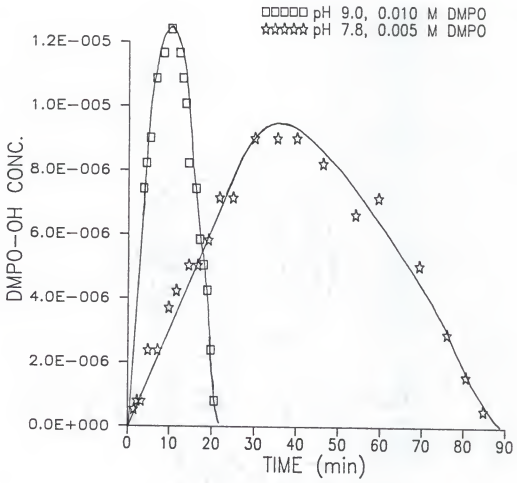

Figure 3-6--continued

were essentially invariant with DMPO concentration at a given pH value. The C_{max} value appeared to be the same at pH 9.0 and 7.8. The average C_{max} value at pH 9.0 was 8×10^{-6} M, and the C_{max} value for the one trial done at pH 7.8 was also 8×10^{-6} M. The t_{dk} and t_{max} values were significantly slower at pH 7.8 than at pH 9.0. Table 3-7 shows t_{dk}, t_{max} and C_{max} data for the different trials where pH and [DMPO] values were varied.

EPR blanks. Blanks of DMPO solution alone and in combination with $[Fe^{III}EDTA]^{-1}$, H_2O_2, or other reaction mixture components were examined in the EPR. No signal formation was noted in any of the blank solutions. Solutions were also allowed to stand at room temperature under normal room lighting conditions for time periods equal to the duration of a typical experiment. No photolytic DMPO-OH production was detected under normal lighting conditions. The results of these blanks indicate that DMPO-OH did not form due to interaction with the reaction mixture components or as result of photolysis or hydrolysis.

Ethanol radical formation. Ethanol and DMPO were included in the $[Fe^{III}EDTA]^{-1}/H_2O_2$ EPR reaction in equal concentrations. Ethanol radicals were formed and trapped in the reaction. The resulting EPR spectrum which was a combination of DMPO-OH and DMPO-ETOH signals is shown in Figure 3-7.

Table 3-7. Data from [DMPO-OH] versus time curves in the $[Fe^{III}EDTA]^{-1}/H_2O_2$ reaction. All reactions were carried out at 20° C.

pH	[DMPO]	t_{max} (min)	t_{dk} (min)	C_{max}*
9.0	0.10	6.0	15.0	1×10^{-5}
	0.010	10.4	20.0	1×10^{-5}
	0.005	7.0	19.5	7×10^{-6}
	0.001	5.0	10.0	7×10^{-6}
7.8	0.005	35.3	85.0	8×10^{-6}

*Concentrations were estimated from peak height relative to known TEMPO standards.

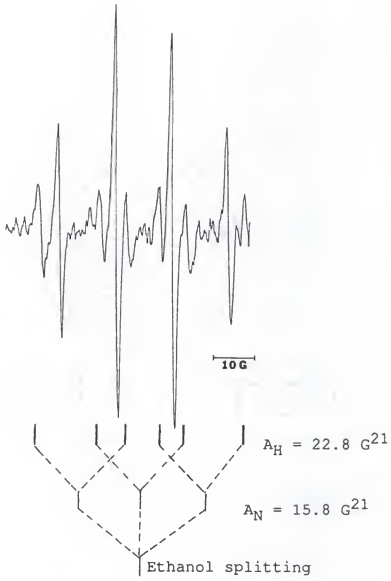

Figure 3-7. EPR spectrum of hydroxyl radical and ethanol radical adducts of DMPO generated during the $[Fe^{III}EDTA]^{-1}/H_2O_2$ reaction.

Protein Effect on the $[Fe^{III}EDTA]^{-1}/H_2O_2$ Reaction

In preliminary $[Fe^{III}EDTA]^{-1}/H_2O_2$ spin-trapping studies, the protein metallothionein was included in the reaction mixture. These studies did not utilize the pH-stat system but were buffered with phosphate buffer. Experimental details are included in chapter 2. The reaction mixture used for these studies contained 1.6×10^{-4} M $[Fe^{III}EDTA]^{-1}$, 1.3 M H_2O_2, 0.06 M DMPO and either 12 μM metallothionein or 12 μM ethanol in pH 7.8, μ 0.2 phosphate buffered solution. Ethanol was chosen for comparison to show the effect of a substrate with a near diffusion rate for reaction with hydroxyl radicals.

Figure 3-8 shows the resulting DMPO-OH concentration versus time plots for these experiments. The effect of ethanol is to decrease the rate of DMPO-OH production as expected. Metallothionein, contrary to prediction, appears to increase the rate of DMPO-OH production.

DMPO-OH Decay Experiments

The DMPO-OH decay rate was determined by following the change in EPR signal with time in both recirculating and non-recirculating experiments. DMPO-OH was generated photolytically as described in the experimental section, and initial DMPO-OH concentrations were on the order of 10^{-6} M. DMPO-OH concentrations for these experiments were determined by double integration of the EPR signal relative to TEMPO standards. The error in concentration measurements was

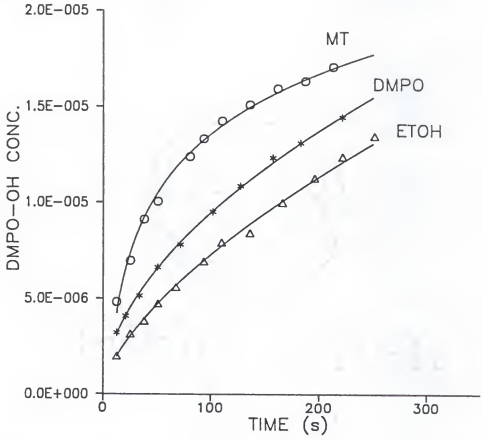

Figure 3-8. The effect of metallothionein on DMPO-OH production in the $[Fe^{III}_{EDTA}]^{-1}/H_2O_2$ reaction. pH 7.8, 25° C.

determined by repeated analysis of TEMPO standards during the course of the experiments. In three separate trials, 3 or 4 replicate samples of different TEMPO standards resulted in an average error of ±25% based on three times the standard deviation for each trial.

DMPO-OH decay rates were determined in the presence of each reaction mixture component at concentrations used in the $[Fe^{III}EDTA]^{-1}/H_2O_2$ reaction. First order decay was observed in all cases. The decay rate was found to be invariant, within experimental error, with pH and ionic strength and was not altered by the presence of any of the reaction components. Figure 3-9 shows representative DMPO-OH decay plots. Decay rates (k_{dk}) for all conditions studied are shown in Table 3-8. The average k_{dk} was $8.6 \pm 2.9 \times 10^{-5}$ $M^{-1}s^{-1}$ yielding an average half-life of 2.3 h.

Though $[Fe^{III}EDTA]^{-1}$ did not accelerate the decay rate the intensity of the DMPO-OH signal decreased instantaneously upon addition of $[Fe^{III}EDTA]^{-1}$. This sudden decrease was attributed to DMPO-OH/$[Fe^{III}EDTA]^{-1}$ complex formation which results in the broadening of the EPR signal via metal/nitroxide coupling interactions.[51-53] The extent of complex formation was determined by titrating DMPO-OH with $[Fe^{III}EDTA]^{-1}$ and measuring the subsequent decrease in EPR signal intensity. The DMPO-OH/$[Fe^{III}EDTA]^{-1}$ binding constant was determined to be 3×10^3 from a Hill plot of

Figure 3-9 DMPO-OH decay plots.
A. 0.43 M $NaClO_4$, pH 6.8
B. 0.43 M $NaClO_4$, pH 7.8
C. 0.43 M $NaClO_4$, 0.0367 M H_2O_2, 33 mM $K_2H_2PO_4$, pH 6.8
D. 0.43 M $NaClO_4$, 0.0152 M H_2O_2 33 mM $K_2H_2PO_4$, pH 9.0

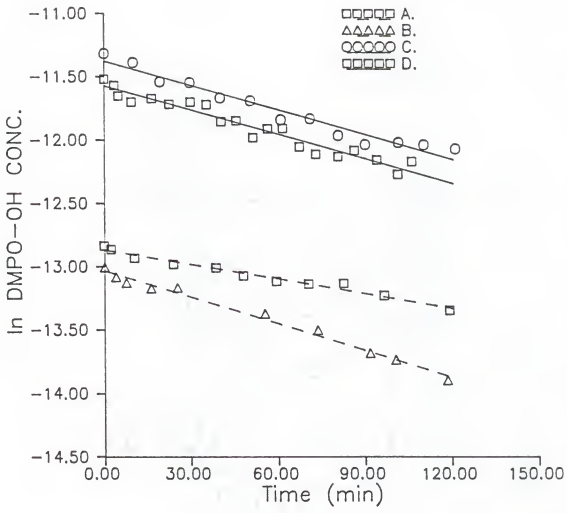
A.
B.
C.
D.
−11.00
−11.50
−12.00
−12.50
−13.00
−13.50
−14.00
−14.50
ln DMPO−OH CONC.
0.00
30.00
60.00
90.00
120.00
150.00
Time (min)

Table 3-8. First order rate constants for DMPO-OH decay under different conditions.

$[DMPO\text{-}OH]_i$	pH	Reaction Mixture	k (s^{-1})*
2.7×10^{-6}	6.8	water	7.0×10^{-5}
2.9×10^{-6}	6.8	water	8.4×10^{-5}
2.7×10^{-6}	6.8	a.	5.8×10^{-5}
2.1×10^{-6}	7.8	a.	1.2×10^{-5}
1.2×10^{-5}	6.8	a,b.	9.6×10^{-5}
5.5×10^{-6}	6.8	a,b,c.	1.1×10^{-4}
1.2×10^{-5}	6.8	a,b,c.	1.1×10^{-4}
1.0×10^{-5}	6.8	a,c,d.	9.4×10^{-5}
6.3×10^{-6}	6.8	a,c,d.	1.2×10^{-4}
8.3×10^{-6}	6.8	a,c,d.	9.3×10^{-5}
2.2×10^{-6}	6.8	a,c,d.	6.2×10^{-5}
1.6×10^{-4}	6.8	a,c,d,(N_2).	1.5×10^{-4}
9.9×10^{-6}	9.0	a,c,d.	1.1×10^{-4}
5.9×10^{-6}	6.8	a,c,e.	6.1×10^{-5}
1.6×10^{-6}	6.8	a,f,g	8.4×10^{-5}

* All reactions were carried out at 20° C.

a. 0.43 M $NaClO_4$ (to adjust ionic strength)
b. 3.67×10^{-2} M H_2O_2
c. 33 mM $K_2H_2PO_4$
d. 1.52×10^{-2} M H_2O_2
e. 3.50×10^{-3} M H_2O_2
f. 1.20×10^{-3} M $Fe(ClO_4)_3$
g. 1.55×10^{-3} M Na_2EDTA

the data. Using the ±25% error limits which were previously determined for EPR concentration measurements, the K_b values at the error limits were calculated to be 4×10^2 and 5×10^4. The K_b value may deviate an order of magnitude from the measured value of 3×10^3. The observed DMPO-OH signal may be 32 to 99% lower than the actual DMPO concentration.

TEMPO Decay

TEMPO is a stable nitroxide radical and shows no decay over several hours in aqueous solutions at room temperature. TEMPO standards stored at 4° C are stable for at least a week. However, TEMPO solutions showed a steady slow decrease in concentration when they were flowing through the EPR recirculation apparatus. This decay ceased when recirculation was stopped. The TEMPO decay effect is thus attributed to TEMPO adsorbing onto the tubing used in the recirculation system. This conclusion is supported by the observation that TEMPO decay does not occur with recirculation if a more appropriate solvent such as ethanol is added to the aqueous solution of TEMPO. Further, no such decay effect is noted with DMPO-OH solutions in the recirculating system.

TEMPO solutions were still useful in examining the behavior of nitroxide radicals in the reacting $[Fe^{II}EDTA]^{-1}/H_2O_2$ system. TEMPO decay was found to be unaffected by the presence of any of the individual reaction

components whether recirculating or not. However, when the reaction was initiated by mixing H_2O_2 and $[Fe^{III}EDTA]^{-1}$ controlling pH to 9.0 and temperature to 20° C, TEMPO decayed rapidly. TEMPO decay was first order with an average rate constant over three trials of $2.67 \pm 0.05 \times 10^{-3}$ s^{-1} and a $t_{½}$ of 4.3 min. TEMPO decay in the recirculating system prior to initiation of the reaction was insignificant and is shown along with the decay data after initiation in Figure 3-10.

Spin Trap Competition Experiments

Gamma radiolysis. EPR spectra of spin trap mixtures exposed to a ^{60}Co source are shown in Figures 3-11 and 3-12. TMPO and PBN yielded complex spectra that did not allow the clear distinction of DMPO and TMPO or PBN spin adduct peaks. TMPO and PBN were thus not used further in the study. 4-POBN produced a spectrum composed of two different spin adducts: a triplet of doublets with A_N = 15.7 G, A_H = 2.4 G and another six line spectrum with A_N = 16.8 G, A_H = 10.3 G. The triplet of doublets was initially thought to be the hydroxyl radical adduct, however, comparison of A_N and A_H values showed that the peaks did not result from the OH· adduct (A_N = 14.95, A_H = 1.68) but were from an unidentified adduct reported by Janzen[54] (A_N = 15.58 - 15.66, A_H = 2.60 - 2.75). The other six line spectrum was attributed to the adduct formed by trapping H (A_N =16.6 G, A_H = 10.25(2) G).[21] DMPO formed a clean DMPO-OH radical spectrum which in some cases included a small amount of the H adduct signal.

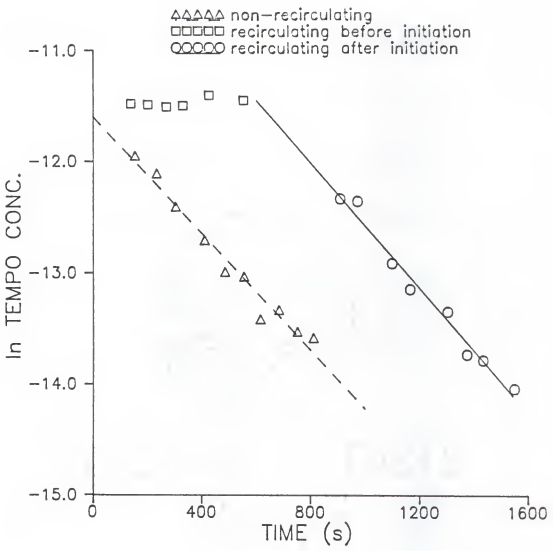

Figure 3-10. TEMPO decay in the $[Fe^{III}EDTA]^{-1}/H_2O_2$ reaction.

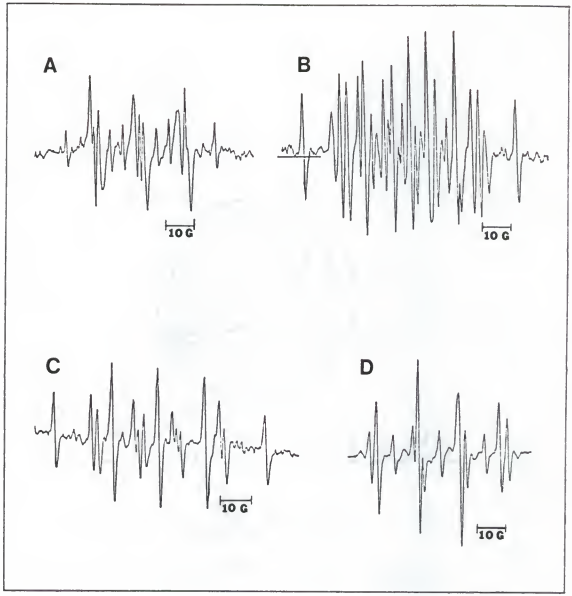

Figure 3-11. Spin adduct formation from radiolysis experiments. A. PBN alone. B. DMPO/PBN mixture. C. TMPO alone. D. DMPO/TMPO mixture.

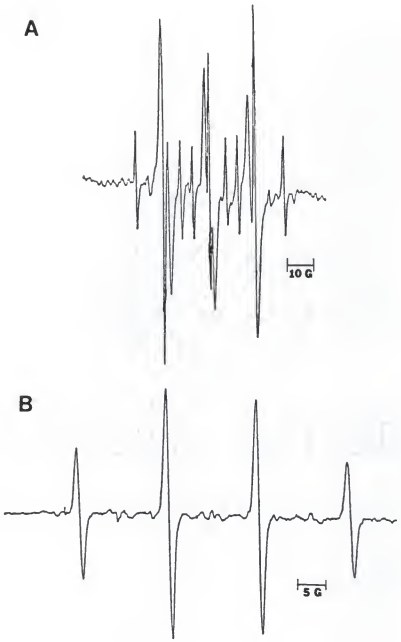

Figure 3-12. Spin adduct formation from radiolysis experiments. A. 4-POBN alone. B. DMPO/ 4-POBN mixture.

When 4-POBN was mixed with DMPO the resulting radical spectrum showed only DMPO-OH peaks. The amount of DMPO-OH formed was so much greater than the 4-POBN adducts that at the decreased gain and modulation necessary to bring DMPO-OH into scale, no 4-POBN adduct signals could be observed.

$[Fe^{II}EDTA]^{-2}/H_2O_2$ reaction. The $[Fe^{II}EDTA]^{-2}/H_2O_2$ reaction was studied at pH 8.0 in the presence of either DMPO, 4-POBN or an equimolar mixture of the two spin traps (0.01 M). In both the mixture and alone, DMPO clearly formed the DMPO-OH spin adduct. 4-POBN alone and in the mixture formed an adduct which produced a six line triplet of doublets spectrum with A_N = 15.7 G and A_H = 3.5 G. This adduct again was not the hydroxyl radical adduct. The spectrum was attributed to the CO_2^- radical adduct which is reported to occur with A_N = 15.5 - 15.8 G and A_H = 3.0 - 3.4 G.[21] Figure 3-13 shows the spectra of 4-POBN alone and mixed with DMPO.

The mixture spectrum shows clearly both DMPO-OH and 4-POBN-CO_2 adducts with no overlapping lines. DMPO-OH and 4-POBN-CO_2 concentrations estimated from peak height relative to standard TEMPO solutions were 1.3 X 10^{-5} and 3.8 X 10^{-5}, respectively. The observed DMPO-OH concentration is lower than the actual DMPO-OH concentration due to complex formation with the 1 mM $[Fe^{III}EDTA]^{-1}$ left at the end of the reaction. Using the binding constant measured for this complex (3 X 10^3), an actual DMPO-OH

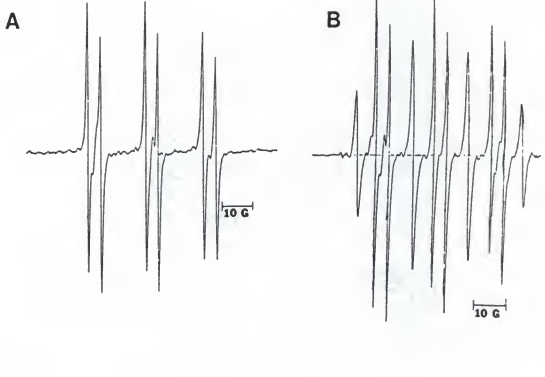

Figure 3-13. Spin adduct formation from the $[Fe^{II}EDTA]^{-2}/H_2O_2$ reaction. A. 4-POBN alone. B. DMPO/4-POBN mixture.

concentration of 5×10^{-5} M is estimated. However, considering the error limits for K_b the actual DMPO-OH concentration could be as low as 2×10^{-5} or as high as 7×10^{-4} M. No complex formation was noted with 4-POBN-CO_2 in the presence of $[Fe^{III}EDTA]^{-1}$, so the observed concentration is assumed to be the actual concentration. This analysis indicates that almost equal concentrations of DMPO-OH and 4-POBN-CO_2 were formed. The CO_2^- adduct of DMPO was not observed in any of the experiments.

4-POBN-CO_2 formation. The CO_2^- radical was assumed to be formed via the degradation of EDTA by the oxidizing intermediate during the $[Fe^{III}EDTA]^{-1}/H_2O_2$ reaction. To confirm that CO_2^- adducts were formed from EDTA, aqueous solutions were sonicated to form hydroxyl radicals in the presence of EDTA and 4-POBN. The 4-POBN-CO_2 adduct was clearly formed in these experiments. Solutions containing no EDTA showed no CO_2^- formation, but did form the unidentified adduct seen in the radiolysis studies. The possibility of CO_2^- forming via reaction of the 4-POBN-OH adduct with EDTA was ruled out by photolyzing 4-POBN solutions in the presence of EDTA. Nitrones form the hydroxyl adduct via photolysis in the absence of hydroxyl radicals.[19] No CO_2^- adduct was observed in the photolyzed solutions, but the unidentified signal noted in radiolysis experiments formed both in the presence and absence of EDTA.

CHAPTER 4
DISCUSSION

Introduction

Study of radical reactions requires a clean radical generating system and a reliable method for quantifying radical production. For biological studies, experimental techniques must be adaptable to aqueous solutions at various pH values. The radical detecting method and the radical generating reaction should not interfere with each other and the radical detection method should be unaffected by all non-radical substances in the reaction medium. Radicals can be detected directly using continuous flow EPR methods, but in protein studies, cost and availability of protein usually make this method impractical. Spin trapping has become the radical detection method of choice since it allows detection and, in some cases, identification of short-lived radical species in aqueous systems at different pH values. Several reviews[12,16,21,25,26,55] detail the potential side reactions and interferences that can occur in spin-trapping studies. Guidelines presented in these reviews are generally followed in spin-trapping studies and are assumed to be sufficient for validation of spin-trapping results. Quantitative

radical studies are generally based on published mechanisms for the radical generating reaction which are assumed to be unchanged by the presence of spin traps. However, little study has been devoted to complete characterization of spin trap behavior in the presence of biological components or in radical generating reactions which might occur in vitro or in vivo.

The $[Fe^{III}EDTA]^{-1}/H_2O_2$ reaction was studied as a potential hydroxyl radical generating system in which radical production could be quantified by the formation of DMPO-OH from the spin trap DMPO. Results of the present study of DMPO spin trapping in the $[Fe^{III}EDTA]^{-1}/H_2O_2$ reaction reveal complications that are not considered in published spin-trapping studies or reviews of the spin-trapping technique. A discussion of these results and a kinetic analysis of spin trapping in the $[Fe^{III}EDTA]^{-1}/H_2O_2$ reaction follows.

Spin-Trapping and the $[Fe^{III}EDTA]^{-1}/H_2O_2$ Reaction

Choice of Radical Generating System

The initial criterion for the successful use of spin traps is the generation of a spin adduct with a clean, clearly identifiable EPR signal. DMPO-OH formation was monitored in several $OH\cdot$ generating reactions shown in Figure 3-1. Iron containing systems were chosen because of the prevalence of iron complexes in vivo and the large

number of in vitro spin-trapping studies conducted in iron containing media. The iron(III)imidazole/peroxide[50] and the iron(II)/cysteine[48] reactions were both reported to form the hydroxyl radical and were thus explored as potential hydroxyl radical generating systems for spin-trapping studies. However, these reactions did not produce identifiable hydroxyl radical adducts of DMPO and were not studied further. A clean DMPO-OH spectrum was produced in the $[Fe^{III}DCYTA]^{-1}$ and $[Fe^{III}EDTA]^{-1}$ reactions with peroxide. DCYTA and EDTA chelates of Fe(III) yielded DMPO-OH signals of equal intensity during the course of the iron/peroxide reaction. Of these two latter reactions, $[Fe^{III}EDTA]^{-1}$ was chosen for further study because EDTA is a more commonly used iron chelate and the $[Fe^{III}EDTA]^{-1}/H_2O_2$ reaction under conditions appropriate for this research had been extensively characterized by Walling and coworkers.[41,56]

$[Fe^{III}EDTA]^{-1}$ and $[Fe^{II}EDTA]^{-2}$ Chemistry

$[Fe^{III}EDTA]^{-1}$ is a heptacoordinate complex with six atoms donated by EDTA and the seventh coordination site occupied by water.[57,58] $[Fe^{III}EDTA]^{-1}$ behaves as a weak acid with a pK_a of 7.6 due to a dissociable proton of the bound water.[58] The complex has an optical absorption at λ_{max} = 256 nm (ε = 9290 $M^{-1}cm^{-1}$) at pH 6.0. As pH increases to 10.7, this absorption shifts to 240 nm (ε = 8800 $M^{-1}cm^{-1}$).[58]

At higher pH values (pH > 8), $[Fe^{III}EDTA]^{-1}$ reacts with H_2O_2 to form a deep purple (λ_{max} 520 nm, ε 528 $M^{-1}cm^{-1}$) iron/peroxide complex ($[Fe^{III}EDTA\text{-}O_2]^{-3}$).[23,57,58] This complex catalyzes the decomposition of H_2O_2 and oxidizes organic substrates.[23]

The $[Fe^{II}EDTA]^{-2}$ structure is thought to be similar to that of $[Fe^{III}EDTA]^{-1}$.[58] Unlike $[Fe^{III}EDTA]^{-1}$, $[Fe^{II}EDTA]^{-2}$ has no optical absorption and shows no acidic character.[58]

Critical Observations

In the present study the following critical observations of the $[Fe^{III}EDTA]^{-1}/H_2O_2$ reaction in the presence of DMPO were made: (1) A clearly identifiable DMPO-OH adduct was produced. (2) Under all conditions, simultaneous production and rapid decomposition of DMPO-OH was observed in the reaction. (3) The spin label TEMPO, which is normally stable for weeks, decayed rapidly when included in the reaction. The decay was first order with a rate constant of 1×10^{-3} s^{-1}. (4) The rate of DMPO-OH or TEMPO decay was not accelerated by any components of the reaction mixture in any combination other than the full reaction conditions. Accelerated decay was found only when the reaction was initiated by mixing iron and peroxide. (5) The DMPO-OH spin adduct signal was quenched, apparently by binding to $[Fe^{III}EDTA]^{-1}$ with a complex formation constant of 3×10^3 M^{-1}. (6) Peroxide decomposed with a first order rate constant of $1.2 \pm 0.2 \times 10^{-4}$ s^{-1} in the

presence of 0.001 to 0.10 M DMPO (see Table 3-6). This rate does not significantly differ from those expected for an organic substrates with the same rate constant for hydroxyl radical reaction.

The significance of the above observations both mechanistically and in terms of the validity of conclusions from spin-trapping applications is discussed below.

Formation of DMPO-OH

Figure 3-1 (D) shows a representative spectrum of the DMPO-OH spin adduct observed in the reaction of $[Fe^{III}EDTA]^{-1}$ with H_2O_2. The spectrum is that formed by the reaction of $OH^{\cdot}$ with DMPO. The occurrence of the DMPO-OH adduct cannot, however, be accepted as definitive proof of the presence of free hydroxyl radicals in the reaction mixture. A review by Finkelstein, et al.[25] comments on the highly reactive nature of nitrones, noting that prior to spin trapping, their main use was as synthetic intermediates. Many potential reactions can occur with nitrones such as DMPO that result in the formation the hydroxyl adduct in the absence of hydroxyl radicals. The formation of spurious DMPO-OH or other DMPO spin adducts via non-radical reactions was examined under the conditions of the current study.

Metal ions may oxidize DMPO into hydroxamic acid which in turn may be oxidized to a nitroxide product called DMPOX (4-1). The DMPOX spectrum is a seven line spectrum with

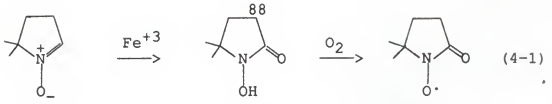

(4-1)

DMPO Hydroxamic acid DMPOX

A_N = 7.2, $A_{\zeta H}$ = $A_{\zeta H}$ = 4.1 G. Hydroxamic acid forms a 1:1 complex with iron that has a visible absorption at 544 nm (ε_{544} = 1075 $M^{-1}cm^{-1}$).[25] Blank solutions containing $[Fe^{III}EDTA]^{-1}$ and DMPO were examined for iron/hydroxamic acid complex formation. These blanks showed that no binding of this nature was occurring under the conditions used in the present study. Further, the DMPOX EPR spectrum was not observed throughout the study in any of the reaction mixtures examined.

The hydroxyl adduct might also form from DMPO in the presence of light or H_2O_2 via the formation of oxazirane (equation 4-2).[25] However blank solutions containing DMPO

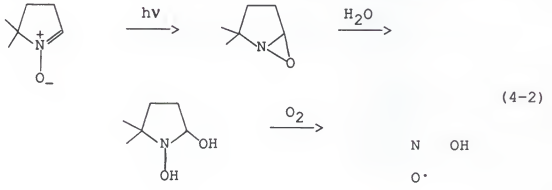

(4-2)

alone or with either iron or peroxide produced no significant EPR signal, ruling out photolytic DMPO-OH formation in the current study.

DMPO also traps superoxide forming an unstable adduct which decomposes into a non-radical species and DMPO-OH.[23] The DMPO trapping rate for superoxide ($10\ M^{-1}s^{-1}$)[23] is not competitive with other superoxide reactions or the OH·/DMPO reaction, so little superoxide trapping is expected.

The formation of the corresponding DMPO radical adduct when organic substrates are included in the reaction is considered verification that DMPO/OH trapping has indeed occurred.[25] Supposedly, the organic substrate reacts with OH· to form secondary radicals resulting in the appearance of a new signal and a decrease of the DMPO-OH signal intensity. Addition of competitive amounts of ethanol to the $[Fe^{III}EDTA]^{-1}/H_2O_2$ reaction in the current study resulted in the formation of ethanol radical adducts of DMPO indicating that radical species were indeed produced by the reaction (Figure 3-7).

According to the generally accepted methods[12,16,21,25,26,55] for verification of OH· production in a reacting system, the observation of the ethanol adduct shows that the hydroxyl radical is definitely formed and trapped in the $[Fe^{III}EDTA]^{-1}/H_2O_2$ reaction. However, in light of the controversial nature of the intermediates in iron/peroxide reactions, the literature standards for definitive OH· trapping are clearly inadequate. Three different oxidizing intermediates have been proposed for the reaction of iron or iron chelates with peroxide. These are

the iron(IV)[59-63] and iron(V)[64-68] ferryl species ($[L\text{-}Fe^{IV}O]^{n-}$, $[L\text{-}Fe^{V}O]^{n-}$) and the hydroxyl radical.[41,56,69-76] It is conceivable that the ferryl species might react to form DMPO-OH in a manner equivalent to and kinetically indistinguishable from the OH· radical.[77-79] Reasonable mechanisms can be written for the formation of DMPO-OH from the ferryl species. The protonated iron(IV) ferryl ion ($[L\text{-}Fe^{IV}OH]^{n-}$) may be written $[L\text{-}Fe^{III}\text{:}OH\cdot]^{n-}$ which is kinetically equivalent to an iron(III)/hydroxyl radical cage complex. As such the iron(IV) ferryl could transfer the OH· to DMPO (equation 4-3). For the iron(V) ferryl, O atom transfer from

$$[L\text{-}Fe^{IV}\text{-}O]^{n-} \xrightarrow{H^+} \{L\text{-}Fe^{III}\text{:}OH\cdot\}^{n-}$$

$$\{L\text{-}Fe^{III}EDTA\text{:}OH\cdot\}^{n-} + DMPO \longrightarrow DMPO\text{-}OH + [L\text{-}Fe^{III}]^{n-} \qquad (4\text{-}3)$$

$[L\text{-}Fe^{V}O]^{n-}$ and subsequent reduction would result in DMPO-OH formation (equation 4-4). Although DMPO-OH formation is expected regardless of the identity of the intermediate, the nature of this intermediate is an important question that has not yet been settled. The different intermediates may not be equally reactive in all cases resulting in significant mechanistic differences depending on the matrix

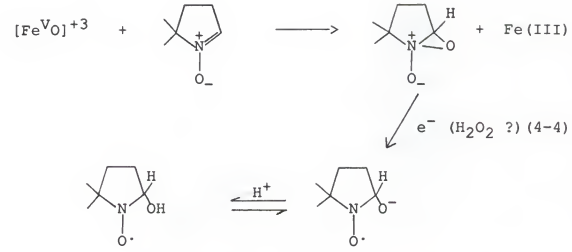

and conditions of the reaction. The mechanism for the reaction of $[Fe^{III}EDTA]^{-1}$ with H_2O_2 is thus the subject of much study and much controversy.

Proposed Reactive Intermediates for Iron/Peroxide Reactions

There are three main mechanisms that have been proposed for the catalytic decomposition of peroxide by iron complexes, and the steps of these mechanisms may vary depending on the reaction conditions of the study. The key difference between the reaction mechanisms is the identity of the intermediate responsible for carrying the chain. As mentioned previously, the potential intermediates are the $[L\text{-}Fe^{V}O]^{n-}$, $[L\text{-}Fe^{IV}O]^{n-}$ or the hydroxyl radical. There are studies in defense of each view by many authors throughout the literature, but the works of Kremer,[64-68] Walling[41,56,69-73] and Richter[62,63] and their coworkers,

are especially applicable to the current study and are discussed as representative work supporting each of the three different intermediates.

Hydroxyl Radical

Walling and coworkers studied the low pH reaction of Fe^{III} with H_2O_2[73] and the reaction of $[Fe^{III}EDTA]^{-1}$ with H_2O_2 at pH values greater than 7.0.[41] He found that peroxide decomposition was slowed by the addition of organic substrates and attributed this observation to the reaction of substrate with hydroxyl radicals. The mechanism proposed by Walling et al.[41] is shown in Figure 4-1 (literature rate constants are listed in Appendix 1). This mechanism yields a rate law that is valid for both low and high pH work with the exception that at high pH an additional propagation step due to the reaction of $OH^{\cdot}$ with EDTA is included. The peroxide decomposition rate law for the mechanism (equation 4-5) reduces to a second order expression (equation 4-6) under the condition of high peroxide to iron ratio.

$$-d[H_2O_2]/dt = 2k_a [H_2O_2][Fe^{III}](1 + k_c[H_2O_2]/k_e[RH]) \quad (4-5)$$

$$-d[H_2O_2]/dt = k_{2nd}[Fe^{III}][H_2O_2] \quad (4-6)$$

Then assuming very little change in iron or iron chelate concentration during the reaction, peroxide decomposition is

$$[Fe^{III}EDTA]^{-1} + H_2O_2 \longrightarrow [Fe^{II}EDTA]^{-2} + H^+ + HO_2\cdot \quad (a)$$

$$[Fe^{II}EDTA]^{-2} + H_2O_2 \longrightarrow [Fe^{III}EDTA]^{-1} + OH^- + OH\cdot \quad (b)$$

$$OH\cdot + H_2O_2 \longrightarrow H_2O + HO_2\cdot \quad (c)$$

$$HO_2\cdot + [Fe^{III}EDTA]^{-1} \longrightarrow [Fe^{II}EDTA]^{-2} + H^+ + O_2 \quad (d)$$

$$OH\cdot + RH \longrightarrow H_2O + R\cdot \quad (e)$$

$$R\cdot + O_2 \longrightarrow RO_2\cdot \quad (f)$$

$$RO_2\cdot + [Fe^{II}EDTA]^{-2} + H^+ \longrightarrow ROOH + [Fe^{III}EDTA]^{-1} \quad (g)$$

Figure 4-1. Mechanism proposed by Walling et al.[41] for the $[Fe^{III}EDTA]^{-1}/H_2O_2$ reaction. (a) initiation, (b-d) propagation, (e-g) termination.

psuedo first order in peroxide (equation 4-7) with a k_{1st} given by equation 4-8. The k_{2nd} value decreases linearly

$$-d[H_2O_2]/dt = k_{1st}[H_2O_2] \quad (4\text{-}7)$$

$$k_{1st} = k_{2nd}[Fe^{III}]$$
$$= (2k_a(1 + k_c[H_2O_2]/k_e[RH])\ [Fe^{III}] \quad (4\text{-}8)$$

as RH concentration increases and when plotted against 1/[RH] gives an intercept equal to $2k_a$ (as in Figure 3-3, for example). The reaction is pH dependent with a rate that is inversely proportional to $[H^+]$. The pH dependence is explained by a complex preequilibrium in the initiation step (equation 4-9).[73]

$$[Fe^{III}EDTA]^{-1} + H_2O_2 \longrightarrow$$

$$H^+ + [Fe^{III}EDTA\text{-}OOH]^{-2} \longrightarrow [Fe^{II}EDTA]^{-2} + HO_2\cdot \quad (4\text{-}9)$$

Walling et al.[41] found that the originally proposed mechanism using literature estimates for relevant rate constants gave calculated slopes for k_{2nd} vs 1/[RH] plots that were only 1/10 of those observed experimentally. He concluded that the hydroxyl radical reacts with EDTA to form a radical species which subsequently terminates the chain by reacting with O_2 or propagates the chain by reducing $[Fe^{III}EDTA]^{-1}$ as shown in equation 4-10. Walling et al.[41]

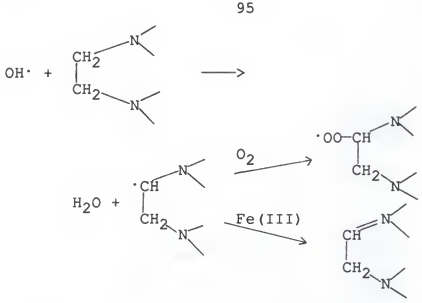

(4-10)

further conclude that since the rate of the EDTA/hydroxyl radical reaction is so rapid ($k = 2.76 \times 10^9\ M^{-1}s^{-1}$), and $[Fe^{III}EDTA]^{-1}$ and the hydroxyl radical are formed in pairs, a significant amount of the hydroxyl radical may react immediately with $[Fe^{III}EDTA]^{-1}$ upon formation. This cage reaction results exclusively in propagation. Inclusion of this propagation sequence in the reaction scheme results in the rate law shown in equation 4-11[41] where α is the

$$-d[H_2O_2]/dt = ((2 + \alpha)\ k_a[H_2O_2][Fe^{III}EDTA]^{-1}]) \times (1 + (k_c[H_2O_2] + k_h[EDTA])/k_e[RH]) \qquad (4\text{-}11)$$

fraction of hydroxyl radicals involved in cage complex reactions and k_h is the rate constant for EDTA/hydroxyl radical reactions. In the presence of high [RH] termination via attack on EDTA is negligible. Recalculation of k_{2nd}

values using equation 4-11 yields 1/RH versus k_{2nd} plots with slopes that more closely match the experimental observations.

In the current study, computer kinetic simulations of the Walling et al. experiments were performed to confirm his mechanistic conclusions. Simulated peroxide decomposition data using the mechanism in Figure 4-1 gives k_{2nd} values that when plotted against 1/RH yield a slope of 1.27×10^{-3} which is 1/10 lower than the slopes obtained experimentally by Walling et al. and in replications of this work in the current study (slopes equal 1.42×10^{-2} and 2.44×10^{-2} respectively). Reaction step (h) ($k_h = 2.76 \times 10^9$) was added to the Figure 4-1 mechanism to account for the propagation due to the hydroxyl radical reaction with EDTA and $[Fe^{III}EDTA]^{-1}$. Kinetic simulations using the modified mechanism resulted in a k_{2nd} versus 1/RH plot with a slope of 1.12×10^{-2} which closely agreed with the experimental

$$[Fe^{III}EDTA]^{-1} + OH\cdot \longrightarrow [Fe^{II}EDTA]^{-2} + H_2O \qquad (h)$$

slopes and those calculated by Walling et al.[41] using equation 4-11.

A consequence of the reaction of the intermediate with EDTA is the eventual degradation of the ligand and the release of iron, which precipitates at high pH. The result is a loss of catalyst over the course of the reaction and a subsequent slowing of the peroxide decomposition rate. The

effect of this catalyst loss was small and was minimized further by including an excess of EDTA in the reaction mixture. No visible precipitation was observed during replication experiments over the time period in which the peroxide concentration was monitored (1 to 2 hours). A reddish precipitate was observed, however, if the reaction was allowed to continue for several hours. Furthermore, the observed plots were found to be first order without detectable retardation indicating that catalyst decomposition was insignificant over the time scale of the current experiments.

In summary, Walling et al.[41] suggests a hydroxyl radical intermediate as a chain carrier in the $[Fe^{III}EDTA]^{-1}/H_2O_2$ reaction. He observed inhibition of the reaction in the presence of organic substrates including acetone and t-butyl alcohol. His mechanism accurately models the experimental observations at low pH and at high pH (with the inclusion of equation (h)). These results have been replicated in the current study, and kinetic simulations are consistent with the Walling et al.[41] mechanistic conclusions. Inhibition of the reaction by organic substrates and the formation of organic radicals are key pieces of evidence used to support the $OH^{\cdot}$ radical as an intermediate. However, Kremer[64-67] proposes that such inhibition may occur in the absence of hydroxyl radicals.

Iron(V) Ferryl

Kremer[65] proposes the mechanism shown in Figure 4-2 for the Fe^{III}/H_2O_2 reaction. Kremer's experiments were carried out only at low pH values where chelates were not necessary. The peroxide decomposition rate law (equation 4-12)[67]

$$-d[H_2O_2]/dt = (k_j/K_M)\ [Fe^{III}][H_2O_2](1 + 2k_k[H_2O_2]/k_1[RH]) \qquad (4\text{-}12)$$

$$K_M = (k_j + k_k)/k_i$$

derived from this mechanism in the case of high organic substrate concentration has the same form as the Walling et al.[41] rate law (equation 4-5) and accurately models low pH experimental observations. For higher pH studies where $[Fe^{III}EDTA]^{-1}$ is used, Walling et al.[41] found that an additional propagation step is necessary to model the experimental observations. Except for k_i, rate constants for the elementary steps in the Kremer[65] scheme are not known. Only rate constant ratios were measured by Kremer[65] and these at low pH values. The rate constants for $[Fe^{V}O]^{+3}$ reactions for chelated iron at high pH values have not been determined. Therefore, since the rate constants are unknown, the Kremer[65] scheme with the appropriate choice of rate constants, can model the high pH experimental observations and cannot be excluded as a potential reaction pathway.

$$H_2O_2 + Fe^{III} \longrightarrow [Fe^{III}\text{-}OOH]^{+2} \quad (i)$$

$$[Fe^{III}\text{-}OOH]^{+2} \longrightarrow OH^- + [Fe^{V}O]^{+3} \quad (j)$$

$$[Fe^{V}O]^{+3} + H_2O_2 \longrightarrow Fe^{III} + H_2O + O_2 \quad (k)$$

$$[Fe^{V}O]^{+3} + RH_2 \longrightarrow R + Fe^{+3} + H_2O \quad (l)$$

Figure 4-2. Mechanism proposed by Kremer for the Fe^{III}/H_2O_2 reaction.[67]

The Kremer[65] scheme (Figure 4-2) is a reasonable mechanism and is consistent with experimental observations. However, there is little support for an $[Fe^{V}O]^{+3}$ intermediate in the literature. Most studies propose either hydroxyl radical or the $[Fe^{IV}O]^{+2}$ ion intermediates in the higher pH, iron chelate/peroxide reaction. The formation of an $[Fe^{V}O]^{+3}$ cannot be discounted, but in light of the lack of literature precedence for $[Fe^{V}O]^{+3}$ and reaction rate constant information, the iron(V)-ferryl is not considered in the current study.

Iron(IV) Ferryl

The product of the reaction shown in equation 4-13 has been the subject of much debate. This step is believed by

$$[L\text{-}Fe^{II}]^{n-} + H_2O_2 \rightarrow \begin{cases} [L\text{-}Fe^{III}]^{n-} + OH^- + OH\cdot \\ [L\text{-}Fe^{IV}O]^{n-} + H_2O \end{cases} \quad (4\text{-}13)$$

some to form the hydroxyl radical and others to form $[L\text{-}Fe^{IV}O]^{n-}$. The iron(IV) ferryl ion has been proposed as the reactive intermediate in iron porphyrin chemistry,[80] and high valent iron-oxo porphyrin species have been characterized spectroscopically.[81] However $[L\text{-}Fe^{IV}O]^{n-}$ formation in $[Fe^{III}EDTA]^{-1}$ or similar chelate chemistry is uncertain since the supposed ferryl adduct has not been spectroscopically characterized.

Rahhal and Richter[62] have studied the reaction of $[Fe^{II}DTPA]^{-3}$ with peroxide (1:10 ratio) at pH 7.0 in the presence of t-butyl alcohol and proposes that $[Fe^{IV}O]^{+2}$ is the reactive intermediate based on her results. By monitoring the rate of $[Fe^{II}DTPA]^{-3}$ conversion to $[Fe^{III}DTPA]^{-2}$, she compared ^{60}Co radiolysis experiments (where OH· formation is well established) to results of the of the $[Fe^{II}DTPA]^{-3}/H_2O_2$ in the presence and absence of t-butyl alcohol.

The surprising outcome of this study was that the $[Fe^{II}DTPA]^{-3}/H_2O_2$ reaction was completely unaffected by the presence of t-butyl alcohol while $[Fe^{II}DTPA]^{-3}$ conversion was significantly slowed by the inclusion of t-butyl alcohol in radiolysis experiments. According to this observation hydroxyl radicals are not formed in the $[Fe^{II}DTPA]^{-3}/H_2O_2$ reaction and further, the intermediate that is formed (presumably $[DTPA\text{-}Fe^{IV}O]^{-3}$) does not react rapidly with the organic substrate.

These findings seem inconsistent with the dramatic decrease in reaction rate observed in the presence of t-butyl alcohol in the Walling et al.[41] study. If the $[Fe^{II}EDTA]^{-2} + H_2O_2$ step of the Walling et al.[41] mechanism produces an $[EDTA\text{-}Fe^{IV}O]^{-2}$ species that is unreactive towards organic substrates as implicated by the Rahhal and Richter[62] results, then no organic substrate effect is expected.

Shiga[82] also studied the iron(II)/peroxide reaction using $[Fe^{II}EDTA]^{-2}$ at pH 7.0 with a 1:10 $[Fe^{II}EDTA]^{-2}/H_2O_2$ ratio. Shiga[82] observed the formation of t-butyl and other alcohol radicals via continuous flow EPR experiments. The formation of organic radicals indicates that the intermediate (whatever its identity) reacts with organic substrates to form radical species. The study also finds that the radical products for various alcohol substrates differ for the $[Fe^{II}EDTA]^{-2}/H_2O_2$ reaction and the known OH· generating reaction of Ti and H_2O_2. Hydroxyl radicals have been shown in photolysis experiments to abstract an α-hydrogen from alcohols.[82] In Shiga's study the Ti/H_2O_2 reaction produced the α-hydrogen radical product while the $[Fe^{II}EDTA]^{-2}/H_2O_2$ reaction yielded the ω-hydrogen radical products. The reactive intermediate does therefore appear to be a species other than the hydroxyl radical.

The seeming inconsistency in the Rahhal/Richter,[62] Shiga[82] and Walling et al.[41] observations illustrate the difficulty encountered when trying to determine the identity of the reactive intermediate in iron/peroxide chemistry. The observations for the Rahhal and Richter[62] study are valid for the conditions, concentrations and chelate used. These results are also supported in related research by Koppenol and coworkers.[77-79] However, these conclusions are not necessarily applicable to iron/peroxide chemistry under different conditions. Rahhal and Richter[62] use the chelate

DTPA, an octadentate ligand that leaves no open coordination site for the inner sphere reaction of H_2O_2. There is evidence that the DTPA ligand behaves differently from EDTA when used as an iron chelate for iron/peroxide and related reactions.[83,84] Though iron(II) and iron(III) clearly react with peroxide in the Rahhal/Richter[62] and other studies,[83-85] some research has shown that the iron/peroxide reactions are inhibited or completely blocked if iron is chelated with DTPA.[42,86] Other studies indicate that the iron catalyzed formation of hydroxyl radical by superoxide in the presence of H_2O_2 is inhibited when DTPA is used as a chelate.[42,86] Further, DTPA is often included in phosphate buffered solutions because it is thought to inhibit OH· production from iron(III) impurities.[42,83,84,87,88] Though it seems unlikely that the use of DTPA blocks iron/peroxide reactions, the literature discrepancies suggest that DTPA chelates may react differently than EDTA chelates. The kinetics of the $[Fe^{II}DTPA]^{-3}$ reaction with peroxide may therefore be very different from those of the $[Fe^{II}EDTA]^{-2}/H_2O_2$ reaction.

The observations of Rahhal and Richter[62] suggest a non-hydroxyl intermediate that is relatively unreactive toward organic substrates. If the intermediate formed in the Rahhal/Richter[62] study is reactive toward organic substrates, the rate of this step is not competitive with other processes in the system when DTPA is the chelate.

Another consideration is that the concentration of the alcohol radicals formed in the Shiga[82] study is unknown. It is also not known if any t-butyl radical was formed in the Richter study. The concentration of an EPR observable amount of t-butyl alcohol radical (as seen in the Shiga[82] study) could be very low and may therefore be too low to observably affect the $[Fe^{II}DTPA]^{-3}/H_2O_2$ reaction rate.

Summary

Since the Walling et al.[41] study uses EDTA as a chelate and begins with $[Fe^{III}EDTA]^{-1}$, the $[Fe^{II}EDTA]^{-2} + H_2O_2$ step (step b Figure 4-1) may differ kinetically from studies that begin with iron(II) due to different $Fe(II)/H_2O_2$ ratios. Thus depending on the $Fe(II)/H_2O_2$ ratio competing reactions may be kinetically more or less significant and result in different product distributions. It is possible that both $[Fe^{IV}O]^{+2}$ and OH· are present in an acid dependent equilibrium. There is general agreement that OH· is produced by iron/H_2O_2 reactions in acidic media.[71] The reaction in equation 4-14 has been proposed to account for this observation.[71] Thus either or both intermediates

$$[Fe^{IV}EDTA\text{-}O]^{-3} + H^+ \longrightarrow [Fe^{III}EDTA]^{-1} + OH\cdot \qquad (4\text{-}14)$$

would be possible, and the predominant species would be determined by pH, iron/peroxide ratio, chelating agent and other variables that alter the rates of elementary reaction steps.

If $[Fe^{IV}O]^{+2}$ is indeed formed as the principle oxidizing chain carrier in the Walling et al.[41] reaction, its reaction with RH must be faster than other competing reactions since addition of RH results in a H_2O_2 decomposition rate decrease that is proportional to the RH concentration. It is also possible that under the conditions of the Walling et al.[41] study the hydroxyl radical is formed and is the principal oxidizing chain carrier as is suggested by Walling and coworkers.[41]

The Rahhal/Richter[62] and Shiga[82] studies indicate that the hydroxyl radical is not the intermediate formed in reaction 4-13. Shiga[82] further shows that the intermediate is capable of reacting in a manner similar to a hydroxyl radical resulting in the formation of organic radicals. It is therefore reasonable to suggest that a ferryl intermediate would also produce the DMPO-OH adduct from DMPO. However, none of the work discussed here conclusively proves the identity of the chain carrying intermediate responsible for DMPO-OH and organic radical formation. Experiments were conducted in the present study to determine the identity of this intermediate.

Spin Trap Competition Experiments

Competition studies of spin traps in radiolysis and chemical reactions were attempted in order to distinguish between hydroxyl radical and alternative (e.g. ferryl)

species following the method of Masarwa et al.[89] Masarwa et al.[89] demonstrated that the ratio of organic radical products in radiolysis experiments, where hydroxyl radical production is well characterized, differed from the ratio observed in chemical reactions of some metals with peroxide. Metals that were known to generate OH· gave the same product ratios as the radiolysis experiments.

An approach similar to that of Masarwa et al.[89] was taken in the present work using spin traps instead of organic substrates. Two different spin traps were included in the $[Fe^{II}EDTA]^{-2}/H_2O_2$ reaction, and the EPR spectra of the resulting spin adducts were compared to EPR spectra of radiolysis experiments using the same spin traps combinations. In N_2O saturated solutions hydroxyl radicals and solvated electrons are produced followed by conversion of the solvated electron to hydroxyl radical via a rapid and well-known sequence of reactions, (equation 4-15).[90] The reaction of $[Fe^{II}EDTA]^{-2}$ with peroxide is the controversial

$$H_2O \longrightarrow e_{aq}^-,\ H,\ OH\cdot,\ HO_2\cdot,\ H_2O_2,\ H_3O^+$$

$$e_{aq}^- + N_2O \longrightarrow N_2 + O^-$$
$$O^- + H_2O \longrightarrow OH\cdot + OH^- \qquad (4\text{-}15)$$

reaction in $[Fe^{III}EDTA]^{-1}/H_2O_2$ mechanism, producing either the hydroxyl radical or the iron(IV) ferryl ion (equation 4-13).

Spin traps TMPO, PBN and 4-POBN were used in combination with DMPO. TMPO and PBN yield complex spectra in radiolysis trials and are thus not useful (Figure 3-11). The radiolysis spectra produced by 4-POBN are clean, and spectral peaks are clearly distinguishable from DMPO peaks, but when mixed, the DMPO adduct signal intensity is much greater than that of 4-POBN which appears only as a noisy baseline (Figure 3-12). EPR spectra show that DMPO clearly forms the DMPO-OH adduct during radiolysis. However, the observed 4-POBN spectrum (A_N = 15.7, A_H = 2.4) is not the OH· adduct as initially thought (A_N = 14.93 - 14.97 G, A_H = 1.68 - 1.69 G)[21] but is an unidentified adduct that has been reported by Janzen.[54] Though Janzen reports that 4-POBN forms a stable long-lived OH· adduct, he gives no decay rate information. Finkelstein et al.[19] report that 4-POBN-OH has a $t_{½}$ of only 23 s. The 4-POBN-OH adduct apparently decays too rapidly to be observed in the radiolysis experiments. As a result, product ratio comparisons between chemical and radiolysis experiments are not possible.

The radical species trapped in the $[Fe^{II}EDTA]^{-2}/H_2O_2$ reaction are of interest (Figure 3-13). The DMPO again cleanly forms the hydroxyl adduct but 4-POBN forms a 4-POBN-CO_2^- adduct. The degradation of EDTA during the reaction is apparently responsible for the release of CO_2^- radicals. The DMPO-OH concentration estimated from the iron

binding constant is 5 X 10^{-5} M, which is nearly equal to the 4-POBN-CO_2 concentration (4 X 10^{-5} M). Considering the error in the K_b value, the DMPO-OH concentration may be as high as 7 X 10^{-4} M, which is almost 20 times that of 4-POBN-CO_2. 4-POBN-CO_2 does not form an iron complex so the measured concentration is equal to the actual concentration. The lack of any observable DMPO-CO_2 adduct formation may be attributed to signal quenching due to iron binding, but no information is available on the DMPO-CO_2/$[Fe^{III}EDTA]^{-1}$ complex formation. A decay rate of 3.0 X 10^{-4} s^{-1} has been measured for DMPO-CO_2, but no information is available on the stability of the DMPO-CO_2 adduct under the current experimental conditions. Without knowledge of the exact actual DMPO-OH concentration and the DMPO-CO_2 decay rate, it would be presumptuous to draw any definite conclusions from this study.

If the DMPO-OH concentration is indeed nearly equal to that of 4-POBN-CO_2 and the DMPO-CO_2 adduct is stable, then these results might suggest that a non-radical intermediate is formed. DMPO and 4-POBN trap OH· at nearly the same rate (3.4 X 10^9 $M^{-1}s^{-1}$ and 3.5 X 10^9 $M^{-1}s^{-1}$, respectively),[37,38] and also trap CO_2^- at nearly equal rates (7.5 X 10^8 $M^{-1}s^{-1}$ and 6.1 X 10^8 $M^{-1}s^{-1}$, respectively).[91] Therefore, if OH· is the intermediate, since DMPO-OH appears to be formed exclusively, 4-POBN would also be expected to form only the OH· adduct. The 4-POBN-OH adduct would then decay rapidly

resulting in no 4-POBN adduct signal. The observation of 4-POBN-CO_2 adduct at concentrations equal to DMPO-OH would then suggest that an intermediate is formed that unlike the hydroxyl radical, reacts with DMPO and POBN at different rates to form the hydroxyl adducts.

On the other hand, the DMPO-OH concentration may be up to twenty times greater than the 4-POBN-CO_2 concentration. In this case, assuming equal adduct formation rates as stated above, it might be concluded that results are consistent with a hydroxyl radical intermediate if the ratio of DMPO-OH to 4-POBN-CO_2 concentrations is appropriate for the known formation constants and the lack of 4-POBN-OH and DMPO-CO_2 is attributed to rapid decay or signal quenching.

The conclusions that may be drawn from the spin-trapping competition studies are obviously dependent on a knowledge of exact complex formation constants (if complexes are formed), spin adduct formation and decay rates, and the ability to accurately measure spin adduct concentration. In the absence of these parameters that are valid for the current reaction conditions, no argument can be made for or against a radical intermediate.

The study does show that the CO_2^- adduct forms, but is not detectable by DMPO under the current conditions. Also, 4-POBN is not suitable for detecting OH· under the current experimental conditions. These results illustrate that the presence of a radical species cannot be ruled out on the

basis of no observable spin adduct formation.

Given proper characterization of spin adduct behavior, spin trap competition studies may provide a means of distinguishing between the potential intermediates in iron/peroxide reactions. The results obtained in these experiments show that there may be a great deal of information to be gained from similar experiments by using a different spin traps in conjunction with DMPO and determining spin adduct decay rates and complex formation constants. A spin trap which may be useful for this study is 4-MePyBN (4-(N-methyl pyridinium) tert-butyl nitrone) (4-16). This spin trap is similar to 4-POBN, but is reported

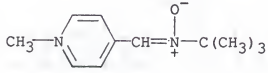

(4-16)

4-MePyBN

by Janzen et al.[92] to form a more stable hydroxyl spin adduct. Janzen et al.[92] gives no indication of the half-life of the $OH^{\cdot}$ adduct, however. The criteria for choosing spin traps for these experiments are to use a spin trap that is as chemically different from DMPO as possible, that forms a long-lived $OH^{\cdot}$ adduct with known hyperfine splitting constants, and that produces an EPR spectrum that can be quantifiably distinguished from that of DMPO-OH.

Results of the present study are consistent with DMPO-OH formation via an oxidizing intermediate, but the identity of the intermediate cannot be determined conclusively. The reaction conditions for the $[Fe^{III}EDTA]^{-1}/H_2O_2$ reaction are the same as those used by Walling et al.[41] The Walling et al.[41] peroxide decomposition results are reproducible and are consistent with the proposed mechanism (Figure 4-1). Peroxide decomposition in the presence of DMPO is also consistent with the proposed mechanism, with DMPO acting as an organic substrate with a high $OH^{\cdot}$ reaction rate. Table 3-6 shows experimental and calculated peroxide decomposition rates for DMPO. The calculated rates used the rate law equation 4-5 and literature rate constant that are shown in Appendix B. The experimental rates are consistently three times lower than the calculated rates. However, the calculated rates are only as accurate as the literature rate constants used. The k_a used for these calculations was estimated by averaging the k_a values from the Walling et al.[41] study. The other rate constants were taken from various sources and some were found to differ from source to source. Therefore agreement between experimental and calculated rates within a factor of three is quite good.

More important than exact rate constant agreement is the experimental consistency with mechanistic predictions. The mechanism (Figure 4-1) predicts that in the presence of an organic substrate (even at very low concentrations) with

an OH· reaction rate equal to that of DMPO, the peroxide decomposition rate will reach a lower limit as the RH term in equation 4-5 approaches zero. Thus, above the limiting RH concentration, the rate will no longer decrease as substrate concentration is increased. Table 3-6 shows this prediction in calculated k_{2nd} values. [Rate constants are psuedo first or psuedo second order and contain an RH concentration term in their calculation. k_{2nd} values are thus expected to change as [RH] changes (see equations 4-5 - 4-8).] The calculated k_{2nd} values remain almost constant as substrate concentration is increased from 0.001 to 0.10 M. Similarly, the experimental k_{2nd} values measured for DMPO show no change over the 0.001 to 0.10 concentration range.

In the presence of the spin trap DMPO, peroxide decomposition rates are close to those predicted for an organic substrate with the same hydroxyl radical trapping rate and are consistent with the Walling et al.[41] mechanistic predictions. Thus the Walling et al. mechanism appears to be predictive in the presence of spin-trapping substrates as well as organic substrates. This mechanism is therefore used to describe the $[Fe^{III}EDTA]^{-1}/H_2O_2$ reaction in the current study and as far as possible model the formation of DMPO-OH from the spin trap DMPO. Though Walling et al.[41] proposes hydroxyl radical formation, another kinetically indistinguishable oxidizing intermediate may easily be substituted for the reactions involving OH·

without changing the predictive accuracy of the mechanism. For the purposes of discussion the oxidizing intermediate is labeled O_x where O_x equals either OH· or $[Fe^{IV}O]^{+2}$ and no judgement between the two is made. Using this convention, the reaction steps involving the OH· in the Figure 4-1 mechanism can be rewritten in two different ways as shown in Figure 4-3. These two sets of equations are equivalent and produce identical simulation results. For consistency, the $O_x = [Fe^{IV}O]^{+2}$ convention will be used in writing mechanisms.

In conclusion, while the DMPO-OH adduct is formed by reaction with O_x, the production of DMPO-OH is not confirmation of hydroxyl radical generation. The formation of DMPO-OH in the reaction is nonetheless of interest and has potential as a probe of the oxidizing intermediate regardless of its identity.

DMPO-OH Production in the $[Fe^{III}EDTA]^{-1}/H_2O_2$ Reaction

DMPO-OH production was monitored in the $[Fe^{III}EDTA]^{-1}/H_2O_2$ reaction by following the appearance of the EPR signal with time. Based on the literature descriptions of spin-trapping studies describing DMPO-OH as a long-lived non-interacting spin adduct, the Walling *et al.*[41] mechanism in Figure 4-1 was altered to describe the spin-trapping reaction (Figure 4-4). The scheme was altered by substituting the spin trap for the organic substrate (RH)

$O_x = OH\cdot$:

$$[Fe^{II}EDTA]^{-2} + H_2O_2 \longrightarrow O_x + OH^- + [Fe^{III}EDTA]^{-1} \quad (b)$$

$$O_x + H_2O_2 \longrightarrow H_2O + HO_2\cdot \quad (c)$$

$$O_x + RH \longrightarrow H_2O + R\cdot \quad (e)$$

$O_x = [Fe^{IV}O]^{+2}$:

$$[Fe^{II}EDTA]^{-2} + H_2O_2 \longrightarrow O_x + OH^- \quad (b)$$

$$O_x + H_2O_2 \longrightarrow H_2O + HO_2\cdot + [Fe^{III}EDTA]^{-1} \quad (c)$$

$$O_x + RH \longrightarrow H_2O + R\cdot + [Fe^{III}EDTA]^{-1} \quad (e)$$

Figure 4-3. Two equivalent ways of expressing the oxidizing intermediate steps using O_x as an unidentified intermediate.

$$[Fe^{III}EDTA]^{-1} + H_2O_2 \longrightarrow [Fe^{II}EDTA]^{-2} + H^+ + HO_2\cdot \quad (a)$$

$$[Fe^{II}EDTA]^{-2} + H_2O_2 \longrightarrow O_x + OH^- \quad (m)$$

$$O_x + H_2O_2 \longrightarrow H_2O + HO_2\cdot + [Fe^{III}EDTA]^{-1} \quad (n)$$

$$HO_2\cdot + [Fe^{III}EDTA]^{-1} \longrightarrow [Fe^{II}EDTA]^{-2} + H^+ + O_2 \quad (d)$$

$$O_x + DMPO \longrightarrow DMPO\text{-}OH + [Fe^{III}EDTA]^{-1} \quad (o)$$

Figure 4-4. Proposed mechanism for the $[Fe^{III}EDTA]^{-1}$ /H_2O_2 reaction in the presence of DMPO.

and eliminating the subsequent reactions involving the organic radical since the spin adduct, once formed, is not expected to react further. The Figure 4-4 mechanism predicts psuedo zero order generation of spin adduct in the initial stages of the reaction, and simulations of the scheme show linear production over approximately the first 20 min of the reaction (Figure 4-5).

Typically studies which quantify DMPO-OH production follow the growth in EPR signal for the first few minutes of the reaction. Production rate and kinetic competition calculations are then based on the assumption that the DMPO-OH production curve depends solely on the nearly diffusion controlled capture of O_x by DMPO. Thus in the Figure 4-4 mechanism the rate of DMPO-OH production is expected to equal the rate of O_x formation. However, experimental results indicate that the assumption that DMPO-OH builds up and is unreactive is in error.

The DMPO-OH concentration versus time curves (Figure 3-6) show that DMPO-OH decays much more rapidly than is reported in the literature. The expected $t_{½}$ for decay was 2.6 h,[19] while the actual decay $t_{½}$ estimated from TEMPO decay rate in the $[Fe^{III}EDTA]^{-1}/H_2O_2$ reaction (see Figure 3-10) was 4.3 minutes. Obviously the DMPO-OH formation curves are a combination of DMPO-OH production and DMPO-OH decay processes under the reaction conditions used in the current study.

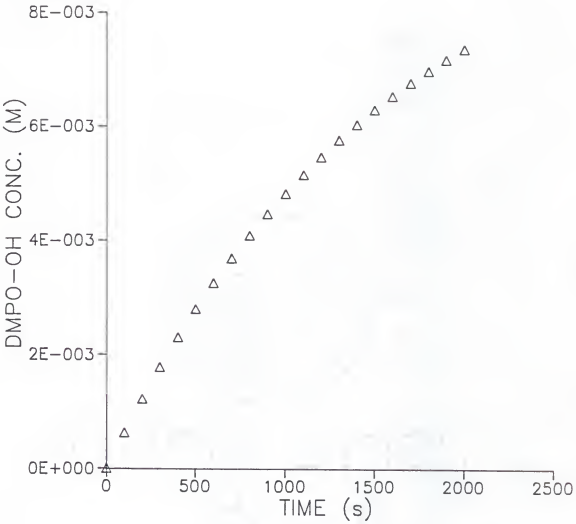

Figure 4-5. Simulated DMPO-OH production using the proposed spin trap mechanism in Figure 4-4. Rate constants are listed in Appendix B.

Studies using similar conditions that only follow DMPO-OH production for the first few minutes of the reaction might incorrectly assume that only linear DMPO-OH production occurs. In pH 9.0 experiments, the curves show apparently linear spin adduct formation for only the first 3 to 5 minutes. At pH 7.8, however, DMPO-OH production is linear for about the first 15 min. Rates of DMPO-OH (or O_x by mechanistic implication) formation based on the linear portion of these curves would be in error due to the unaccounted for DMPO-OH decay.

For example, Finkelstein et al.[19] used competition kinetic techniques to measure the DMPO/hydroxyl radical trapping rate in both peroxide photolysis and $Fe(II)/H_2O_2$ reactions. They observed DMPO-OH production in the presence of ethanol as a competitive inhibitor for a 1 minute initial reaction period. The calculated second order rate constants for the DMPO/OH reaction were consistently lower for the $Fe(II)/H_2O_2$ system. Finkelstein et al.[19] attributed this observation to an inhibition of the $Fe(II)/H_2O_2$ reaction by ethanol and did not consider the possibility of accelerated DMPO-OH decay.

In the current study the initial fall off in DMPO-OH production might also be attributed to factors that slow the $[Fe^{III}EDTA]^{-1}/H_2O_2$ reaction such as catalyst decomposition. However, peroxide decomposition rates are stable for 1 to 2 hours indicating that no significant catalyst

decomposition occurs. In addition catalyst decomposition would not account for the complete disappearance of DMPO-OH over such a short time period.

Another source of error occurs in the measurement of DMPO-OH concentration in the presence of $[Fe^{III}EDTA]^{-1}$. The concentration determined by double integration of the EPR spectrum is generally assumed to represent the total DMPO-OH present. However, the DMPO-OH signal is quenched upon formation of a complex with $[Fe^{III}EDTA]^{-1}$. The actual DMPO-OH concentration must be calculated taking into account the signal attenuation due to $[Fe^{III}EDTA]^{-1}$ binding.

It is apparent that DMPO does not behave in the manner predicted by the modified scheme in Figure 4-4 nor does the spin adduct behave in a manner consistent with literature descriptions of spin trapping. The key difference is the rapid decay of the DMPO-OH spin adduct. The decay kinetics of DMPO were therefore examined under the conditions of the current study.

DMPO-OH Decay in the $[Fe^{III}EDTA]^{-1}/H_2O_2$ Reaction

Finkelstein et al.[19] reports that DMPO-OH decay is first order with a half-life of 2.6 hr (k_{dk} = 7.4 X 10^{-5} s^{-1}) in the presence of 0.6% H_2O_2 at pH 7.4. Buettner[26] points out however that half-lives as short as 5 sec have been observed under strong oxidizing conditions. In results from his laboratory, Buettner[26] has seen varying life-times

for spin adducts of DMPO generated with the Fenton reaction depending on the peroxide and iron concentration in the spin-trapping mixture. No exhaustive study exists on the decay rate of DMPO-OH under different conditions. In the absence of decay rate information specifically applicable to the current study, DMPO-OH was generated photolytically, and adduct decay was measured by monitoring the EPR signal intensity with time. Decay rates were measured in the presence of each component of the $[Fe^{III}EDTA]^{-1}/H_2O_2$ reaction and at different pH values.

DMPO-OH decay was found to be independent of the reaction mixture components (except for the full complement), concentration of spin adduct or pH (see Table 3-8 and Figure 3-9). The decay was first order in all cases, and the average half life was 2.3 hr which compares favorably with that reported by Finkelstein et al.[19] The DMPO-OH decay rate in the $[Fe^{III}EDTA]^{-1}/H_2O_2$ reaction is obviously much faster than that in the non-reacting solution. Accelerated decay must therefore be attributed to interaction with the reaction intermediates. Accelerated decay of the chemically similar nitroxide spin-label TEMPO (Figure 3-10), when included in the $[Fe^{III}EDTA]^{-1}/H_2O_2$ reaction, confirms that some component of the reaction system is responsible for the nitroxide decay. TEMPO, though normally stable for weeks, decayed with a first order rate constant of 2.7×10^{-3} s^{-1} upon initiation of the $[Fe^{III}EDTA]^{-1}/H_2O_2$ reaction. This

rate constant is 100 times faster than the normal decay of DMPO-OH. By analogy, the k_{dk} for DMPO-OH in the reaction is expected to be at least as fast as that for TEMPO.

DMPO-OH and other nitroxides have greatly reduced lifetimes when included in the reacting $[Fe^{III}EDTA]^{-1}/H_2O_2$ system. Accelerated decay is not noted in the presence of any of the components or under any of the conditions studied until the reaction is initiated by mixing iron and peroxide. The decay is attributed to reaction intermediates, but the identity of the intermediate cannot be determined from the available information. The mechanism presented for the $[Fe^{III}EDTA]^{-1}/H_2O_2$ in the presence of a spin trap (Figure 4-4) does not accurately describe the reaction. No literature information or mechanism describing DMPO-OH or other spin adduct decay is available. Kinetic simulation studies were therefore undertaken in an attempt to describe the observations of the current study using plausible reaction schemes.

$[Fe^{III}EDTA]^{-1}/H_2O_2$ Spin-Trapping Reaction Mechanism

In order to model the DMPO-OH concentration curves, the reaction mechanism must include a trap decay step. An accurate mechanism must also include the DMPO-OH/$[Fe^{III}EDTA]^{-1}$ complex equilibrium since this lowers the total spin adduct concentration and also slows the peroxide decomposition rate by lowering the available $[Fe^{III}EDTA]^{-1}$.

In addition to spin adduct production, the reaction mechanism must accommodate the observed peroxide decay rate in the presence of DMPO. Table 3-6 shows that peroxide consumption in the presence of DMPO has an average first order rate constant of $1.2 \pm 0.3 \times 10^{-4}$ s^{-1} at pH 9.0 and 30°C which is independent of DMPO concentration in the 0.001 to 0.10 M range. DMPO-OH production curves show a similar lack of dependence on spin trap concentration over the same range concentration range (see Table 3-7).

The Walling et al.[41] mechanism obviously cannot be simply adapted, as attempted in Figure 4-4, to model spin-trapping experiments. It is desirable therefore to develop a predictive reaction mechanism which can account for the experimental observations. The complexity of the $[Fe^{III}EDTA]^{-1}/H_2O_2$ reaction has been previously discussed, and, in light of this discussion, numerous possible reaction steps are available for consideration. Initial attempts to model the experimental results are based on the mechanism in Figure 4-1 since it is consistent with peroxide decomposition observations in the presence of spin traps or other organic substrates.

A simple model including only H_2O_2 decomposition, DMPO-OH production and DMPO-OH decay is shown in the first 6 steps of Figure 4-6. Partial success with this scheme was achieved by adjustment of the rate constants as indicated in Figure 4-6 and required the addition of the catalyst decay

$$[Fe^{III}EDTA]^{-1} + H_2O_2 \longrightarrow [Fe^{II}EDTA]^{-2} + H^+ + HO_2\cdot \quad (a)$$

$$[Fe^{II}EDTA]^{-2} + H_2O_2 \longrightarrow O_x + OH^- \quad (m)$$

$$O_x + H_2O_2 \longrightarrow H_2O + HO_2\cdot + [Fe^{III}EDTA]^{-1} \quad (n)$$

$$HO_2\cdot + [Fe^{III}EDTA]^{-1} \longrightarrow [Fe^{II}EDTA]^{-2} + H^+ + O_2 \quad (d)$$

$$O_x + DMPO \longrightarrow DMPO\text{-}OH + [Fe^{III}EDTA]^{-1} \quad (o)$$

$$DMPO\text{-}OH \longrightarrow Prods. \quad (p)$$

$$[Fe^{III}EDTA]^{-1} \longrightarrow i[Fe^{III}EDTA]^{-1} \quad (q)$$

Figure 4-6. Mechanism attempting to model DMPO-OH and H_2O_2 behavior in the $[Fe^{III}EDTA]^{-1}/H_2O_2$ reaction. $k_a = 0.05\ M^{-1}s^{-1}$; $k_p = 5 \times 10^{-3}\ s^{-1}$; $k_q = 2 \times 10^{-4}\ s^{-1}$.

step (q). A slow catalyst consumption step reflects any processes that may result in a decrease in the available $[Fe^{III}EDTA]^{-1}$. This step may also reflect any other unknown inhibition reaction that is not accounted for. One such process that was mentioned previously is the release of iron as EDTA is degraded by the oxidative intermediate. At the pH values used for this study, free iron precipitated as hydroxides. The occurrence of this process is mentioned by Walling et al.[41] but was not observed during the time course of the current experiments. There may be other processes occurring that render $[Fe^{III}EDTA]^{-1}$ catalytically inactive.

The best fit that can be obtained with the Figure 4-6 scheme is shown in Figure 4-7. This scheme closely models the experimental peroxide decomposition and produces the correct DMPO-OH curve shape. However, the maximum concentration of the DMPO-OH is too high, and the t_{max} (time at which maximum concentration is reached) and t_{dk} (time at which complete decay has occurred) values are much longer than observed experimentally. The mechanism was thus expanded (Figure 4-8) to include the DMPO-OH/$[Fe^{III}EDTA]^{-1}$ complex equilibrium (steps r and s) and the additional propagation step proposed by Walling et al.[41] (step t). The peroxide and DMPO-OH curves in Figure 4-9 show that this step with various rate constants (10^{-5} to 10^{9} $M^{-1}s^{-1}$) did scheme (Figure 4-8) more accurately models H_2O_2

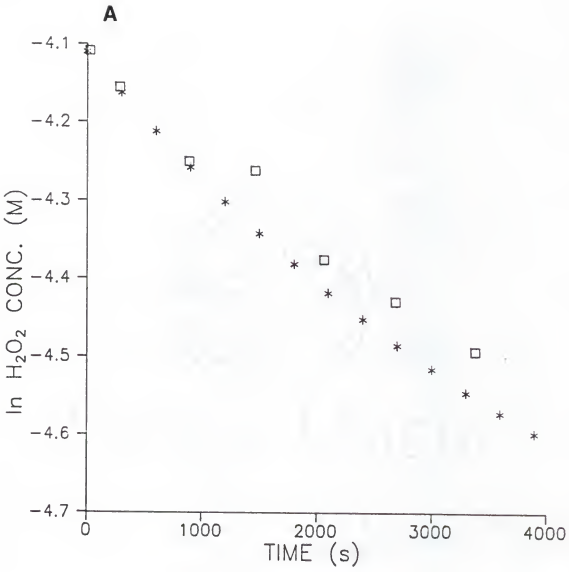

Figure 4-7. Simulations of the Figure 4-6 mechanism. A. Peroxide decomposition: * simulation; □ experimental. B. DMPO-OH production.

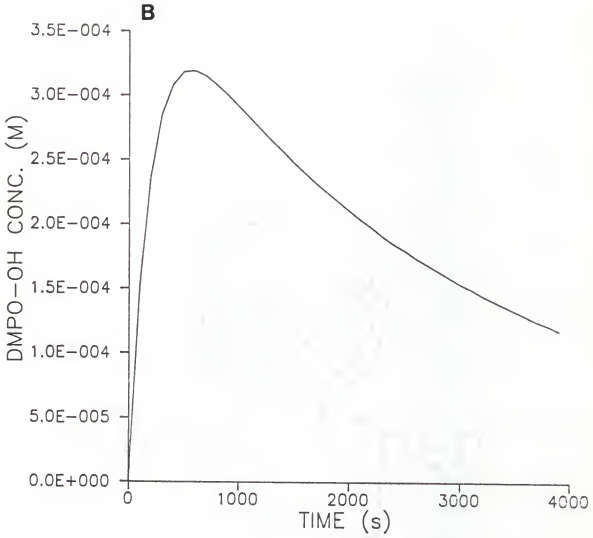

Figure 4-7--continued

$$[Fe^{III}EDTA]^{-1} + H_2O_2 \longrightarrow [Fe^{II}EDTA]^{-2} + H^+ + HO_2\cdot \quad (a)$$

$$[Fe^{II}EDTA]^{-2} + H_2O_2 \longrightarrow O_x + OH^- \quad (m)$$

$$O_x + H_2O_2 \longrightarrow H_2O + HO_2\cdot + [Fe^{III}EDTA]^{-1} \quad (n)$$

$$HO_2\cdot + [Fe^{III}EDTA]^{-1} \longrightarrow [Fe^{II}EDTA]^{-2} + H^+ + O_2 \quad (d)$$

$$O_x + DMPO \longrightarrow DMPO\text{-}OH + [Fe^{III}EDTA]^{-1} \quad (o)$$

$$DMPO\text{-}OH \longrightarrow Prods. \quad (p)$$

$$[Fe^{III}EDTA]^{-1} \longrightarrow i[Fe^{III}EDTA]^{-1} \quad (q)$$

$$[Fe^{III}EDTA]^{-1} + DMPO\text{-}OH \longrightarrow C \quad (r)$$

$$C \longrightarrow [Fe^{III}EDTA]^{-1} + DMPO\text{-}OH \quad (s)$$

$$[Fe^{III}EDTA]^{-1} + O_x \longrightarrow [Fe^{II}EDTA]^{-2} \quad (h)$$

Figure 4-8. Alteration of the Figure 4-6 mechanism.

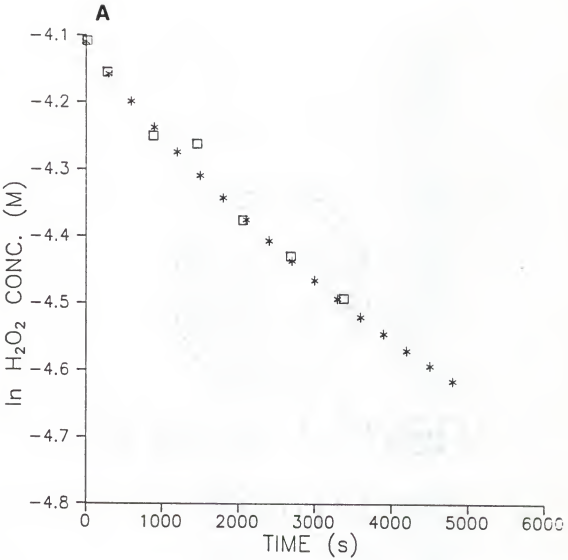

Figure 4-9. Simulations of the Figure 4-8 mechanism. A. Peroxide decomposition: * simulation; □ experimental. B. DMPO-OH production.

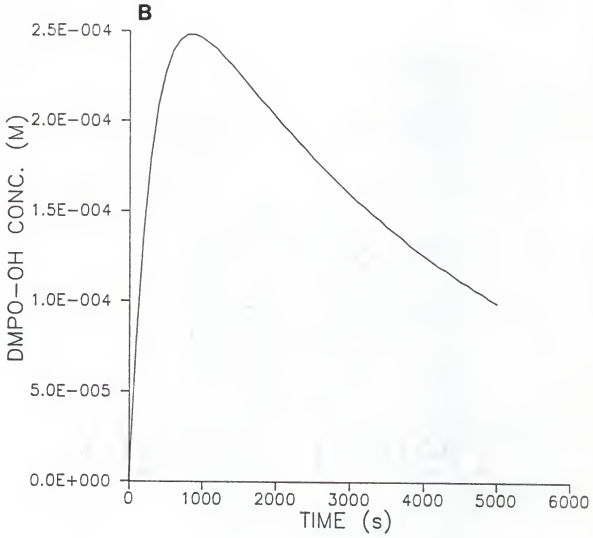

Figure 4-9--continued

decomposition but again is unsuccessful at reproducing the experimental DMPO-OH curves.

Since DMPO-OH decay is attributed to reaction with intermediates, the first order decay step in the above mechanisms was replaced by reactions involving the intermediates. $[Fe^{II}EDTA]^{-2}$ or $HO_2\cdot$ are the most likely candidates for DMPO-OH reaction so equations 4-16 and 4-17

$$[Fe^{II}EDTA]^{-2} + \text{DMPO-OH} \longrightarrow \text{DT} \qquad (4\text{-}16)$$

$$HO_2\cdot + \text{DMPO-OH} \longrightarrow \text{DT} \qquad (4\text{-}17)$$

were included in the mechanism (DT = "dead" trap, no EPR signal). However, inclusion of one or both of these steps in place of or in addition to the first order DMPO-OH decay not reproduce the experimental curves.

In addition to attempts to modify the Walling et al.[41] mechanism, other schemes based on different combinations of reasonable steps were explored. The rational for developing these schemes was to choose the simplest combinations of possible steps for the peroxide decomposition and DMPO-OH generation. Then DMPO-OH decay step(s) and $[Fe^{III}EDTA]^{-1}$ binding equilibrium were added. The steps for these schemes were taken from the many potential reactions proposed by Richter, Walling and others for iron/peroxide systems. None of these schemes, however, was able to model the experimental observations.

Returning to the Figure 4-8 scheme, it is found that although the peroxide decomposition is accurately modeled, the rate of peroxide decay still shows a small change as trap concentration is varied (see k_{1st} values in Table 4-1). Elimination of step (h) in the Figure 4-8 mechanism decreases the influence of trap concentration on k_{1st} values (Table 4-1). Removal of both step (h) and step (m) from the Figure 4-8 mechanism yields the mechanism shown in Figure 4-10. Simulation of the Figure 4-10 mechanism results in a peroxide decomposition rate that is independent of trap concentration (Table 4-1), which is consistent with experimental observations for peroxide decomposition in the presence of DMPO (Table 3-6).

It is significant that both steps that were removed from Figure 4-8 involve the reactive intermediate O_x. The k_{1st} values for simulations at high trap concentration (DMPO = 0.10 M) do not change when steps (h) and (m) are absent because at high trap concentration these steps are not competitive with the O_x/DMPO reaction (step(o)). At lower trap concentrations, steps (h) and (m) become competitive with step (o). The elimination of step (h) results in less rate acceleration as trap concentration is decreased, as shown in Table 4-1. When step (m) is removed,the trap concentration dependence is no longer seen. This effect can be explained by referring to the Figure 4-1 mechanism rate law (equation 4-5). In this equation the

$$[Fe^{III}EDTA]^{-1} + H_2O_2 \longrightarrow [Fe^{II}EDTA]^{-2} + H^+ + HO_2\cdot \quad (a)$$

$$[Fe^{II}EDTA]^{-2} + H_2O_2 \longrightarrow O_x + OH^- \quad (m)$$

$$HO_2\cdot + [Fe^{III}EDTA]^{-1} \longrightarrow [Fe^{II}EDTA]^{-2} + H^+ + O_2 \quad (d)$$

$$O_x + DMPO \longrightarrow DMPO\text{-}OH + [Fe^{III}EDTA]^{-1} \quad (o)$$

$$DMPO\text{-}OH \longrightarrow Prods. \quad (p)$$

$$[Fe^{III}EDTA]^{-1} \longrightarrow i[Fe^{III}EDTA]^{-1} \quad (q)$$

$$[Fe^{III}EDTA]^{-1} + DMPO\text{-}OH \longrightarrow C \quad (r)$$

$$C \longrightarrow [Fe^{III}EDTA]^{-1} + DMPO\text{-}OH \quad (s)$$

Figure 4-10. An accurate mechanism for H_2O_2 decomposition. $k_n = 2.65 \times 10^7\ M^{-1}s^{-1}$; $k_d = 1.3 \times 10^8\ M^{-1}s^{-1}$; $k_p = 5 \times 10^{-3}\ s^{-1}$.

Table 4-1. k_{1st} rate constants for peroxide decay from simulations of: (A). The Figure 4-8 mechanism; (B). The Figure 4-8 mechanism without step (h); (C). The Figure 4-8 mechanism without steps (h) and (m) (Figure 4-10), at different DMPO concentrations.

	k_{1st} (s^{-1})		
[DMPO]	(A)	(B)	(C)
0.10 M	1.02×10^{-4}	1.02×10^{-4}	1.02×10^{-4}
0.01 M	1.10×10^{-4}	1.05×10^{-4}	1.02×10^{-4}
0.005 M	1.29×10^{-4}	1.12×10^{-4}	1.02×10^{-4}

$k_c[H_2O_2]/k_e[RH]$ term approaches zero as RH concentration increases. At high RH concentration the $k_c[H_2O_2]/k_e[RH]$ term drops out and the rate becomes independent of RH concentration. In the spin trap case, when the analogous step, (n), is removed from the Figure 4-8 mechanism, $k_n[H_2O_2]$ drops out, and the $k_n[H_2O_2]/k_o[DMPO]$ term becomes $1/k_o[DMPO]$. The term $1/k_o[DMPO]$ is very small even at low trap concentrations ($k_o = 3.4 \times 10^9\ M^{-1}\ s^{-1}$).[19] Thus the reaction rate becomes independent of trap concentration in the absence of step (n).

The Figure 4-10 mechanism, by the elimination of steps (h) and (n) (Figure 4-8), reproduces the experimental peroxide decomposition in the presence of spin traps. However, the increase in decomposition rate that is predicted by the Figure 4-8 mechanism as DMPO concentration decreases from 0.10 to 0.005 M is only 21%. This change is too small to be detected by the method of the current study. It can be concluded that the participation of steps (h) and (n) is minimal under the current conditions and it is therefore reasonable to leave them out of the reaction scheme. Since the rate constant used for step (n) is that of the hydroxyl radical with peroxide, it can also be concluded that the reaction O_x with peroxide does not occur at a rate greater than that of $OH\cdot$ with peroxide (2.65×10^7).[41] If step (n) were occurring at a higher rate,

a peroxide decomposition dependence on trap concentration should be measurable experimentally.

The fit of a simulated first order peroxide decomposition line (using the Figure 4-10 scheme) to the experimental data is shown in Figure 4-11. The average experimental k_{1st} for peroxide decomposition was $1.2 \pm 2.5 \times 10^{-4}$ s^{-1}. Using a k_a value of 0.05 $M^{-1}s^{-1}$ the simulation of Figure 4-10 gave a k_{1st} constant of 1.1×10^{-4} s^{-1}. The simulated rate constant varies as k_a is changed without affecting the appearance of the decay plot. This mechanism also reproduces the experimental observations as the initial concentration of DMPO is varied. Simulations with DMPO concentrations of 0.10 M and 0.01 M give identical peroxide decay curves (Figure 4-12) (A limitation of the simulation program would not allow 0.001 M DMPO to be modeled, but 0.005 M gave identical results) successfully replicating the experimental observation of little or no change in peroxide decay rate as DMPO concentration was varied.

Though the mechanism in Figure 4-10 models the peroxide decomposition accurately, it is not correct for DMPO-OH production and decay. The DMPO-OH curve produced by simulation of this scheme is shown in Figure 4-13. The simple first order decay step included in the reaction does not

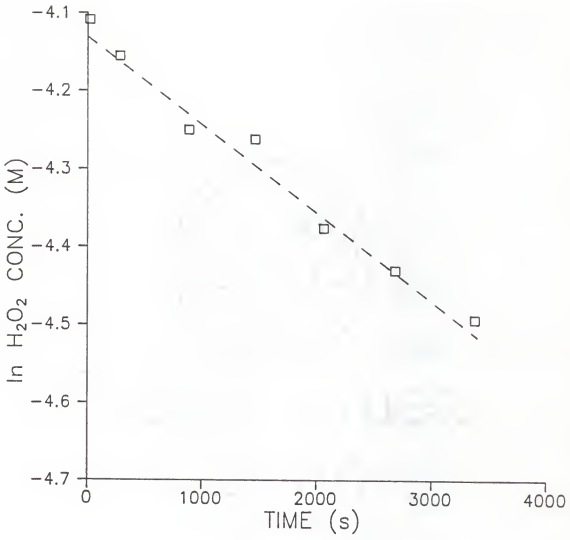

Figure 4-11. Figure 4-10 mechanism fit of simulated peroxide decomposition data to experimental data. □ Experimental data points. ---- Simulated best fit line.

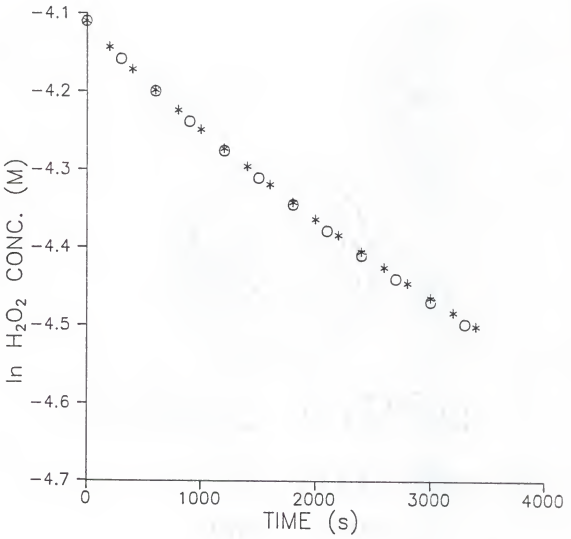

Figure 4-12. Invariance of peroxide decomposition to trap concentration using the Figure 4-10 mechanism. * 0.10 M trap; o 0.01 M trap.

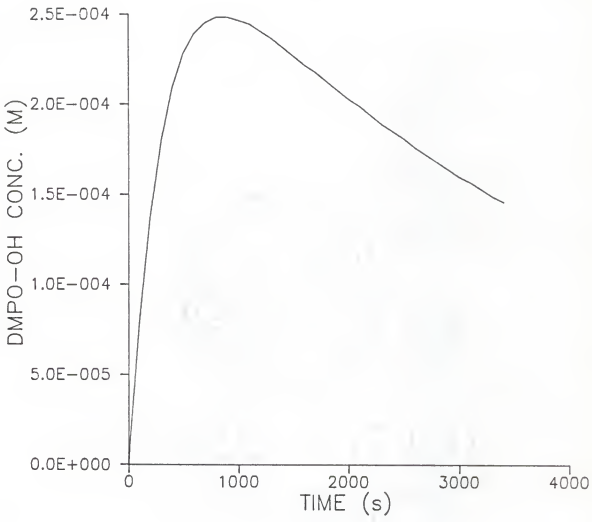

Figure 4-13. DMPO-OH production curve from the Figure 4-10 mechanism.

replicate the DMPO-OH decay necessary to reproduce the experimental DMPO-OH curves. With $k_p = 5 \times 10^{-3}$ s^{-1} the maximum DMPO-OH concentration is too high and decreases too slowly. The proper DMPO-OH curve cannot be obtained by simply increasing the k_p value. As before (equations 4-16 and 4-17), reactions of DMPO-OH with $[Fe^{II}EDTA]^{-2}$ or $HO_2\cdot$ do not produce successful models.

Since H_2O_2 decay is accurately modeled by the Figure 4-10 scheme it is assumed that the DMPO + O_x step is correct, and thus DMPO-OH production is correctly modeled. More information about the decay step is necessary to model the observed DMPO-OH curves. Analysis of DMPO-OH production using kinetic simulations was undertaken to provide information about the nature of the DMPO-OH decay process necessary to reproduce the experimental curves.

Simulated DMPO-OH production using the Figure 4-10 mechanism without the DMPO-OH decay step (p) is shown in Figure 4-14. The production curve is almost linear over the time studied with a psuedo zero order rate constant of 1.2×10^{-6} M s^{-1}. Therefore, a zero order decay step with a similar rate constant is necessary to reproduce the experimental DMPO-OH curve.

The mechanism in Figure 4-10 was altered by adding a zero order DMPO-OH decay step with a rate constant of 1.2×10^{-6} M s^{-1} (Figure 4-15). The simulated DMPO-OH concentration plot using the Figure 4-15 mechanism is shown

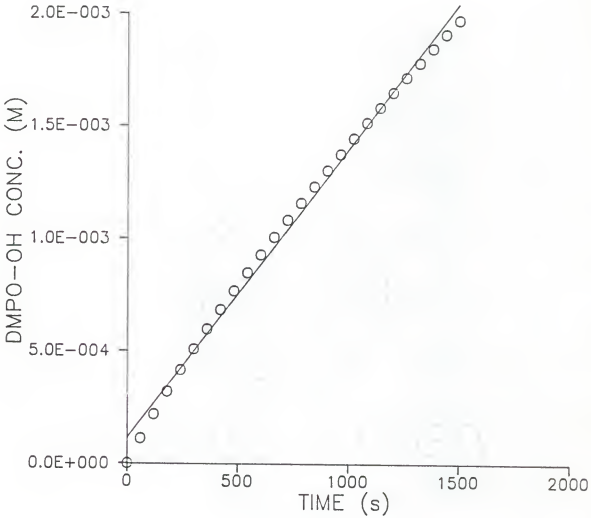

Figure 4-14. DMPO-OH production curve using the Figure 4-10 scheme without the DMPO-OH decay step (p).

$$[Fe^{III}EDTA]^{-1} + H_2O_2 \longrightarrow [Fe^{II}EDTA]^{-2} + H^+ + HO_2\cdot \quad (a)$$

$$[Fe^{II}EDTA]^{-2} + H_2O_2 \longrightarrow O_x + OH^- \quad (m)$$

$$HO_2\cdot + [Fe^{III}EDTA]^{-1} \longrightarrow [Fe^{II}EDTA]^{-2} + H^+ + O_2 \quad (d)$$

$$O_x + DMPO \longrightarrow DMPO\text{-}OH + [Fe^{III}EDTA]^{-1} \quad (o)$$

$$[Fe^{III}EDTA]^{-1} \longrightarrow i[Fe^{III}EDTA]^{-1} \quad (q)$$

$$[Fe^{III}EDTA]^{-1} + DMPO\text{-}OH \longrightarrow C \quad (r)$$

$$C \longrightarrow [Fe^{III}EDTA]^{-1} + DMPO\text{-}OH \quad (s)$$

$$DMPO\text{-}OH + cat. \longrightarrow Prod. \quad (t)^*$$

$$Prod. \longrightarrow cat. \quad (u)^*$$

* Steps t an u comprise a catalytic cycle resulting in psuedo zero order decay of DMPO-OH at a rate of 1.2×10^{-6} Ms^{-1}

Figure 4-15. Inclusion of a catalytic DMPO-OH decay cycle (steps t and u) in the Figure 4-10 mechanism. $k_a = 0.044$ $M^{-1}s^{-1}$; $k_t = 5 \times 10^2$ $M^{-1}s^{-1}$; $k_u = 1 \times 10^6$ s^{-1}.

in Figure 4-16. The curve very closely models the experimental data and is consistent with DMPO-OH decay by a psuedo zero order process. The k_a value was adjusted down to 0.044 $M^{-1}s^{-1}$ to maintain the accuracy of the simulated H_2O_2 decomposition curve which is also shown in Figure 4-16.

There is no precedent for the zero order decay of DMPO-OH. Previous studies[12,19,21,26] all indicate that DMPO-OH decay is first order, and, based on the TEMPO decay curve (Figure 3-10) observed in the $[Fe^{III}EDTA]^{-1}/H_2O_2$ reaction, DMPO-OH decay is expected to be first order in the current studies also. Psuedo zero order decay could not be achieved by simulations of simple reactions involving the known reaction intermediates $[Fe^{II}EDTA]^{-2}$ and superoxide.

One pathway leading to psuedo zero order trap decay might be the involvement of a spin adduct decay step in a simple catalytic cycle (equation 4-18). Zero order decay

$$\begin{aligned} \{\text{iron/peroxide reaction}\} &\longrightarrow \text{cat., DMPO-OH, etc.} \\ \text{DMPO-OH} + \text{cat.} &\longrightarrow \text{product} \\ \text{product} &\longrightarrow \text{cat.} \end{aligned} \qquad (4\text{-}18)$$

in such a cycle can be demonstrated by simulations of equation 4-18. These simulations show that in order to achieve the zero order decay rate necessary to model the observations of the current study (1.2×10^{-6} M s^{-1}) psuedo zero order cat. production must occur at a rate of 7×10^{-9} M s^{-1}. The rate constants of the DMPO-OH + cat.

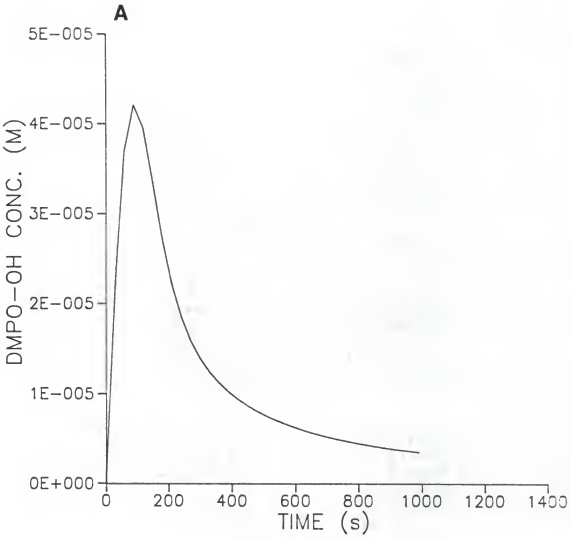

Figure 4-16. Simulation of the Figure 4-15 mechanism. A. DMPO-OH curve. B. H_2O_2 decomposition curve, * ---- simulation; o ——— experimental

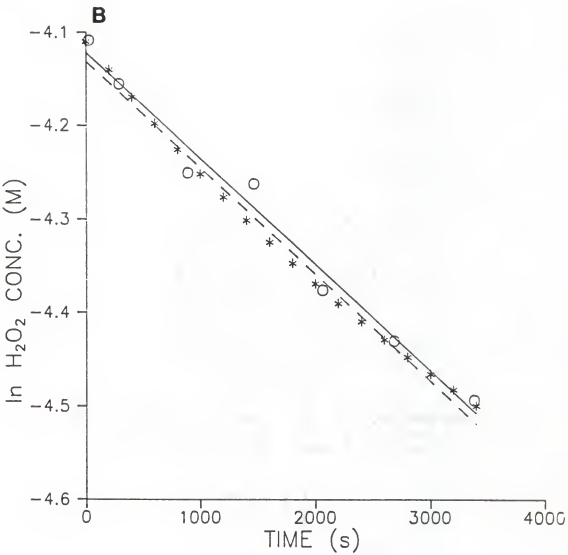

Figure 4-16--continued

step, and the product ⟶ cat. step, must then be 5×10^2 $M^{-1}s^{-1}$ and 1×10^6 s^{-1}, respectively. The nature of the reactive intermediate that might be involved in such a catalytic cycle in the current experiment cannot be determined from the available data. Alternatively, pseudo zero order DMPO-OH decay could be achieved by a fixed catalyst concentration, where the catalyst is saturated by DMPO-OH (equation 4-19). In this instance -[DMPO-OH]/dt

$$\text{DMPO-OH} + \text{cat.} \longrightarrow \{\text{DMPO-OH-cat.}\}$$
$$\{\text{DMPO-OH-cat.}\} \longrightarrow \text{prod.} + \text{cat.} \qquad (4\text{-}19)$$

reduces to k[cat.]. The cat. concentration is constant so the decay would be pseudo zero order. reaction sequences may be involved in the DMPO-OH decay reaction.

The mechanism in Figure 4-15 is consistent with experimental observations for both H_2O_2 decomposition and DMPO-OH production. The types of processes that are occurring in the $[Fe^{III}EDTA]^{-1}/H_2O_2$ reaction in the presence of DMPO are identified in this mechanism. However, the exact molecular steps involved cannot be determined from the available data. This mechanism shows that DMPO is not a non-interfering species in the $[Fe^{III}EDTA]^{-1}/H_2O_2$ but participates in a complex manner that is not completely understood. Significant DMPO-OH decay occurs during the course of the reaction and this decay process is not the simple first order decay that is predicted for DMPO-OH. It

is likely that DMPO-OH decay involves a reaction intermediate and possibly proceeds through a catalytic process.

Proteins in the $[Fe^{III}EDTA]^{-1}/H_2O_2$ Reaction

Peroxide Decomposition

Peroxide decomposition was studied in presence of the protein bovine serum albumin (BSA). BSA is a large protein (molecular weight 65,000 kDa) that is expected to act as an oxidizable substrate and severely retard the rate of peroxide decomposition. However, BSA had no effect on the rate of peroxide decomposition in the $[Fe^{III}EDTA]^{-1}/H_2O_2$ reaction. This observation implies that BSA is not attacked by the reaction intermediate or that a balance of propagating and terminating reactions occur with BSA. It seems unlikely that a hydroxyl radical intermediate would not react with BSA, but a chelated ferryl ion may be sterically inhibited from approaching a BSA reaction site by the bulk of the protein. It seems more likely, that the intermediate reacts with some sites on BSA resulting in propagation and with other sites resulting in termination.

DMPO-OH Production

The effect of a protein on DMPO-OH production in the $[Fe^{III}EDTA]^{-1}/H_2O_2$ reaction was studied using the metalloprotein metallothionein. Metallothionein is a small

protein (molecular weight 6500 g) which is unique because of its high sulfur content (21 S atoms per mole). Twenty of the sulfur atoms occur in cysteine amino acid residues and are used to bind 7 metal atoms, usually cadmium and zinc into two metal thiolate clusters.[35] The protein was chosen for study because it has been suggested that metallothionein has a possible role as a radical scavenging protein.[35,93] Thornalley and Vasak[35] measured a rate constant of 10^{12} $M^{-1}s^{-1}$ for the reaction of metallothionein with the hydroxyl radical using competition kinetic techniques with the spin trap DMPO. This rate constant is two orders of magnitude greater than the diffusion limit and thus seems impossibly high.

The results of DMPO-OH production measurements in the presence of metallothionein in the current study suggest that metallothionein does not act as a radical scavenger and that the large rate constant that was determined by Thornalley and Vasak[35] is in error. Figure 3-8 shows that while 12 μM ethanol ($k_{OH\cdot}$ = 1 X 10^9 $M^{-1}s^{-1}$)[94] slightly retards the rate of DMPO-OH formation, metallothionein appears to increase the rate of formation. If the experimental error of the technique is considered the metallothionein, ethanol and no substrate plots do not differ significantly (also, only one trial of this experiment was performed), so it cannot be definitely concluded that metallothionein accelerates the rate of DMPO-

OH formation. However, if metallothionein scavenges hydroxyl radical at the rate of 10^{12} $M^{-1}s^{-1}$, there should be a dramatic decrease in the DMPO-OH formation rate when metallothionein is included in the reaction mixture. Clearly, metallothionein did not behave as a highly reactive scavenger in the current study.

In light of the potential complications of spin-trapping studies, the observed decrease in DMPO-OH production when metallothionein was present may reflect accelerated DMPO-OH decay or signal quenching due to interaction of the spin adduct with the protein. The Thornalley and Vasak[35] rate constant determinations were made in a H_2O_2, UV photolysis radical generating system. The pH was controlled with phosphate buffer and DTPA was included to sequester metal impurities. The presence of DTPA is not sufficient to eliminate the reaction of iron impurities with peroxide, so iron/peroxide reactions could be a source of error. Obviously, without further information on DMPO-OH behavior in the Thornalley and Vasak[35] reaction system, it is not acceptable to attribute the observed decrease in DMPO-OH formation solely to radical scavenging by metallothionein.

CHAPTER 5
CONCLUSIONS

The $[Fe^{III}EDTA]^{-1}/H_2O_2$ reaction was evaluated as a radical-generating system for spin-trapping studies using the spin trap DMPO. This reaction was chosen as a hydroxyl radical-generating system, and the formation and decay of the DMPO-OH spin adduct was monitored via EPR spectroscopy. Of primary interest in this study was the characterization of DMPO as a spin trap in an *in vitro* radical-producing reaction.

DMPO is widely used to detect radicals under a variety of *in vitro* and *in vivo* conditions. Standard precautions have been established for spin-trapping experiments, and if these guidelines are followed, the technique is considered relatively straightforward. Upon preliminary investigation using the $[Fe^{III}EDTA]^{-1}/H_2O_2$ reaction, DMPO performed as expected: the DMPO-OH spin adduct was readily observed; the concentration was determined by double integration of the EPR spectral peaks; and DMPO-OH production curves were nearly linear over the first few minutes of the reaction. According to the accepted verification measures, DMPO-OH formation was legitimate and confirmed the presence o hydroxyl radicals as intermediates in the reaction.

However, a closer examination of this spin-trapping system revealed complications that were not identified or eliminated by following the standard experimental spin-trapping precautions, and that may lead to erroneous results and conclusions.

Although the results of the current study apply specifically to the $[Fe^{III}EDTA]^{-1}/H_2O_2$ reaction, similar in vitro and in vivo reaction mixtures are often studied. The conclusions of this study may therefore apply specifically to the spin-trapping technique in various applications where iron and/or peroxide are present. Even for applications where the current results are not directly applicable, the findings of this study identify the errors that might occur in spin-trapping systems. The observations of the current study allowed the identification of basic considerations which must be taken into account in any spin-trapping study. These observations are reviewed below in light of the potential interpretation errors that might arise in spin-trapping studies if these considerations are neglected.

(1) The first consideration must be the origin of the spin adduct formation: Does DMPO-OH formation result from the reaction of the hydroxyl radical with DMPO? Although adventitious DMPO-OH production was ruled out in the $[Fe^{III}EDTA]^{-1}/H_2O_2$ experiments, DMPO-OH production does not prove the existence of hydroxyl radicals in the reaction system. The iron catalyzed decomposition of peroxide may

proceed via either a hydroxyl radical, a high valent iron intermediate, or by some other pathway. The identity of the critical intermediate(s) has not been proven conclusively in the literature. The results of the current study are also inconclusive on this point. It is therefore appropriate in the iron/peroxide system to recognize the formation of a highly reactive oxidizing intermediate that can be detected via reaction with DMPO to form DMPO-OH. However, it is not appropriate to assume that the legitimate formation of DMPO-OH conclusively proves the presence of hydroxyl radicals in the reacting system.

The possibility that legitimate DMPO-OH formation does not prove the existence of hydroxyl radicals must be considered as a general precaution for spin-trapping studies. Spin-trapping investigations (both *in vitro* and *in vivo*) often attempt to determine if hydroxyl radicals are produced under the conditions of interest. This approach may be useful for *in vitro* experiments in simple systems where all other DMPO-OH forming species can be ruled out. However, *in vivo* environments are obviously more complex than the reaction system of the current study, and under conditions where radical formation is postulated iron and peroxide are likely to be present. Thus, even assuming that all adventitious DMPO-OH formation can be ruled out (which

is difficult to accomplish), DMPO-OH formation may not necessarily prove the existence of free hydroxyl radicals in the system of interest.

(2) The stability of the DMPO-OH adduct is another major consideration. Rapid DMPO-OH decay was an unexpected complication in the $[Fe^{III}EDTA]^{-1}/H_2O_2$ reaction. DMPO-OH decay is greatly accelerated in the reacting system. This accelerated decay is not unique to DMPO-OH but also occurs with the stable nitroxide spin label TEMPO. From these limited studies, it appears that the accelerated decay is a general phenomenon for nitroxides in the $[Fe^{III}EDTA]^{-1}/H_2O_2$ reaction.

The findings of the current study emphasize that literature DMPO-OH decay rates cannot be assumed to be generally applicable. Spin adduct decay rates must be measured for each different spin trapping environment. Two major errors in interpretation may result from unexpectedly rapid spin adduct decay. First, if no spin adduct is observed, the absence of radical species may be concluded while in fact radical species are present but are not observed due to rapid spin adduct decay. Secondly, kinetic competition experiments require accurate rate measurements for DMPO-OH formation. Rapid spin adduct decay may not be suspected if nearly linear production is observed during the first few minutes of the reaction. Spin adduct production in these studies is typically only monitored for the first 1

to 5 minutes of the reaction.[19,35] Though linear, these initial curves will reflect both production and decay processes. Production rates taken directly from these curves are thus likely to be in error. The metallothionein study by Thornalley and Vasak[35] (discussed previously) is an example of a spin-trapping kinetic-competition study. The metallothionein rate constant for reaction with hydroxyl radical is questionably high and inconsistent with observations of the current study. Rapid spin adduct decay may be a source of error in the Thornalley and Vasak[35] study since DMPO-OH decay rates were not determined for the reaction conditions under study.

(3) The quenching of the DMPO-OH EPR signal in the presence of $[Fe^{III}EDTA]^{-1}$ is another unexpected observation of the current study. Because of this phenomenon, DMPO-OH concentration measurements (in the presence of $[Fe^{III}EDTA]^{-1}$) based on double integration of EPR spectral peaks do not reflect the actual spin adduct concentration. It is apparent that spin-adduct signal quenching complexes may form with other species in different spin-trapping environments. The errors in quantitative spin trapping studies due to unanticipated spin-adduct signal quenching are apparent. In qualitative studies, EPR signal-quenching complex formation may again result in negative spin adduct observation where radicals are in fact present.

(4) An initial aim of the current study was to determine the rate of the intermediate oxidant formation by assuming, based on published reaction mechanisms, that the rate of DMPO-OH formation was equal to the rate of O_x formation. Obviously, in light of the unexpected DMPO-OH behavior in the $[Fe^{III}EDTA]^{-1}/H_2O_2$ reaction, the rate of intermediate oxidant formation cannot be determined directly from the rate of DMPO-OH formation. Although the mechanism for the system is apparently adequate for prediction of peroxide decomposition, even in the presence of DMPO, spin adduct quantification cannot be achieved from this scheme.

For spin adduct studies in general it is necessary to confirm that mechanisms for reaction used as radical-generating systems are applicable in the presence of spin traps. Free radical and spin adduct formation are often evaluated on the basis of reaction mechanisms that have not been derived specifically for the system of interest. Existing mechanisms may be applicable, but their accuracy must be verified. Conclusions from quantitative spin-trapping studies based on mechanisms that have not been proven valid in the presence of the spin trap are suspect and must be viewed with caution.

In conclusion, it is apparent that spin trapping is not as simple and straightforward as would be assumed from its wide use as a semiquantitative method of radical quantification. Although standard precautions have been

established, this work shows that most studies require more rigorous measures to insure that their conclusions are valid. Many studies that have been published to date have not taken the necessary measures to validate their results. The conclusions from these studies may therefore be inaccurate due to unexpected and undetected complications in spin trap or spin adduct behavior. The considerations pointed out in the current study should be kept in mind when planning spin-trapping experiments and evaluating the results of literature spin-trapping studies.

Spin trapping remains a powerful and valuable technique for the study of free radical reactions. In order for the full potential of the spin-trapping technique to be realized, extensive in vitro investigations of spin trapping in radical generating systems under biochemically relevant conditions are necessary The observations of the current study stress the importance of this kind of research.

Radical reactions in biological systems are a reality that require serious attention. The many diseases and disorders that are attributed to radical formation may be prevented by understanding the etiological role of radical reactions. A knowledge of radical defense mechanisms, such as radical scavenging molecules, may allow treatments to be developed that reduce or eliminate the presence of undesirable radical reactions. An understanding of desirable radical reactions and their control may aid in

developing disease prevention and radical elimination treatments. Once completely understood, these desirable reactions could potentially be activated in situations where they could be useful, such as to destroy bacteria, cancerous cells or other undesirable species *in vivo*. Spin-trapping techniques may be the key to unlocking the complexities of biological radical reactions.

APPENDIX A
KINETIC SIMULATIONS

Kinetic simulations were performed by using a computer simulation program provided by Dr. R. J. Hanrahan. The program analyzes the kinetics of a reaction mechanism by numerical integration. The program is capable of handling mechanisms of up to 16 first or second order elementary reaction steps and can be run on any PC that is equipped with a math coprocessor. The program consists of two parts (HICHEM and FCHEM) that are compiled and run separately. HICHEM takes the input mechanism file and generates an output file for use in the second program FCHEM. FCHEM uses the HICHEM output file to generate concentration versus time data for the desired reaction components. This data is displayed on the screen as well as stored in an output file. Descriptions of the input file for HICHEM and the operation of both HICHEM and FCHEM programs follows.

HICHEM Input File

An example of a HICHEM input file is shown below. This file can be created using any word processor but must be saved as a DOS file. The input file must be typed in with no spaces as shown below.

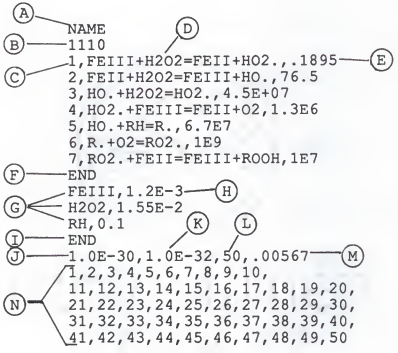

Legend

(A) Name of file, up to 8 characters. (B) Internal flags which control data output. These must not be changed. (C) Reaction step number. (D) Reaction step. Only two reactants and two products are allowed. (E) Rate constants in units of $M^{-1}s^{-1}$ or s^{-1} as appropriate. (F) End of reaction mechanism. (G) ReactantS. (H) Initial reaction concentration. (I) End of concentration input. (J) Initial time increment used for integration. (K) Minimum time increment used for integration. (L) Time increment for data output (in seconds) should be smaller than the time increment specified during operation of the HICHEM program. (M) Internal precision number. (N) These numbers must be included in order to allow output of 50 data points.

HICHEM Program Execution

The HICHEM program is started by typing "HICHEM" and pressing enter. An example of the HICHEM program operation is included below. User input is underlined. All user input must be followed by enter. Program statements are indicated by quotation marks. Comments on program usage are enclosed in brackets.

HICHEM

"HICHEM: DEC, 1908"
"ENTER NAME OF INPUT DATA FILE"
NAME {Use the mechanism data file described above}

"ENTER NAME OF OUTPUT DATA FILE"
NAME {Use the name desired for the FCHEM input file
This name must be different from the name
above}

"INPUT TIME MULTIPLIER, 1.0 OR WHAT?"
100 {Any number greater than one can be used here.
This number determines the time increment
between data points. For instance, if 100
is entered here, concentration values will be
determined at t=0, 100 s, 200 s, etc. This
number must be greater than (usually 2 times)
than the number in item (L) of the mechanism
input file shown above.}

"INPUT TIME ADD AMOUNT, 0 OR WHAT?"
0 {This number determines the time at which
the first data point will be calculated.
Fifty data points will be generated
incremented by the time specified previously
beginning with time specified here. For
example
if 25 is entered here then points will be
generated at t=25 s, 125 s, 225 s etc.}

"MECHANISM MATRIX JS(I,K)"

{The mechanism matrix is displayed here and the program
execution terminates}

FCHEM Program Execution

FCHEM generates the concentration versus time data points using the output file from HICHEM. The data is stored in an output file which can be imported into spread sheet or plotting programs. Program execution is started by typing "FCHEM" and pressing enter. The program prompts for all input just as in HICHEM. The prompts are self-explanatory and are thus not included here. An example of a FCHEM output file is shown below. This file was generated using a time increment of 100 and a time add of 0. Column 1 is the time. The other columns are concentrations of the species specified in the FCHEM program.

FCHEM Output File

```
  .000E+00    1.640E-02    1.000E-30
 1.000E+02    1.615E-02    4.190E-05
 2.000E+02    1.591E-02    2.362E-05
 3.000E+02    1.568E-02    1.385E-05
 4.000E+02    1.545E-02    9.856E-06
 5.000E+02    1.523E-02    7.622E-06
 6.000E+02    1.502E-02    6.190E-06
     |            |            |
     |            |            |
     |            |            |
     |            |            |
     |            |            |
 4.800E+03    1.007E-02    3.879E-07
 4.900E+03    1.001E-02    3.744E-07
 5.000E+03    9.955E-03    3.615E-07
```

APPENDIX B
RATE CONSTANTS FOR ELEMENTARY REACTION STEPS

The rate constants used in computer simulations were taken from different sources in which constants were either measured under a variety of conditions or were estimated. Literature rate constants were varied if necessary, and where literature values were not available, rate constants were estimated. The rate constants listed here are, at best, approximations of the true rate constants under the current experimental conditions, but are reasonable values that allow succesful computer simulation of the experimental observations. Temperature and pH data are given where available. These rate constants were used in all computer simulations unless otherwise noted in the text. Where more than one rate constant is listed, the one used in kinetic simulations is denoted by an asterisk.

Step	Rate Constant*	Source	Comments
(a)	*0.18	41	pH 9.0, t 30° C
	0.002	73	pH 1.7, t 30° C
(b)	76.5	73	used for calcs. imef. 74 for pH 1.7 and t 30° C.
(c)	4.5×10^7	73	
	*2.65×10^7	41	
(d)	1.3×10^6	95	
(e)	6.7×10^7	41	Acetone
	5.7×10^8	41	t-BuOH
	2.76×10^9	41	EDTA
(f)	10^9	--	estimated
(g)	10^7	--	estimated
(h)	2.76×10^9	41	
(i)	----	41	$K = 3.65 \times 10^{-5}$, 20° C
(j)	----	--	unknown
(k)	$3.2\ s^{-1}$	67	pH 2.6, t 27° C
(l)	----	--	unknown
(m)	----	--	used step (b) value
(n)	----	--	used step (c) value
(o)	3.4×10^9	19	pH 7.4, t 20° C
(p)	5×10^{-3}	--	estimated
(q)	2×10^{-4}	--	estimated
(r)	1×10^3	--	estimated
(s)	$1\ s^{-1}$	--	estimated
(t)	5×10^2	--	estimated
(u)	1×10^6	--	estimated

* $M^{-1}s^{-1}$ unless otherwise indicated.

REFERENCES

1. Ihde, A. J., Pure and Applied Chemistry, 1967, 15, 1.

2. Dumas, J. B. A.; Boullay, P., Ann. Chim., 1828, 37, 15.

3. Gomberg, M., J. Am. Chem. Soc., 1900, 22, 757.

4. Gilbert, D. L. ed. Oxygen and Living Processes. An Interdisciplinary Approach. New York: Springer-Verlag, 1981.

5. McCord, J. M.; Fridovich, I., J. Biol. Chem., 1969, 244, 6049.

6. Halliwell, B., FASEB J., 1987, 1 358.

7. Bolli, R.; Patel, B. S.; Jeroudi, M. O.; Lai, E. K.; McCay, P. B., J. Clin. Invest., 1988, 82, 476.

8. Floyd, R. A., Biochem. Biophys. Res. Comm., 1981, 99, 1209.

9. Floyd, R. A., Can. J. Chem., 1982, 60, 1577.

10. Hill, H. A. O., Phil. Trans. R. Soc. Lond. B, 1985, 311, 605.

11. Koppenol, W. H.; Liebman, J. F., J. Phys. Chem., 1984, 88, 99.

12. Janzen, E. G. In Free Radicals in Biology, Vol. IV; Pryor, W. A., Ed.; New York: Academic Press, 1980; p 115.

13. Williams, R. J. P., Phil. Trans. R. Soc. Lond. B, 1985, 311, 593.

14. Symons, M. C. R., Phil. Trans. R. Soc. Lond. B, 1985, 311, 451.

15. Davies, M. J., Chemistry and Physics of Lipids, 1987, 44, 149.

16. Janzen, E. G., Accounts of Chemical Research, 1971, 4, 31.

17. Aurich, H. G., Can. J. Chem., 1982, 60, 1414.

18. Harbour, J. R.; Chow, V.; Bolton, J. R., Can. J. Chem., 1974, 52, 3549.

19. Finkelstein, E.; Rosen, G. M.; Rauckman, E. J., J. Am. Chem. Soc., 1980, 102, 4994.

20. Castlehano, A. L.; Griller, D.; Ingold, K. U., Can. J. Chem., 1982, 60, 1501.

21. Buettner, G. R., Free Radical Biology & Medicine, 1987, 3, 259.

22. Buettner, G. R.; Oberley, L. W., Biochem. Biophys. Res. Comm., 1978, 83, 69.

23. Finkelstein, E.; Rosen, G. M.; Rauckman, E. J., Molecular Pharmacology, 1979, 16, 676.

24. Marriott, P. R.; Perkins, M. J.; Griller, D., Can. J. Chem., 1980, 58, 803.

25. Finkelstein, E.; Rosen, G. M.; Rauckman, E. J., Archives of Biochemistry and Biophysics, 1980, 200, 1.

26. Buettner, G. R. In Superoxide Dismutase, Vol. II; Oberley, L., Ed.; Boca Raston, FL: CRC Press Inc., 1982.

27. McCay, P. B., Lai, E. K.; Poyer, J. L.; Dubose, C. M.; Janzen, E. G., J. Biol. Chem., 1984, 259, 2135.

28. Poyer, J. L.; McCay, P. B.; Weddle, C. C.; Downs, P. E., Biochemical Pharmacology, 1981, 30, 1517.

29. Lai, E. K.; Crossley, C.; Sridhar, R.; Misra, H. P.; Janzen, E. G.; Mccay, P. B., Archives of Biochemistry and Biophysics, 1986, 244, 156.

30. Kubow, S.; Janzen, E. G.; Bray, T. M., J. Biol. Chem., 1984, 259, 1.

31. Lai, C.; Piette, L. H., Biochem. Biophys. Res. Comm., 1977, 78, 51.

32. Sibille, J.; Doi, K; Aisen, P., J. Biol. Chem., 1987, 262, 59.

33. Floyd, R. A.; Lewis, C. A., Biochemistry, 1983, 22, 2649.

34. Faraggi, M.; Carmichael, A.; Riesz, P., Int. J. Radiat. Biol., 1984, 46, 703.

35. Thornalley, P. J.; Vasak, M., Biochim. Biophys. Acta, 1985, 827, 36.

36. Baxendale, J. H.; Wilson, J. A., Trans. Faraday Soc., 1957, 53, 344.

37. Riesz, P.; Christman, C. L., Federation Proceedings, 1986, 45, 2485.

38. Makino, K; Mossoba, M. M.; Riesz, P. J. Phys. Chem., 1983, 87, 1369.

39. Carmichael, A. J.; Makino, K.; Riesz, P., Radiation Research, 1984, 100, 222.

40. Sargent, F. P.; Gardy, E. M., Can. J. Chem., 1976, 54, 275.

41. Walling, C.; Partch, R. E.; Weil, T., Proc. Nat. Acad. Sci. USA, 1975, 72, 140.

42. Buettner, G. R.; Oberley, L. W.; Leuthauser, S. W., Photochemistry and Photobiology, 1978, 28, 693.

43. Lai, C. S.; Piette, L. H., Tetrahedron Letters, 1979, 9, 775.

44. Sutton, H. C.; Winterbourn, C. C., Archives of Biochemistry and Biophysics, 1984, 235, 106.

45. Hamer, J.; Macaluso, A. Chem. Rev., 1964, 64, 473.

46. Day, Jr., R. A.; Underwood, A. L. Quantitative Analysis, 4th Ed. Englwood Cliffs, New Jersey: Prentice Hall Inc., 1980.

47. Poole, C. P. Electron Spin Resonance. New York: Interscience Publishers, 1967, pp. 776-806.

48. Searle, A. J. F.; Tomas, A. J., Inorganic Biochemistry, 1982, 17, 161.

49. Dressick, W., J. Am. Chem. Soc., 1980, 102, 6227.

50. Johnson, C. R.; Shephered, R. E.; Marr, B.; O'Donnell, S.; Dressick, W., J. Am. Chem Soc., 1980, 102, 6227.

51. Caneschi, A.; Grand, A.; Laugier, J.; Rey, P.; Subra, R., J. Am. Chem. Soc., 1988, 110, 2307.

52. Eaton, S. S.; Eaton, G. R., Coordination Chemistry Reviews, 1988, 83, 29.

53. Wilbur, D.; Kreilick, R., J. Chem. Phys., 1970, 52, 1643.

54. Janzen, E. G.; Wang, Y. Y.; Shetty, R. V., J. Am. Chem. Soc., 1978, 100, 2923.

55. Janzen, E. G.; Nutter, D. E.; Davis, E.R.; Blackburn, B. J., Can. J. Chem., 1978, 56, 2237.

56. Walling, C.; Kurz, M.; Schugar, H. J., Inorg. Chem., 1970, 9, 931.

57. Lind, M. D.; Hamor, M. J.; Hamor, T. A.; Hoard, J. L., Inorganic Chemistry, 1964, 3, 34.

58. Bull, C.; McClune, G. J.; Fee, J. A., J. Am. Chem. Soc., 1983, 105, 5290.

59. Balasubramanian, P. N.; Bruice, T. C., J. Am. Chem. Soc., 1986, 108, 5495.

60. Bray, W. C.; Gorin, M. H., J. Am. Chem. Soc., 1932, 54, 2124.

61. Groves, J. T. In Metal Ion Activation of Dioxygen; Spiro, T. G. Ed.; New York: Wiley, 1980; p 125.

62. Richter, H. W.; Rahhal, S., J. Am. Chem. Soc., 1988, 110, 3126.

63. Rahhal, S.; Richter, H. W., Radiat. Phys. Chem., 1988, 32, 129.

64. Kremer, M. L.; Stein, G., Trans. Faraday Soc., 1959, 55, 959.

65. Kremer, M. L., Trans. Faraday Soc., 1962, 58, 702.

66. Kremer, M. L., Trans. Faraday Soc., 1963, 59, 2535.

67. Kremer, M. L., Int. J. Chem. Kinet., 1985, 17, 1299.

68. Flicstein, J. M.; Kremer, M. L., Journal of Catalysis, 1967, 8, 145.

69. Walling, C.; Taliawi, G. M.; Johnson, R. A., J. Am. Chem. Soc., 1974, 96, 133.

70. Walling, C., Accounts of Chemical Research, 1975, 8, 125.

71. Walling, C.; Amarnath, K., J. Am. Chem. Soc., 1982, 104, 1185.

72. Walling, C.; Weil, T., Int. J. Chem. Kinet., 1974, IV, 507.

73. Walling, C.; Goosen, A., J. Am. Chem. Soc., 1973, 95, 2987.

74. Barb, W. G.; Baxendale, J. H.; George, P.; Hargrave, K. R., Trans. Faraday Soc., 1951, 47, 591.

75. Barb, W. G.; Baxendale, J. H.; Geroge, P.; Hargrave, K. R., Trans. Faraday Soc., 1951, 47, 462.

76. Lei, C. S.; Piette, L. H., Tetrahedron Letters, 1979, 9, 775.

77. Koppenol, W. H., Journal of Free Radicals in Biology & Medicine, 1985, 1, 281.

78. Rush, J. D.; Koppenol, W. H., The Journal of Biological Chemistry, 1986, 261, 6730.

79. Rush, J. D.; Koppenol, W. H., J. Am. Chem. Soc., 1988, 110, 4957.

80. Groves, J.T.; Watanabe, Y., J. Am. Chem. Soc., 1986, 108, 507.

81. Balch, A. L.; Latos-Grazynski, L.; Renner, M. W., J. Am. Chem. Soc., 1985, 107, 2983.

82. Shiga, T., J. Phys. Chem., 1965, 69, 3805.

83. Cohen, G.; Lewis, D., J. Inorg. Biochem., 1981, 15, 143.

84. Buettner, G. R.; Doherty, T. P.; Patterson, L. K., FEBS Letters, 1983, 158, 143.

85. Rush, J. D.; Koppenol, W. H., Journal of Inorganic Biochemistry, 1987, 29, 199.

86. Halliwell, B., FEBS Letters, 1978, 92, 321.

87. Finkelstein, E.; Rosen, G. M.; Rauckman, E. J., Molecular Pharmacology, 1982, 21, 262.

88. Rosen, H.; Klebanoff, S. J., Archives of Biochemistry and Biophysics, 1981, 208, 512.

89. Masarwa, M.; Cohen, H.; Meyerstein, D.; Hickman, D. L.; Bakac, A.; Espenson, J. H., J. Am. Chem. Soc., 1988, 110, 4293.

90. Buxton, G. V., In Radiation Chemistry Principles and Applications; Farhataziz, Rodgers, M. A. Eds.; New York: VCH Publishers Inc., 1987; p.321.

91. Faraggi, M.; Carmichael, A.; Riesz, P., Int. J. Radiat. Biol., 1984, 46, 703.

92. Janzen, E. G.; Dudley, R. L.; Shetty, T. V., J. Am. Chem. Soc., 1979, 101, 243.

93. Matsubara, J.; Tajima, Y.; Karasawa, M., Environmental Research, 1987, 43, 66.

94. Anbar, M.; Neta, P., International Journal of Applied Radiation and Isotopes, 1967, 18, 493.

95. Butler, J.; Halliwell, B., Archives of Biochemistry and Biophysics, 1982, 218, 174.

BIOGRAPHICAL SKETCH

Fran Saunders was born in Newton, North Carolina, on December 31, 1960. She graduated eighth in her class from Newton-Conover High School in 1979. From August 1979 to May 1981 she attended Catawba College in Salisbury as a psychology major. In August 1981 she changed her major to chemistry and transferred to the University of North Carolina at Wilmington. While attending UNC-Wilmington, she worked in the Chemical Projects Group of General Electric-Nuclear Energy Division in Wilmington, NC. She was also involved in undergraduate research under the direction of Dr. Ned Martin. In December 1983 she graduated from UNC-Wilmington, magna cum laude, and received the Bachelor of Science degree in chemistry. She continued to work at General Electric until August 1984 when she enrolled at the University of Florida and began her graduate study under the direction of Dr. David Richardson. In February 1990 she joined the National Council for Air and Stream Improvement staff in Gainesville, Florida, as a research chemist. Upon completion of her degree she will continue her career with NCASI.

I certify that I have read this study and that in my opinion it conforms to acceptable standards of scholarly presentation and is fully adequate, in scope and quality, as a dissertation for the degree of Doctor of Philosophy.

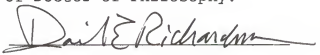

David E. Richardson, Chair
Associate Professor of
Chemistry

I certify that I have read this study and that in my opinion it conforms to acceptable standards of scholarly presentation and is fully adequate, in scope and quality, as a dissertation for the degree of Doctor of Philosophy.

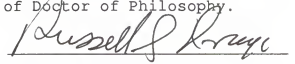

Russell S. Drago
Graduate Research Professor of
Chemistry

I certify that I have read this study and that in my opinion it conforms to acceptable standards of scholarly presentation and is fully adequate, in scope and quality, as a dissertation for the degree of Doctor of Philosophy.

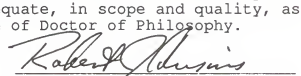

Robert J. Cousins
Boston Family Professor of
Human Nutrition

I certify that I have read this study and that in my opinion it conforms to acceptable standards of scholarly presentation and is fully adequate, in scope and quality, as a dissertation for the degree of Doctor of Philosophy.

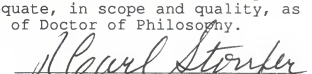

R. Carl Stoufer
Associate Professor of
Chemistry

I certify that I have read this study and that in my opinion it conforms to acceptable standards of scholarly presentation and is fully adequate, in scope and quality, as a dissertation for the degree of Doctor of Philosophy.

Kirk S. Schanze
Assistant Professor of
Chemistry

This dissertation was submitted to the Graduate Faculty of the Department of Chemistry in the College of Liberal Arts and Sciences and to the Graduate School and was accepted as partial fulfillment of the requirements for the degree of Doctor of Philosophy.

December 1990

Dean, Graduate School